The impact of rat cytomegalovirus gamma chemokine on dendritic cells

DISSERTATION

Zur Erlangung des akademischen Grades

Doctor rerum naturalium

(Dr. rer. nat.)

im Fach Biologie

Eingereicht an der

Lebenswissenschaftlichen Fakultät

der Humboldt-Universität zu Berlin

von

Julia Cecilia Madela-Mönchinger

Präsidentin der Humboldt-Universität zu Berlin

Prof. Dr.-Ing. Dr. Sabine Kunst

Dekan der Lebenswissenschaftlichen Fakultät

Prof. Dr. Bernhard Grimm

Gutachter:

1. Prof. Dr. Detlev H. Krüger

2. PD Dr. Sebastian Voigt

3. Prof. Dr. Martin Messerle

Tag der mündlichen Prüfung: 23.04.2021

The experiments described in this dissertation have been conducted from January 2017 to July 2020 at the Robert Koch Institute under the supervision of Prof. Dr. Detlev H. Krüger and PD Dr. Sebastian Voigt.

Für Stephan und meine Schwestern

Nauka jest jak niezmierne morze, im więcej jej pijesz, tym bardziej jesteś spragniony.

Science is like an immeasurable sea, the more you drink it, the thirstier you are.

Stefan Żeromski

Table of contents

Index of figures and tables

Figures

Images of rats were obtained from Pixabay.com and modified in Adobe Illustrator.

Tables

Abbreviations

°C	Degree Celsius
µ	micro
µg	micrograms
A647	Alexa 647
AA	Amino acid
ACK	Ammonium-Chloride-Potassium
Ag	Antigen
al.	alii, aliae
ANOVA	Analysis of variance
APC	Antigen presenting cell
APC	Allophycocyanin
ATAC	activation-induced T-cell-derived and chemokine-related molecule
bp	Base pairs
BSA	Bovine serum albumin
BV421	Brilliant Violet 421
CCR7	CC chemokine receptor 7
CD	Cluster of differentiation
cDC	Conventional dendritic cell
cDNA	Complementary DNA
CHE	Switzerland
CMV	Cytomegalovirus
CO_2	Carbon dioxide
conc.	Concentration
CPE	Cytopathic effect
CRISPR	Clustered Regularly Interspaced Short Palindromic Repeats
Ct	Cycle threshold
CTL	Cytotoxic T lymphocyte
DAPI	4′,6-diamidino-2-phenylindole
DC	Dendritic cell
DEG	Differentially expressed genes
DIG	Digoxigenin
DMEM	Dulbecco’s modified eagle medium
DMSO	Dimethyl sulfoxide

DNA	Deoxyribonucleic acid
DNK	Denmark
dNTP	Deoxynucleoside triphosphate
dpi	Days post infection
E	Early
e.g.	Example given
EDTA	Ethylenediaminetetraacetic acid
ELISA	Enzyme-linked immunosorbent assay
EM	Electron microscopy
ER	Endoplasmic reticulum
FACS	Fluorescence Activated Cell Sorting
FCS	Fetal calf serum
FITC	Fluorescein isothiocyanate
FMO	Fluorescence minus one
FR	France
FSC-H /-A	Forward scatter-Height/ -Area
fwd	forward
g	gram
g	Gravity
gB	Glycoprotein B
GDP	Guanosine diphosphate
GER	Germany
GFP	Green fluorescent protein
GO	Gene ontologies
GPCR	G protein-coupled receptor
gRNA	Guide RNA
GTP	Guanosine triphosphate
H_2O	Water
HCl	Hydrochloric acid
HCMV	Human Cytomegalovirus
HHV	Human herpesvirus
hpi	Hours post infection
HR	Croatia
HRP	Horseradish peroxidase
i.p.	Intraperitoneal
i.v.	Intravenous
ICTV	International Committee on Taxonomy of Viruses

IE	Immediate early
IFN	Interferon
IgG	Immunoglobulin G
IL	Interleukin
kbp	Kilobase pairs
KCl	Potassium chloride
kDa	Kilo dalton
KEGG	Kyoto Encyclopedia of Genes and Genomes
L	Late
l	liters
M	Molar, moles per liter
MCMV	Mouse Cytomegalovirus
MDC	Max Delbrück Center
$MgCl_2$	Magnesium Chloride
MHC	Major histocompatibility complex
min	Minute
ml	milliliters
MOI	Multiplicity of infection
mRNA	Messenger RNA
MuHV	Murid herpesvirus
MWCO	Molecular weight cut-off
n	Size of statistical sample
Na_2CO_3	Sodium carbonate
NaCl	Sodium chloride
$NaHCO_3$	Sodium bicarbonate
NaN_3	Sodium azide
ng	nanograms
NH_4Cl	Ammonium chloride
NK	Natural killer
NL	Netherlands
nm	nanometers
ns	Not significant
OD	Optical density
ORF	Open reading frame
PacO	Pacific Orange
PBS	Phosphate buffered saline
PBST	Phosphate buffered saline with tween

PCR	Polymerase chain reaction
pDC	Plasmacytoid dendritic cell
PE	Phycoerythrin
PFA	Paraformaldehyde
pfu	Plaque forming units
pH	Potential of hydrogen
PI	Propidium iodide
PMA	Phorbol-12-myristat-13-acetat
p-value	Probability-value
qRT	Quantitative real time
RCMV	Rat Cytomegalovirus
RCMV-B	Rat Cytomegalovirus Berlin
RCMV-E	Rat Cytomegalovirus England
RCMV-M	Rat Cytomegalovirus Maastricht
RCTL	C-type lectin homolog
REA	REAfinity Recombinant Antibodies
REF	Rat embryonic fibroblasts
rev	reverse
RKI	Robert Koch Institute
RNA	Ribonucleic acid
rpm	Revolutions per minute
RPMI	Roswell Park Memorial Institute medium
RT	Room temperature
SCM-1	single C motif-1
SD	Standard deviation
SDS	Sodium dodecyl sulfate
sec	seconds
SEM	Standard error of the mean
SG	Salivary glands
SIRPα	Signal regulatory protein alpha
SN	Supernatant
SSC-H /-A	Side scatter-Height/ -Area
TAP	Transporter associated with antigen processing
TierSchG	German animal protection law
TMB	3,3',5,5'-Tetramethylbenzidine
U	Unit
UK	United Kingdom

UL	Unique long
UMC	University Medical Center
US	Unique short
USA	United States of America
UV	Ultraviolet
v	Volume
VSB	Virus standard buffer
w	Weight
wt	wildtype
XCL1	X-C Motif Chemokine Ligand 1
XCR1	XC chemokine receptor 1

1. Introduction

1.1 Cytomegalovirus

1.1.1 Classification of Cytomegaloviruses

Cytomegaloviruses (CMV) are members of *Herpesviridae,* a family of large double stranded DNA viruses that infect a wide spectrum of species, including reptiles, birds and mammals. Members of this family share the ability to establish a life-long latency in their host. *Herpesviridae* are divided into three subfamilies named *Alpha*-, *Beta*-, and *Gammaherpesvirinae.* These are differentiated by nucleotide or predicted amino acid sequences. *Betaherpesvirinae* are characterized by genes found in the *Human betaherpesvirus 5* (HHV-5), also known as Human cytomegalovirus (HCMV) (ICTV 2019, Lefkowitz et al. 2017). *Betaherpesvirinae* consist of four genera: *Cytomegalovirus*, *Muromegalovirus*, *Proboscivirus* and *Roseolovirus*. Viruses of these genera are species-specific and exclusively infect mammals. While HCMV is a member of the genus *Cytomegalovirus*, Rat and Mouse CMV (RCMV, MCMV) belong to *Muromegalovirus* (Figure 1).

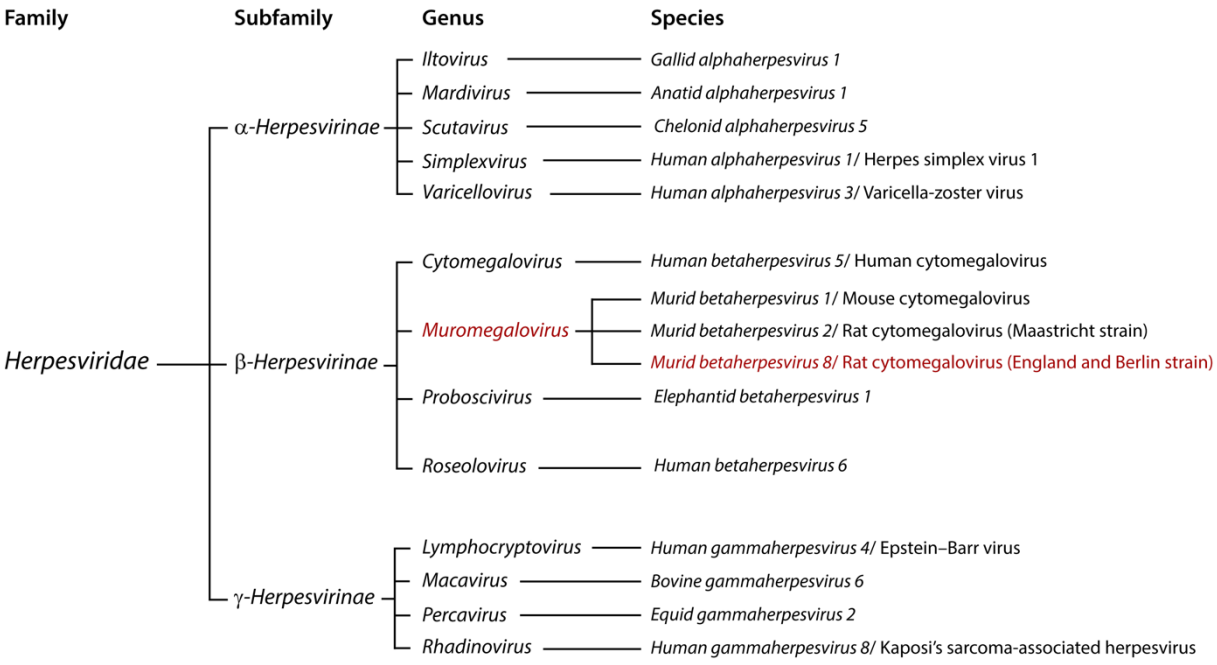

Figure 1: Taxonomy of *Herpesviridae*. The herpesvirus family is subclassified into the *Alpha*-, *Beta*-, *Gammaherpesvirinae*. Each subfamily consists of distinct genera. Only one to three representative species are shown for each genus. The phylogenetic tree was created based on the latest version of the International Committee on Taxonomy of Viruses (ICTV 2019). Species that is investigated in this work is colored in red.

Muromegaloviruses infect rodents and as *Cytomegalovirus* consist of a large genome (> 200 kb) that cause pathognomonic cytomegalia. Rodent CMV include *Murid betaherpesvirus 1*

(MuHV-1), also known as MCMV, and MuHV-2, known as RCMV-Maastricht (RCMV-M). Additionally, the two isolates RCMV-England and RCMV-Berlin have been described and grouped within the genus *Muromegalovirus* under the name MuHV-8 since 2011 (Voigt and Hayward 2011).

1.1.2 Rat cytomegalovirus

38 years ago, Bruggeman *et al.* isolated an infectious particle from salivary glands from rats (*Rattus norvegicus*) captured in the Netherlands (Bruggeman et al. 1982). Further investigations showed that the infectious particles displayed a variety of similarities to MCMV and HCMV, including particle size and morphology, the ability to form plaques in fibroblast monolayers and to induce cytomegalia, and the preference to persist in salivary glands. The infectious particles were confirmed to resemble a RCMV strain. Additional similarities to HCMV, such as the virus being excreted in urine and saliva, leukocyte-associated viremia and the persistence of the virus in the kidney without clinical disease, suggested that the isolated RCMV, named RCMV-Maastricht, could be used as a model to study CMV infections in humans (Bruggeman et al. 1985). During the same time another group isolated a similar infectious particle from *Rattus norvegicus* in England that exhibited characteristics comparable to HCMV. This virus was named RCMV-England (RCMV-E) (Priscott and Tyrrell 1982). A few years later, analysis of genome sizes, growth characteristics and genome sequences revealed that these viruses represent two highly diverged species, leading to the classification of RCMV-M as MuHV-2 and RCMV-E as MuHV-8 (Beisser et al. 1998a, Ettinger et al. 2012, Geyer et al. 2015, Vink et al. 2000, Voigt et al. 2005). Whole genome comparison analysis revealed that MuHV-8 differs significantly from MuHV-2 in size, base composition and genomic content. The genome of RCMV-E has a size of 203 kbp and is 27 kb smaller than RCMV-M. In 2015, a new infectious virus was isolated from *Rattus norvegicus* in Berlin that showed high sequence similarities to RCMV-E that was also classified as MuHV-8. The identification of the new MuHV-8 isolate, named RCMV-Berlin (RCMV-B) (Geyer et al. 2015), gave evidence that the smaller genome size of 203 kbp was not a result of accidental deletion by passage in cell culture as it was reported for the HCMV strains AD169 and Towne (Cha et al. 1996, Sinzger et al. 1999) but represents a distinct MuHV-8. Furthermore, it has been shown that MuHV-8 shares more sequence similarity with its mouse ortholog MCMV (MuHV-1) compared to its rat ortholog RCMV-M (MuHV-2) (Geyer et al. 2015). Despite its smaller genome size, MuHV-8 has unique genes that are not present in other CMVs. These genes encode homologs of the X-C Motif Chemokine Ligand 1 (XCL1), the C-type lectin receptor (Clr) ligand and CD200 which were named vXCL1, RCTL and e127, respectively (Foster-Cuevas et al. 2011, Geyer et al. 2014, Voigt et al. 2007, Voigt et al. 2005). Resulting from million years of co-evolution with their hosts, CMV evolved

strategies to adapt and broadly influence the innate and the adaptive immune systems of their hosts with the help of numerous genes that encode protein homologs important for regulating the immune response (Miller-Kittrell and Sparer 2009). In accordance with these findings and as it has been shown for RCTL (Voigt et al. 2007), vXCL1 and e127 might also interfere with the immune system.

1.1.3 CMV structure and replication

All CMV exhibit a common virion structure composed of an outer membrane envelope that takes the form of a lipid bilayer, a phosphoprotein tegument layer and an icosahedral capsid enclosing the linear double-stranded DNA (Figure 2). The outer membrane bears several glycoproteins that are necessary for viral attachment. The particle size ranges from 150 to 200 nm. Their genome size varies from 203 kb for MuHV-8 to 241 kb for *Panine herpesvirus 2*, also known as Chimpanzee Cytomegalovirus (CCMV) (Davison et al. 2003, Ettinger et al. 2012).

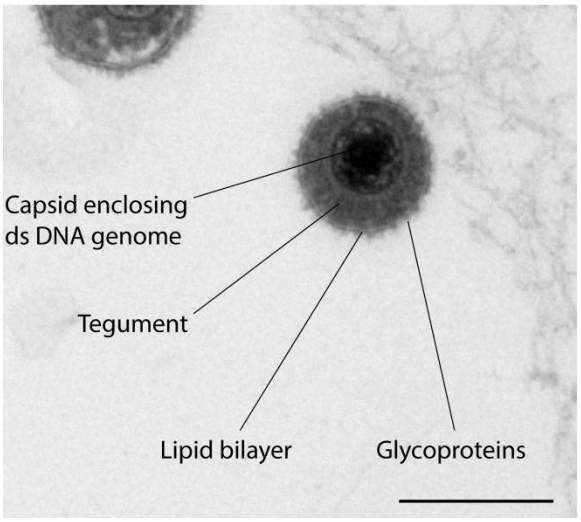

Figure 2: Electron microscopic image of RCMV-E. Bar = 200 nm. Image taken by Lars Möller, Robert Koch Institute.

CMV infect a broad range of host cells, including epithelial and endothelial cells, fibroblasts, monocytes/macrophages and dendritic cells (DC) (Sinzger et al. 2008). It has been shown that latent infection is associated with cells of the monocyte series, including macrophages and DC (Jarvis and Nelson 2002). The attachment of CMV occurs through interaction of specific viral glycoprotein complexes, e.g., gH, gL and MCK-2 in the case of MCMV, with various host cell receptors which can differ among cell types (Wagner et al. 2013, Wang and Shenk 2005). After fusion of the virus' lipid bilayer with the host membrane the viral DNA is released into the nucleus (Granzow et al. 1997, Sodeik et al. 1997). Viral transcription, viral DNA synthesis and capsid assembly take place in nuclear factories. The transcription of

genes follows a temporally regulated cascade with three chronological phases: immediate early (IE), early (E) and late (L) phase (Wathen and Stinski 1982). IE genes are the first to be transcribed. They function as transcription factors for early proteins, which play an essential role in viral replication. The late genes are transcribed last and encode structural components of the virion. They are necessary for virion assembly and egress. After nucleocapsids have formed in the nuclear factories tegumentation occurs in the cytoplasm followed by budding into vesicles of the trans-Golgi network and exocytosis (Mettenleiter 2002, Novoa et al. 2005). Like all Herpesviruses, CMV has the ability to establish life-long latency following the initial acute infection (Jarvis and Nelson 2002). During latency, no infectious particles are produced while the circularized DNA remains as an episome in the nucleoplasm. In this phase, only a few specific latency-associated genes are transcribed. The major sites of persistence as well as transmission of CMV are salivary glands (Campbell et al. 2008).

1.2 Immune system and response to CMV infection

The immune system is a complex interacting network that comprises an innate immunity that is not antigen-specific and an adaptive immunity that is antigen-specific. Key features of the innate immunity are the recognition of danger, triggered by pathogens or cell injury, and the transport of this signal to cells of the adaptive immune system (Banchereau et al. 2000). The interaction between the innate and the adaptive immune response plays a crucial role in the immune system and requires a communication platform. This is facilitated by antigen presenting cells (APC), including macrophages, B cells and DC. As part of the innate immune response APC recognize potentially dangerous particles. After intracellular processing, antigens are presented to cells of the adaptive immune system, including T cells.

1.2.1 Dendritic cells and antigen presentation

DC are highly adapted to their role as antigen-presenting cells and directing immune responses (Brinkman et al. 2013). DC are derived from bone marrow hematopoietic progenitor cells and are especially abundant in skin, mucosa and lymphoid tissues (Austyn 1996). In contrast to macrophages, DC can leave the tissue by getting attracted to the site of infection. DC subsets can be distinguished based on their phenotype, location or functionality (Guilliams et al. 2014). In mice and humans, there are three major groups of DC: conventional DC 1 and 2 (cDC1 and cDC2) as well as plasmacytoid DC (pDC) (Guilliams et al. 2014, Naik et al. 2007). cDC process ingested peptides that can be presented to T cells, while pDC produce antiviral type 1 interferons (IFN-α and -β) to activate further immune responses (Hochrein et al. 2002).

Immature cDC exhibit a high phagocytic capacity. This is important for the ingestion and procession of antigens that are presented to T cells. Three major ways of antigen presentation have been characterized: the Major histocompatibility complex (MHC) class I pathway, the MHC class II pathway and Cross-presentation.

The MHC class I pathway involves proteasomal processing of endogenous peptides or antigens that originate from the cell or from a pathogen replicating within the cell. Peptides derived from degraded proteins are transported via transporter associated with antigen processing (TAP) to the endoplasmic reticulum (ER). There, antigens are loaded on MHC class I and are ultimately presented to $CD8^+$ T cells (also known as cytotoxic T lymphocytes, CTL). If a foreign antigen is presented, the cell that bears this antigen is getting defeated by the primed CTL (Vyas et al. 2008).

In the MHC class II pathway, exogenous peptides are taken up by professional APC via phagocytosis, pinocytosis or receptor-mediated endocytosis. Antigens are loaded on MHC class II molecules within a phagosome or endosome, depending on the modes of previous internalization, followed by the transport to the cell surface and presentation to $CD4^+$ T cells. $CD4^+$ T cells are also known as T helper cells. They can further differentiate into T helper subsets that activate macrophages, B cells or cytotoxic T cells (Guermonprez et al. 2002, Zhu Jinfang and Paul 2010).

The third pathway, designated as cross-presentation, exhibits parts of both the MHCI and the MHCII pathways. Here, exogenous antigens are loaded on MHCI molecules and presented to $CD8^+$ T cells (Sigal et al. 1999). Cross-presentation can occur through a cytosolic or vacuolar pathway that are regulated differentially. In particular, the cytosolic cross-presentation has two ways of antigen loading: exogenous antigens can be processed by the proteasome and loaded onto MHCI molecules in the ER or reimported to the phagosome where antigens are loaded onto MHCI (Joffre et al. 2012). During vacuolar cross-presentation, antigens undergo phagosomal degradation followed by phagosomal loading on MHCI molecules (Figure 3).

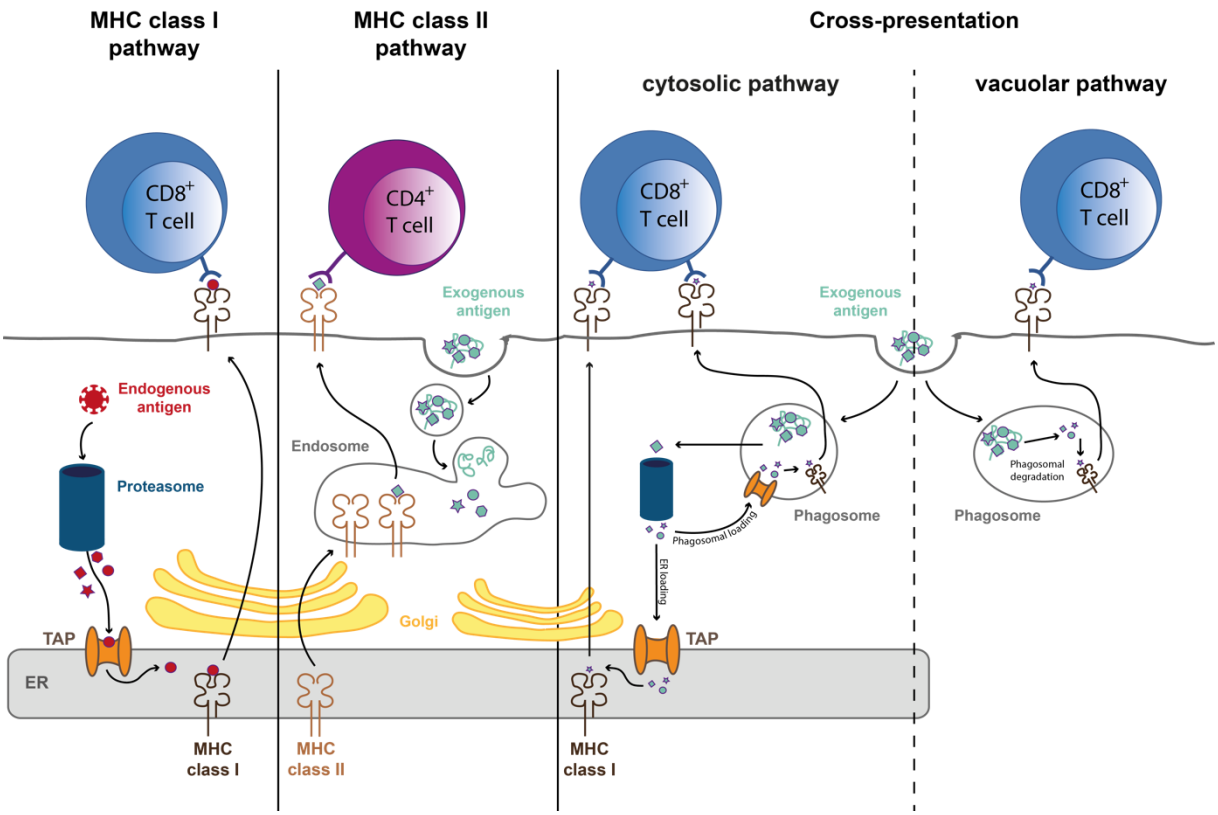

Figure 3: Antigen presentation pathways in dendritic cells (DC). DC can present antigens via MHC class I and MHC class II molecules to T cells. In the MHC class I pathway, peptides derived from proteins degraded in the cytosolic proteasome (endogenous antigens) are transported via a transporter associated with antigen processing (TAP) to the endoplasmic reticulum (ER), loaded onto MHCI and after vesicular transport to the cell surface presented to $CD8^+$ T cells. In the MHC class II pathway exogenous antigens are loaded onto MHCII in the endosome, transported to the cell surface and then presented to $CD4^+$ T cells. During cross-presentation exogenous antigens are loaded onto MHCI and presented to $CD8^+$ T cells. In the cross-presentation cytosolic pathway exogenous antigens are transported from the phagosome to the cytosol, where they undergo proteolysis. Antigens can then undergo ER loading or be re-imported to the phagosome for phagosomal loading. In the vacuolar pathway exogenous antigens are degraded and loaded onto MHCI in the phagosome. Modified after (Joffre et al. 2012, Villadangos and Schnorrer 2007).

To date, the intracellular pathways of cross-presentation are insufficiently understood. Nevertheless, it appears that the control of endocytic and phagocytic pathways, including the antigen export to the cytosol, might be of significant importance for this process (Alloatti et al. 2016, Gros and Amigorena 2019). Practically, cross-presenting DC can be determined by their phenotype. Mouse studies showed that the XC chemokine receptor 1 (XCR1) is expressed on $CD8\alpha^+$ DC which are capable of antigen cross-presentation, suggesting that cross-presentation is exclusively restricted to $XCR1^+$ DC (Bachem et al. 2012). Since XCR1 is a conserved selective marker for mammalian cell homologs of murine $CD8\alpha^+$ DC, it is an appropriate lineage marker for cross-presenting DC in other species (Crozat et al. 2010).

After antigen uptake or exposure to pathogens, DC undergo a complex transformation called maturation. This implies extensive morphological and functional changes. DC maturation can be divided into three main phases, starting with the early maturation (0 to 6 h of maturation), followed by maturing DC (from 7 to 20 h of maturation) and finally the establishment of fully

matured DC (over 20 h of maturation) (Alloatti et al. 2016). A fully mature DC has a reduced capacity to phagocyte and process antigens but shows an increased T cell stimulatory capacity, apparent by the upregulated expression of co-stimulatory molecules like CD40, CD80 and CD86 (De Smedt et al. 1996, Reis e Sousa 2006). Maturation also initiates the upregulation of the CC chemokine receptor 7 (CCR7), leading to migration to the local draining lymph nodes where interaction with naïve T cells occurs (Braun et al. 2011, Ritter et al. 2004).

1.2.2 CMV host entry, spread and immune response

Most CMV infections occur by transmission of body fluids and blood from acutely or chronically infected individuals (Keen 1985). However, to date no oral target cells have been identified, hence the oral entry of CMV is still unproven (Farrell et al. 2019). It has been suggested that CMV and other herpesviruses enter the host via olfactory epithelia (Milho et al. 2012, Shivkumar et al. 2013). In case of an intraperitoneal (i.p.) infection, which is a common experimental route, MCMV colonizes circulating monocytes, inducing a biphasic, monocyte-associated viraemia with primary spread to liver and spleen followed by secondary spread to the salivary glands where latency takes place (Collins et al. 1994). In addition, after olfactory infection with MCMV, infected DC were identified in draining lymph nodes, blood and salivary glands suggesting that viral spread was facilitated by DC being used as a transport vehicle (Farrell et al. 2017).

The immune response to CMV engages both humoral and cellular immunity. During primary infection the complement system is activated, bridging innate and humoral immune responses by the induction of inflammatory mediators, opsonization of pathogens and degradation of infected cells (Miller-Kittrell and Sparer 2009). Furthermore, specific antibodies that recognize epitopes of various CMV proteins are generated by the host. In particular, tegument proteins, envelope glycoproteins and nonstructural proteins such as the immediate early 1 (IE1) protein are targets of these antibodies (Jonjić et al. 1988, La Rosa and Diamond 2012). The most striking feature of CMV infection is the maintenance of a great number of CMV-specific memory T cells, a phenomenon termed memory inflation (Karrer et al. 2003). The T cell response to CMV is broadly specific, targeting CMV proteins from all three phases of lytic infection (immediate early, early and late) as well as all types of structural and non-structural proteins (Elkington et al. 2003). The generation of a $CD8^+$ T cell response is essential to control acute infection and reactivation. Interestingly, it is suggested that the priming of $CD8^+$ T cells is dominated by antigen cross-presentation (Busche et al. 2013). The number of memory T cells increases lifelong and constitutes approximately 10% of the circulating $CD4^+$ and $CD8^+$ memory T cell repertoires of HCMV-exposed individuals (Sylwester et al. 2005).

During early primary infection cells of the innate immune system recognize the virus. Activated pDC secrete IFN-α/β and Interleukin-12 (IL-12), promoting the activation of DC, macrophages and Natural Killer (NK) cells to limit viral replication and to protect adjacent cells against infection (Dalod et al. 2003, Swiecki et al. 2010). NK cells are cytotoxic cells of the innate immune response that play an important role in detecting and eliminating infected cells. They are responsible for the immediate control of viral infections. In general, infections lead to a reduction of MHCI surface expression. Since NK cell activation is controlled by inhibitory receptors interacting with MHCI on the cell surface of target cells in a healthy individual, an infection-induced reduction of MHCI leads to an activation of NK cells and therefore to the lysis of the cell. This process is also called “Missing self recognition” (Ljunggren and Kärre 1990).

During the acute infection phase NK cells expressing the C-type lectin receptor Ly49H$^+$ are indispensable to control MCMV *in vivo*. Once activated, they recruit inflammatory effector cells by secreting specific cytokines and chemokines, inter alia IFN-γ and XCL1 (Dorner et al. 2004). XCR1$^+$ CD8α$^+$ DC are attracted to the site of infection, where they take up antigens and interact with NK cells to keep the balance between positive and negative effects of IFN-α/β for the optimal control of MCMV infection (Thomas and Yang 2016). NKT cells are also efficient regulators of early host responses. NKT cells are a specialized population of T cells that co-express restricted T cell receptors (TCR) and receptors of the NK lineage (Bendelac et al. 1997). It appears that NKT cells do not play a critical role in restricting early acute-phase infection but may play a role in helping to activate immune responses that control viral replication at later stages (Van Dommelen et al. 2003). The antiviral response in MCMV infected submaxillary salivary glands involves both innate and acquired regulatory and effector cells that are sustained in higher numbers throughout the chronic phase of infection. Here, especially CD8$^+$ T cells primed against IE1 dominate the immune response (Cavanaugh et al. 2003). Despite the strong immune response launched by the host against CMV, the virus cannot be eliminated.

1.2.3 Immune evasion by CMV

Due to million years of co-evolution, herpesviruses evolved mechanisms to modulate both innate and adaptive immune responses to their own benefit. For HCMV more than 40 gene products were recognized that play a role in modulating the host immune response including the complement and interferon system, the chemokine network and immune cell interaction (Miller-Kittrell and Sparer 2009, Mocarski et al. 2013). Since antigen presentation by MHC class I molecules results in a CD8 T cell response, it might be expected that CMV evolved strategies to subvert MHCI and MHCII pathways disturbing antigen presentation and T cell

activation (Rölle and Olweus 2009). Since DC are key players in T cell activation, it is not surprising that CMV targets these cells. *In vitro*, CMV can infect DC while inhibiting their function on several levels: maturation, migration, antigen processing and T cell activation. DC infected with HCMV or MCMV show a downregulation of MHCI and MHCII resulting in a reduced antigen-presenting capacity (Andrews et al. 2001, Raftery et al. 2001). US6, encoded by HCMV, impedes antigen processing by preventing the transport of peptides through the TAP pore (Patro 2019). In addition, CMV infection inhibits DC maturation through the downregulation of costimulatory molecules CD40, CD80 and CD86, and by impairment of cytokine production (Andrews et al. 2001, Beck Kerstin et al. 2003, Moutaftsi et al. 2002). Furthermore, DC migration is prevented by the downregulation of certain chemokine receptors like CCR7 that are responsible for homing to lymphoid organs (Moutaftsi et al. 2004). Many of the CMV immune modulating genes are homologs of host genes that are involved in the immune response and which exhibit similar functions as the CMV genes. For example, to avoid NK-mediated clearance, CMV imitates host MHCI (Beck Stephan and Barrell 1988, Farrell et al. 1997). The RCMV-E C-type lectin homolog RCTL is another gene used to control NK cell activation. RCTL interacts directly with the NKR-P1B inhibitory receptor on NK cells leading to protection of the infected cell (Voigt et al. 2007).

Although CMV has developed various strategies to interfere with the host immune system and paralyzes the most potent APC, virus infection is largely controlled by a healthy immune system. Consequently, the balance between immune response and CMV evasion allows survival of both the virus and the host.

1.3 Chemokines, chemokine receptors and viral mimicry

One immune evasive strategy evolved by herpesviruses is the exploitation of the chemokine system by expressing homologs of chemotactic cytokines and receptors. These viral homologs can cause interference of cell migration, gene expression and leukocyte communication (Alcami 2003, Pontejo and Murphy 2017).

1.3.1 Classification and characterization of chemokines and chemokine receptors

Chemokines are small secreted molecules with a molecular weight of 8 to 12 kDa. Together with their receptors, they direct cell migration and control inflammation, lymphoid development and angiogenesis (Rossi and Zlotnik 2000). Chemokines are classified into four groups based on the number and spacing of conserved cysteine residues located at their N-terminus (Rollins 1997). The groups designate the date of discovery (α, β, γ and δ) and describe the number and position of the cysteine residue(s) (CXC, CC, C and CX3C) (Figure 4). Chemokines mediate their biological effects via binding to G protein-coupled receptors

(GPCR). The GPCR family is characterized by seven transmembrane domains. Since the specificity of each GPCR subtype strictly follows the associated chemokine class, they are named according to the structural subgroup they bind followed by an “R” for receptor and a number corresponding to the date of discovery (Bacon et al. 2003).

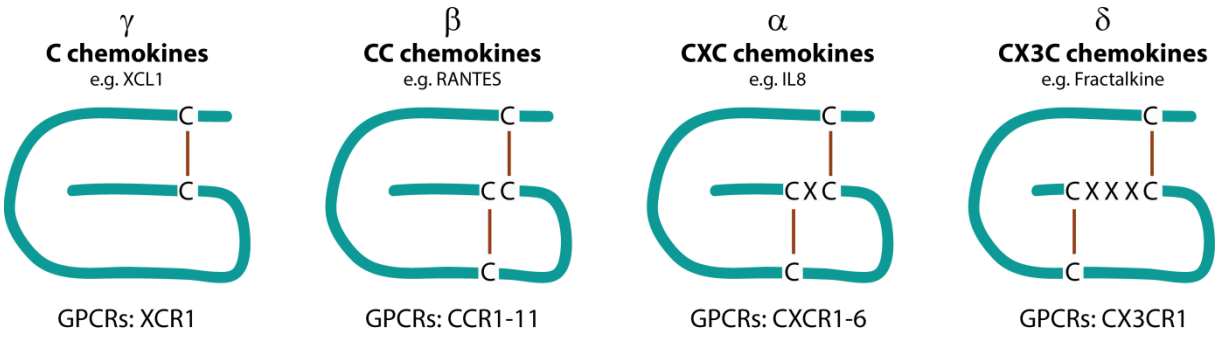

Figure 4: The four chemokine classes and their respective GPCR. Chemokines are classified into four groups, based on the number and relative position of their N-terminal cysteine residues (C, CC, CXC, CX3C) or the date of discovery (γ, β, α, δ). For each class, one representative chemokine is listed. C is a cysteine residue and X a non-cysteine amino acid. Modified after (Sodhi et al. 2004).

Chemokines are produced as pro-peptides that are cleaved during secretion. The pro-peptide comprises a signal peptide that guides the pro-peptide through the protein secretion pathway to the protein target location. The signal peptide consists of around 20-30 amino acids, involving a positive charged domain at the N-terminus, a hydrophobic core and an uncharged to negative charged region within the cleavage site (Owji et al. 2018, von Heijne 1990). As active mature proteins, chemokines bind GPCR which activates G proteins. Activated G proteins stimulate, according to their receptor-coupling specificities, effector molecules, including phospholipases, protein kinases and GTPases, turning on signaling cascades within the cell (Sodhi et al. 2004). This triggers intracellular signaling pathways that regulate cellular migration and activate other cellular events (Mackay 2001).

1.3.2 Viral mimicry

Since chemokines and GPCR are the initial activators of crucial physiological processes, it appears plausible that viruses imitate and use them to their own advantage. This molecular mimicry can facilitate viral infection, replication, dissemination or immune evasion (Murphy 2001). On the one hand, viral mimics can exhibit similar sequences and splicing patterns indicating divergent evolution. On the other hand, there are molecules with structures unrelated to chemokines or chemokine receptors but which bind to chemokines and GPCR to distract their function. The latter might be an example for convergent evolution. On this basis chemokine mimics can be divided into three subclasses: chemokine homologs, chemokine receptor homologs and chemokine binding proteins with a unique structure

(Murphy 2001). Chemokines encoded by viruses can operate as agonists that activate or antagonists that block their target receptors.

Four chemokine-like genes in the HCMV genome have been described so far: *UL128*, *UL130*, *UL146* (vCXCL1) and *UL147* (vCXCL2) (Pontejo and Murphy 2017). The HCMV open reading frame (ORF) *UL128* encodes the CC chemokine homolog CCL2 that was shown to be necessary for monocyte infection and inhibition of migration (Straschewski et al. 2011). Although this chemokine homolog has also been identified in RCMV-E and MCMV, the diverse patterns of genomic organization and low amino acid sequence identity suggest that they cannot be considered as orthologs (Pontejo and Murphy 2017). UL128 exhibits an additional function as part of a protein complex with gH, gL, UL130 and UL131A that mediates the cell-entry process (Ryckman et al. 2008, Vanarsdall and Johnson 2012). Furthermore, ORF *UL146* encodes vCXCL1, an agonist that is secreted by HCMV infected endothelial cells and attracts neutrophils. These cells contribute to the vascular dissemination of HCMV (Grundy et al. 1998, Yamin et al. 2016).

Most CMV encode two or more viral chemokines except for MCMV that encodes only one CC chemokine MCK-2 (Saederup et al. 1999). Like UL128, MCK-2 also forms a complex with gH and gL to promote infection of macrophages (Wagner et al. 2013). MCK-2 is translated from a spliced transcript that includes ORF *m131* and *m129* (MacDonald et al. 1999). RCMV-E-encoded *e131/e129* is an ortholog that exhibits the same genomic organization as *m131/m129* with two syntenic ORF (Voigt et al. 2005). Unlike its counterparts, RCMV-M ORF *r131/r129* encodes two separate CC chemokines, RCK-2 and RCK-3 (Kaptein et al. 2004).

All viral chemokines require additional viral or host GPCR to execute their proper function. Four HCMV-encoded viral GPCR have been described: US27, US28, UL33 and UL78 (Chee et al. 1990, Vischer et al. 2014). Among them, only UL33 and UL78 are conserved across all CMV species (MCMV *m33* (Rawlinson et al. 1996); RCMV-M *r33*, *r78* (Vink et al. 2000); RCMV-E *e33, e78* (Voigt et al. 2005)). Viral GPCR are present on the viral envelope, possibly facilitating cell interaction and viral entry (Margulies et al. 1996, Varnum et al. 2004). Furthermore, UL33 and UL78 were shown to form heteromers with human CCR5 and CXCR4, resulting in translocation followed by impaired cell migration towards CCR5 and CXCR4 specific chemokines (Tadagaki et al. 2012). Figure 5 depicts known CMV chemokines and chemokine receptors.

	Chemokines	Chemokine receptors	References
 HCMV	UL146 (vCXCL1) UL147 (vCXCL2) UL128 UL130	US27 US28 UL33 UL78	Chee et al., 1990 Vischer et al., 2014 Pontejo and Murphy, 2017
 RCMV-M	r131 (RCK-2) r129 (RCK-3)	R33 R78	Beisser et al., 1998 Vink et al., 2000 Kaptein et al., 2004
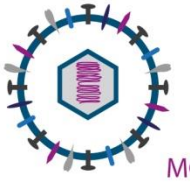 MCMV	m131/m129 (MCK-2)	M33 M78	Rawlinson et al., 1996 Davis-Poynter et al., 1997 MacDonald et al., 1999 Oliveira and Shenk, 2001
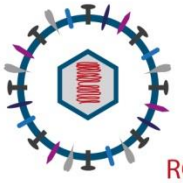 RCMV-E	e131/e129 (ECK-2) e156.5 (vXCL1)	E33* E78*	Voigt et al., 2005 Ettinger et al., 2012 Geyer et al., 2014 Bauer et al., 2020 *no experimental evidence

Figure 5: Chemokines and chemokine receptors encoded by different CMV species.

1.3.3 XCL1 and XCR1

Among the chemokine classes, the γ-chemokines include only one member that is conserved among mammalian species. According to the chemokine nomenclature, this chemokine is designated XCL1 but was earlier described as lymphotactin, single C motif-1 (SCM-1) or activation-induced T-cell-derived and chemokine-related molecule (ATAC) (Kelner et al. 1994, Kennedy et al. 1995, Yoshida et al. 1995). During a bacterial, parasitic or viral infection XCL1 is expressed by innate immune cells like NK cells and NKT cells (Dorner et al. 2004, Hedrick et al. 1997) as well as adaptive immune cells including activated $CD8^+$ and $CD4^+$ T cells (Dorner et al. 2002).

XCL1 elicits its function by chemoattracting XCR1-expressing cells and then activating its target receptor (Figure 6). XCR1 is the only receptor for XCL1 and is solely expressed on a $CD8\alpha^+$ subpopulation of mouse DC, $CD141^+$ subpopulation of human DC and equivalent DC subsets among all mammalian species (Bachem et al. 2010, Crozat et al. 2010, Dorner et al. 2009, Yoshida et al. 1998). Most of XCR1-expressing DC are found in the spleen and in the

subcapsular sinus and paracortical areas of lymph nodes (Dorner et al. 2009, McLellan et al. 2002). XCR1$^+$ DC are capable of cross-presentation that induces an antigen-specific cytotoxic immune response via CD8$^+$ T cell activation (Bachem et al. 2010). Besides infection, the XCL1-XCR1 axis appears to play a crucial role in the thymic establishment of self-tolerance by antigen presentation to medullary thymic epithelial cells (Lei and Takahama 2012).

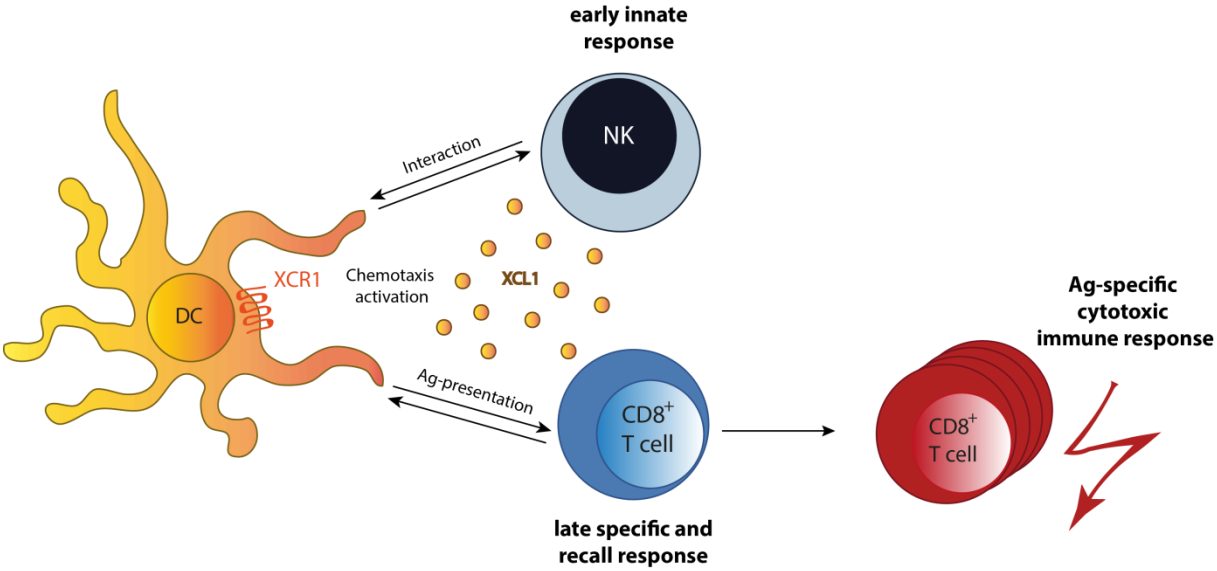

Figure 6: XCR1-XCL1 related immune response. In response to a bacterial, parasitic or viral infection XCL1 NK, NKT and T cells secrete XCL1. During the early innate response activated NK cells secrete, among other cytokines, XCL1 which chemoattracts XCR1$^+$ DC. In the adaptive phase, secretion of XCL1 by activated CD8$^+$ T cells optimizes the dialog with antigen cross-presenting DC and facilitates differentiation of CD8$^+$ T cells to cytotoxic effector cells (Kroczek and Henn 2012).

1.3.4 The RCMV-E homolog vXCL1 (*e156.5*)

In 2014 the first viral γ-chemokine encoded by *e156.5* of RCMV-E was identified and named vXCL1 (Geyer et al. 2014). vXCL1 shares a strong amino acid identity with rat (64%), mouse (58%) and human XCL1 (46%). In addition, vXCL1 chemoattracts and binds exclusively XCR1-expressing cells (Bauer 2018, Geyer et al. 2014). In rats, splenic CD4$^-$ DC that express XCR1 are assumed to be the equivalent of mouse CD8α$^+$ and human CD141$^+$ DC (Hubert et al. 2006). vXCL1 consists of 114 or 115 amino acids for RCMV-B and RCMV-E, respectively, with a predicted molecular weight of 13 kDa and cysteine residues at position 30 and 67 that are conserved within rXCL1 and vXCL1. The N-terminal signal peptide is cleaved off for secretion of the mature chemokine which is a glycosylated protein with 96 amino acids that can be detected in the supernatant of infected rat embryonic fibroblasts 13 h post infection (hpi) (Geyer et al. 2014). To date, among all viruses, only RCMV-E and the second isolate of MuHV-8, RCMV-B, were shown to encode vXCL1 (Geyer et al. 2015).

1.4 Objectives

By encoding an XCL1 homolog, MuHV-8 evolved a unique strategy to interact with XCR1 expressing DC that are possibly capable of antigen cross-presentation. Previous work revealed that vXCL1 chemoattracts only the XCR1-expressing DC subset and binds solely to this receptor (Bauer 2018, Bauer et al. 2020, Geyer et al. 2014). Furthermore, it was shown that vXCL1 acts as an agonist that competes with rXCL1 for XCR1. Therefore, the aim of this study was to investigate the impact of vXCL1 on DC and the role of the vXCL1-XCR1 axis during RCMV infection. The main objectives were:

1. Characterization of rat DC subsets
2. Identification of DC and lymphocytes in salivary glands
3. Transcriptome and surface protein expression analysis of DC after RCMV-E wt and RCMV-E ∆*vxcl1* infection
4. Comparative analysis of recombinant rXCL1 and vXCL1 regarding a potential downregulation effect on XCR1
5. The impact of XCR1 and vXCL1 on RCMV-B spread and immune cell migration to salivary glands

2. Materials

2.1 Media, buffers and solutions

Table 1: Media, buffers and solutions and their composition.

Cell cultivation				
DMEM	3.7	g/l	$NaHCO_3$	
	13.3	g/l	DMEM	pH 7.2
RPMI 1640	2	g/l	$NaHCO_3$	
	10.43	g/l	RPMI 1640	pH 7.2
Complete DMEM	2-5.0	%	FCS	
	100.0	U/ml	Penicillin	
	0.1	mg/ml	Streptomycin	
	2.0	mM	L-glutamine	
	1	x	DMEM	
Complete RPMI 1640	10	%	FCS or Rat serum	
	100.0	U/ml	Penicillin	
	0.1	mg/ml	Streptomycin	
	2.0	mM	L-glutamine	
	50	µM	β-Mercaptoethanol	
	1	x	RPMI	
Chemotaxis medium	1	%	BSA	
	100	U/ml	Penicillin	
	0.1	mg/ml	Streptomycin	
	50	µM	β-Mercaptoethanol	
	1	x	RPMI	
1x Phosphate buffered saline (PBS)	137.0	mM	NaCl	
	2.7	mM	KCl	
	4.0	mM	Na_2HPO_4	
	1.5	mM	KH_2PO_4	pH 7.4
Freezing medium				
Rat embryonic fibroblasts	10.0	%	DMSO	
	90.0	%	FCS	
Rat leukocytes	10.0	%	DMSO	
	45	%	FCS	

	45	%	RPMI	
Virus DNA preparation and plaque assay				
Plaque overlay medium	8.0	g/l	Methylcellulose	
	100.0	U/ml	Penicillin	
	0.1	mg/ml	Streptomycin	
	5.0	%	FCS	
	1	x	DMEM	
TE9 buffer	0.5	M	Tris	
	20	mM	EDTA	
	10	mM	NaCl	pH 9.0
Sucrose/Virus standard buffer	15	% (w/v)	Saccharose	
	50	mM	Tris	
	10	mM	KCl	
	5	mM	EDTA	pH 7.8
Methylene blue staining solution	0.5	M	$NaCH_3COO$	
	0.1	% (w/v)	Methylene blue	
	0.1	% (w/v)	NaN_3	
Cell isolation and flow cytometry				
ACK-lysis buffer	155	mM	NH_4Cl	
	10	mM	$KHCO_3$	
	0.1	mM	EDTA	pH 7.2
MACS PBS	0.5	% (w/v)	BSA	
	2.0	mM	EDTA	
	1	x	PBS	pH 7.2
FACS PBS	2.0	% (v/v)	FCS	
	0.1	% (w/v)	NaN_3	
	1	x	PBS	pH 7.2
Permeabilization buffer	0.5	% (w/v)	Saponin	
	1	x	FACS PBS	
ELISA				
Coating buffer	0.1	M	$NaHCO_3$	
	0.1	M	Na_2CO_3	pH 9.5
Washing buffer	1	x	PBS	
	0.05	% (v/v)	Tween 20	

Blocking buffer	1	x	PBS	
	1.0	% (w/v)	BSA	
	0.1	% (v/v)	Tween 20	
Tissue disruption for *Xcr1* genotyping				
Ear buffer	100	mM	Tris	
	5	mM	EDTA	
	200	mM	NaCl	
	0.2	% (w/v)	SDS	pH 8.5
TE/RNase buffer	10	mM	Tris-HCl	
	1	mM	EDTA	
	20	µg/ml	RNase A	pH 8.0
DNA electrophoresis				
Tris acetate EDTA buffer	40	mM	Tris	
	20	mM	Glacial acetic acid	
	1	mM	EDTA	pH 7.8

2.2 Equipment

Table 2: Laboratory equipment and devices.

Equipment	Company
AxioCam ICm1	Zeiss, Jena, GER
Bacteria incubator type 3032	GFL, Burgwedel, GER
BioDocAnalyze	Biometra, Jena, GER
Centrifuge 5415 D	Eppendorf, Hamburg, GER
CO_2 Incubator	Memmert, Schwabach, GER
CO_2 incubator HERAcell 240i	Thermo Scientific, Schwerte, GER
Flow Cytometer Cytoflex	Beckman Coulter, Brea, USA
Flow cytometer Fortessa	BD Pharmingen, San Diego, USA
Flow cytometer MACSQuant Analyzer 10	Miltenyi Biotec, Bergisch Gladbach, GER
FLUOstar Omega microplate reader	BMG Labtech, Ortenberg, GER
Freezer -20°C	Liebherr, Bulle, CH
Gel electrophoresis chamber	Peqlab Biotechnologie GmbH, Erlangen, GER

Gentle MACS Dissociator	Miltenyi Biotec, Bergisch Gladbach, GER
GFL® Waterbath	Gesellschaft für Labortechnik mbH, Burgwedel, GER
Heraeus Fresco 17 centrifuge	Thermo Scientific, Schwerte, GER
Heraeus Fresco 21 centrifuge	Thermo Scientific, Schwerte, GER
Heraeus Multifuge 1S-R centrifuge	Thermo Scientific, Schwerte, GER
Hot plate magnetic stirrer IKA® RCT basic	IKA-Werke GmbH & Co. KG, Staufen, GER
Laminar Flow Safe 2020	Thermo Scientific, Schwerte, GER
Light microscope Axiovert 25	Zeiss, Jena, GER
Light microscope Nikon Eclipse TS100	Nikon, Düsseldorf, GER
LightCycler® 480	Roche Life Science, Penzberg, GER
Liquid nitrogen tank Biosafe®	Cryotherm, Kirchen/Sieg, GER
Mastercycler epgradient S	Eppendorf, Hamburg, GER
MaxQ™ 7000 Water Bath Orbital Shaker	Thermo Scientific, Schwerte, GER
Microwave 800	Severin, Sundern, GER
MP FastPrep® -24	MP Biomedicals, Santa Ana, USA
NanoDrop 8000	Thermo Scientific, Schwerte, GER
Neubauer counting chamber	Marienfeld, GER
Neubauer counting chamber	VWR International GmbH, Darmstadt, GER
Pipetus®	Hirschmann Laborgeräte GmbH & Co. KG, Eberstadt, GER
Refrigerator	Bosch, Gerlingen, GER
Sorvall Lynx 4000 centrifuge	Thermo Scientific, Schwerte, GER
Sorvall RC6+ centrifuge	Thermo Scientific, Schwerte, GER
Thermocycler T 3000	Biometra, Jena, GER
Thermomixer comfort	Eppendorf, Hamburg, GER
Ultracentrifuge XL90	Beckman Coulter, USA
UV Stratalinker™ 2400	Stratagene, Cedar Creek, USA
Vortex Genie 2	Scientific Industries, Inc., New York, USA

2.3 Consumables

Table 3: Consumable list.

Consumables	Company
0.2 ml thin wall PCR tubes	Thermo Scientific, Schwerte, GER
1 ml, 2 ml, 5 ml, 10 ml and 50 ml syringes	B. Braun Melsungen AG, Melsungen, GER
10 cm and 15 cm cell culture dishes	TPP, Trasadingen, CHE
15 ml and 50 ml centrifuge tubes	Azer Scientific Inc., Hamburg, GER
24-well tissue culture plates	TPP, Trasadingen, CHE
30 µm MACS smart strainer	Miltenyi Biotec, Bergisch Gladbach, GER
50 µm filter CellTrics®	Sysmex Europe GmbH, Norderstedt, GER
6-well tissue culture plates	Sarstedt, Nümbrecht, GER
70 µm and 100 µm nylon cell strainer BD Falcon™ Corning	BD Pharmingen, San Diego, USA
96-well MaxiSorp microtiter plates	Nunc, Roskilde, DNK
96-well tissue culture plates	Sarstedt, Nümbrecht, GER
96-well U-bottom plates	Nunc, Roskilde, DNK
Art tips (20 µl, 200 µl, 1000 µl)	Thermo Scientific, Schwerte, GER
Cluster tubes	Corning, Salt Lake City, USA
C-Tubes	Miltenyi Biotec, Bergisch Gladbach, GER
MACS cell separation columns (MS columns)	Miltenyi Biotec, Bergisch Gladbach, GER
Minisart® Syringe Filter (0.22 µm and 0.45 µm) sterile filter	Sartorius Stedim Biotech, Göttingen, GER
Nunc™ CryoTube™ vials	Thermo Fisher Scientific, Jiangsu, CHN
PD-10 columns	GE Healthcare, München, GER
Polyallomer tubes (25x89 mm)	Beckmann Coulter, Krefeld, GER
RNase-Free Tubes	Zymo Research, Irvine, USA
Serological pipettes (5 ml, 10 ml, 25 ml)	Sarstedt, Nümbrecht, GER
Single-use pipetes (50 ml)	Carl Roth, Karlsruhe, GER
Slide-A-Lyzer Dialysis cassette	Thermo Fisher Scientific, Schwerte, GER
Transwell system, 6.5 mm	Corning, Schiphol-Rijk, NL

2.4 Software

Table 4: Software used in this study.

Software	Manufacturer
Adobe Illustrator CS6	Adobe Systems Inc., San José, USA
EndNote	Thomson Reuters, London, UK
FACSDiva Software	BD Pharmingen, San Diego, USA
FlowJo Software v10.4	Tree Star Inc., Ashland, USA
Geneious Prime	Biomatters Ltd, Auckland, NZ
GraphPad Prism 8	GraphPad Software, Inc., La Jolla, USA
LightCycler® 480 Software	Roche Life Science, Penzberg, GER
MACSQuantify™ Software	Miltenyi Biotec, Bergisch Gladbach, GER
MARS Data Analysis Software	BMG Labtech, Ortenberg, GER
Microsoft Office	Microsoft Corporation, Redmond, USA
R	R Core Team
ZEN (blue edition) 2.3	Carl Zeiss Microscopy GmbH, Jena GER

2.5 Chemicals

Table 5: Chemicals.

Chemical	Supplier
200 mM L-Glutamine	PAA Laboratories, Cölbe, GER
2x MEM	Gibco, Thermo Fisher Scientific, Schwerte, GER
Agarose	Carl Roth, Karlsruhe, GER
Bovine serum albumin, low endotoxin	Gemini Bio-Products, West Sacramento, USA
ddH_2O	Sigma-Aldrich, Inc., St. Louis, USA
Dulbecco's Modified Eagle medium	Thermo Scientific, Waltham, USA
Fetal calf serum	PAN Biotech GmbH, Regensburg, GER
GelRed Nucleic Acid Gel stain	Biotium, Fremont, USA
Ionomycin calcium salt from *Streptomyces conglobatus*	Sigma-Aldrich, Inc., St. Louis, USA

Isoflurane	Baxter GmbH, Unterschleißheim, GER
Methylcellulose	Sigma-Aldrich, Inc., St. Louis, USA
NycoPrep® 1.077	Progen, Heidelberg, GER
OptiPrep™ (Iodixanol)	Progen, Heidelberg, GER
Pacific Orange™ Succinimidyl Ester	Thermo Fisher Scientific, Schwerte, GER
Pancoll rat	PAN Biotech, Aidenbach, GER
Penicillin/Streptomycin (100x)	PAA Laboratories, Cölbe, GER
Phorbol 12-myristate 13-acetate	Sigma-Aldrich, Inc., St. Louis, USA
Puromycin Dihydrochlorid (Calbiochem)	Merck Chemicals GmbH, Darmstadt, GER
Roswell Park Memorial Institute medium	Thermo Scientific, Waltham, USA
TRIzol® LS Reagent	Life Technologies, Carlsbad, USA
Trypsin-EDTA 1x in PBS	Biowest, Nuaillé, FR
Trypan blue	Sigma-Aldrich, Inc., St. Louis, USA

2.6 Reagents

Table 6: Reagents.

Reagent	**Supplier**
1 kb DNA ladder	Thermo Scientific, Schwerte, GER
100 bp DNA ladder	Thermo Scientific, Schwerte, GER
6x Loading dye	Thermo Scientific, Schwerte, GER
100 mM dNTP set	Thermo Scientific, Schwerte, GER
dNTP mix, 10 mM each	Thermo Scientific, Schwerte, GER
TMB Substrate Solution	Thermo Scientific, Schwerte, GER
Lamda-DNA-TE buffer	Fermentas, Massachusetts, USA

2.7 Kits

Table 7: Utilized kits.

Kit	**Manufacturer**
BigDye Terminator v3.1 Cycle Sequencing Kit	Applied Biosystems, Darmstadt, GER

DNeasy Blood & Tissue Kits	Qiagen, Hilden, GER
NEBNext® Ultra II Directional RNA Library Prep Kit for Illumina®	New England Biolabs, Massachusetts, USA
Platinum™ *Taq* DNA Polymerase	Invitrogen, Massachusetts, USA
RNA Clean & Concentrator-25 kit	Zymo Research, Irvine, USA

2.8 Primers and Probes

Primers were ordered from Invitrogen™ (Thermo Fisher Scientific) and dissolved in nuclease free water (Sigma-Aldrich) to 100 µM. For PCR reactions primers were diluted to 10 µM and stored at -20°C. TaqMan probes used in quantitative real-time PCR were purchased from TIB MOLBIOL, dissolved in nuclease free water to a working concentration of 10 µM and stored at -20°C.

Table 8: Nucleotide sequences of used primers.

Primer/ Probe name	**Sequence (5′ to 3′)**
***Xcr1* genotyping**	
XCR1 Intron 3204 fwd	CCTCCCATTCTATAGACCATCTC
XCR1 Exon 3659 rev	AACCAGGCTGTTACCCACCAGG
RCMV-E *vxcl1* region	
SG vATAC Seq fwd	TAACGTACAATGCGATCATATTC
HG6 fwd 1284	CGACATGGGCCGTCAATGTG
vATAC seq 186691	CACGAAACCATCTGCGTAAG
RCMV-B *vxcl1* region	
vXCL1 B rev	CTTCCAGTCCCTTACAGCGG
vXCL1 B fwd	TGATATGGCGGATCCGTTCG
Seq vXCL1 B rev	TGCTTCTATATCAGCACTGTGATCT
Seq vXCL1 B fwd	CGATACGATGGACATGATATACACG
RC-2425	GCAAAGAAGGAGCTATGCGAG
RC-2424	GTTTTGAATCGGAAGTCGCT
RC-2423	GTCACTGCATGGATTGTAGA
Quantitative real-time PCR	
RCMV gB-1008F	CAAGGCCATCAGAACGGATC
RCMV gB-1118R	TCACTCCCCGATGCGTTATA

myc-6015F	GCCAGAGGAGGAACGAGCT
myc-6095R	GGGCCTTTTCATTGTTTTCCA
RNASeq qPCR	
NEBnext_qPCR_fwd	TCC CTA CAC GAC GCT CTT CCG ATC
NEBnext_qPCR_rev	GTT CAG ACG TGT GCT CTT CCG ATC
TaqMan probes	
gB (55-1050 TM)	FAM-CACAAACGTTGCGGTCAGACTTTTCGAC-TAMRA
c-myc (myc-6049TM)	FAM-TGCCCTGCGTGACCAGATCC-TAMRA

2.9 Plasmids

Table 9: List of plasmids used and generated in this study.

Plasmid Name	Description	Reference
pTopo2.1-gB	gB standard curve for quantitative real-time PCR	Ettinger, 2012
pTopo2.1-c-myc	c-myc standard curve for quantitative real-time PCR	Ettinger, 2012
RP-557 EFS puro-T2A-Cas9 - RC-2425 - RC-2424 - RC-2423	Generation of RCMV-B vXCL1 deletion mutant	Kindly provided by Robert Jan Lebbink, UMC Utrecht

2.10 Antibodies and beads

Fluorophore-coupled antibodies were titrated and stored at 4°C. Dig-coupled antibodies were stored at -80°C.

Table 10: Antibodies used in this study.

Specifity	Clone	Label	Source
Anti-mouse IgG		A647	Life Technologies, Carlsbad, USA
Anti-mouse IgG		HRP	Dako, Hamburg, GER
CD103	Ox-62	A647	BioLegend, London, UK
CD103	Ox-62	BV428	BD Pharmingen, San Diego, USA
CD103	Ox-62	Microbead	Miltenyi Biotec, Bergisch Gladbach, GER

CD161a	NKR-P1A	PE	BD Pharmingen, San Diego, USA
CD161a	REA227	PE-Vio770	Miltenyi Biotec, Bergisch Gladbach, GER
CD172a (SIRPα)	Ox-41	PE	BioLegend, London, UK
CD3	REA223	APC-Vio770	Miltenyi Biotec, Bergisch Gladbach, GER
CD3	REA223	VioBlue	Miltenyi Biotec, Bergisch Gladbach, GER
CD4	W3/25	PE-Cy7	BioLegend, London, UK
CD45RA	Ox-33	PerCP-Cy5.5	BioLegend, London, UK
CD45RA	Ox-33	PE	BD Pharmingen, San Diego, USA
CD45RA	Ox-33	APC-Cy7	BD Pharmingen, San Diego, USA
CD8a	REA437	FITC	Miltenyi Biotec, Bergisch Gladbach, GER
Isotype Mouse IgG2b, κ	MPC-11	PE	BioLegend, London, UK
MHCII	REA510	PerCP-Vio700	Miltenyi Biotec, Bergisch Gladbach, GER
MHCII (RT1B)	Ox-6	FITC	BD Pharmingen, San Diego, USA
rXCL1		Dig	Torrey Pines Biolabs, Secaucus, USA
StrepMAB-Immo Oyster	Strep-tag® II	A645	IBA GmbH, Göttingen, GER
Streptavidin		APC	BioLegend, London, UK
vXCL1	RCMV-11		S. Jonjic, University of Rijeka, Rijeka, HR
XCR1	ZET	PE	BioLegend, London, UK

2.11 Viruses

All viruses were titrated by plaque assay and stored at -80°C.

Table 11: RCMV-E and RCMV-B recombinant viruses.

Virus	Description	Source
RCMV-E wild type	RCMV isolated from *Rattus norvegicus* propagated on rat embryonic fibroblasts (REF).	William H. Burns, Baltimore, USA (Voigt et al. 2005)
RCMV-E Δ*vxcl1*	The *vxcl1* ORF was replaced by a mCherry-cassette followed by removing the fluorescent marker by Cre recombinase.	Generated by Anna Novak (Voigt laboratory)

RCMV-E *gfp*	A green fluorescent protein (*gfp*)-cassette was introduced adjacent to *e32.*	Generated by Aila Daugs (Voigt laboratory)
RCMV-B wild type	RCMV isolated from salivary glands of a rat (*Rattus norvegicus)* captured in Berlin and plaque purified (SG1 D12) on REF.	Isolated by Sebastian Voigt, plaque purified by Henriette Geyer (Geyer et al. 2015)
RCMV-B Δ*vxcl1*	REF were transfected with RP-557 EFS puro-T2A-Cas9 containing three different guide RNAs (RC-2425, RC-2424, RC-2423) targeting RCMV-B *vxcl1* and then infected with RCMV-B wt. Mutants were screened and plaque purified (RCMV-B Δ*vxcl1* H3)	Generated by Julia Madela-Mönchinger with technical assistance of Yue Yu (part of this dissertation 4.5)

2.12 Eukaryotic cells

To propagate virus and conduct infection experiments, REF were obtained from William H. Burns (Baltimore, USA).

2.13 Rat strains

8 to 9-week-old male inbred Lewis rats were purchased from Charles River. *Xcr1* knockout rats were generated from the Sprague Dawley-Hannover outbred strain by Elena Popova and Michael Bader in the Max Delbrück Center for Molecular Medicine (MDC). *Xcr1* knockout rats were characterized by Agnieszka Bauer (Bauer 2018). All rats were kept and bred in the animal facility of the Robert Koch Institute under pathogen-free conditions.

3. Methods

3.1 Molecular biology

3.1.1 Polymerase Chain Reaction (PCR)

In order to amplify DNA fragments, PCR was performed using *Taq* DNA Polymerase kit (Invitrogen) with 1x PCR reaction buffer, 1.5 mM $MgCl_2$, 0.2 mM of dNTP mix, 0.2 µM of each primer and 2 Units (U) of Platinum *Taq* DNA polymerase. Amplification was performed in a thermal cycler (Mastercycler epgradient S, Eppendorf) with thermal cycling conditions shown in Table 12. Annealing temperatures were calculated in Geneious according to the primer melting temperature. PCR-products were loaded on a 0.8-2% agarose gel supplemented with 1x GelRed nucleic stain to allow an analysis under ultraviolet (UV) light by using a gel documentation station (BioDocAnalyze, Biometra).

Table 12: Standard cycling conditions for PCR.

Step	Temperature	Time	Cycles
Initial denaturation	94°C	2 min	1
Denaturation	94°C	30 sec	
Annealing	50-60°C	30 sec	35-40
Elongation	72°C	60 sec/kb	
Final elongation	72°C	1-5 min	1
Hold	4°C	∞	1

3.1.2 Genotyping of *Xcr1* knockout rats

To genotype rats, ear biopsies were incubated in 100 µl Ear buffer containing 1 mg/ml proteinase K at 55°C until the tissue was completely digested. Proteinase K was heat inactivated at 95°C for 5 min followed by mixing the sample with TE/RNase buffer. Table 13 shows the PCR set up. The PCR reactions were conducted with *Taq* DNA Polymerase kit (Invitrogen) with 1.8 mM $MgCl_2$ and 3 U Platinum *Taq* Polymerase. PCR-products were loaded on a 1.5% agarose gel containing 1x GelRed nucleic stain and analyzed under UV light by using a gel documentation station (BioDocAnalyze, Biometra).

Table 13: PCR cycling conditions for Xcr1 genotyping.

Step	Temperature	Time	Cycles
Initial denaturation	94°C	3 min	1
Denaturation	94°C	20 sec	
Annealing	58°C	30 sec	35
Elongation	72°C	40 sec/kb	
Final elongation	72°C	5 min	1
Hold	4°C	∞	1

3.1.3 Quantitative real-time PCR (qRT-PCR)

In order to detect and quantify glycoprotein B (*gB*) in different rat tissues, a quantitative PCR was performed using *Taq* DNA Polymerase kit (Invitrogen) with 1x buffer, 4 mM $MgCl_2$, 0.4 mM dNTP Mix, 300 nM of each primer, 100 nM of probe and 1 U of Platinum *Taq* DNA polymerase. qRT-PCRs were conducted in the LightCycler® 480 (Roche) with cycling conditions listed in Table 14. To quantify copy numbers, a standard curve with a defined number of copies of plasmids containing the target gene were used. The detected copy number of *gB* was normalized to the housekeeping gene *c-myc*.

Table 14: Quantitative real-time PCR.

Step	Temperature	Time	Cycles
Initial denaturation	95°C	5 min	1
Denaturation	95°C	15 sec	45
Amplification	60°C	30 sec	

3.1.4 DNA isolation from tissue

Frozen organs were thawed and equilibrated to RT and transferred to a tube with Teflonbeads. After 180 µl Buffer ATL (Qiagen DNeasy Blood and Tissue Kit) was added, organs got homogenized with TissueLyzer Fastprep (MP) with 6.5 m/s 45 s two times. Then, homogenates were centrifuged for 2 min at 10000*g and incubated with 2 mg/ml proteinase K (provided in Qiagen Kit) for at least 3 h at 56°C in a ThermoMixer. After incubation 1 mg/ml RNase A was added and incubated for 5 min at RT. DNA extraction was performed according to the instructions of Qiagen DNeasy Blood and Tissue Kit. DNA concentration was measured with a NanoDrop 8000 spectrophotometer.

3.1.5 Isolation of virion DNA

RCMV virion DNA was isolated from REF infected with a low multiplicity of infection (MOI) of 0.05-0.1. When the cytopathic effect (CPE) reached 100%, plates were frozen at -80°C. Following thawing at 37°C cell debris were removed by centrifugation at 9200*g for 10 min at RT and virus was pelleted at 27000*g for 3 h at 4°C. To remove cellular DNA, the virus pellet was incubated with 0.2% (v/v) FCS and 1 µg/ml of both, RNase and DNase I for 15 min at 37°C. After centrifugation at 30600*g for 90 min at RT, the virus capsid was destabilized with 2.7 ml TE9 buffer containing 0.24 mg/ml proteinase K in 10% (w/v) SDS at 37°C while shaking at 200 rpm overnight. The next day, viral DNA was mixed with a phenol/ chloroform/ isoamylalcohol mixture (Roti-phenol) and transferred to a Phase Lock Gel heavy 15 ml falcon followed by centrifugation at 4000 rpm for 10 min. The viral DNA containing upper aqueous phase was mixed with 1/10 volume of 3 M sodium acetate and 2.5 volumes of ice-cold 96% (v/v) ethanol and centrifuged at 13000*g for 30 min at 4°C. The pellet was dried overnight at RT and reconstituted in 150 µl H_2O. DNA concentration was determined by using a NanoDrop 8000 spectrophotometer.

3.1.6 DNA Sequencing

In order to determine *vxcl1* deletion mutants, supernatants of single plaques were incubated at 95°C for 5 min. To enrich the area of interest a first PCR was performed as described in Table 12. 5 µl of the amplified DNA was then purified with 2 µl ExoSAP-IT™ PCR Product Cleanup Reagent (Applied Biosystems™) with settings listed in Table 15. For the sequencing PCR BigDye Terminator v3.1 cycle sequencing kit was used with 1x buffer, 0.5 µM of each primer and 1x BigDye Premix in 10 µl H_2O with reaction conditions shown in Table 16. Products were sequenced by the Sanger method which was accomplished by the sequencing facility MF2 at the Robert Koch Institute. Digital raw data were evaluated by using Geneious.

Table 15: PCR clean-up protocol.

Step	Temperature	Time
Degradation of primers and nucleotides	37°C	4 min
Inactivation of ExoSAP-IT™ reagent	80°C	1 min
Hold	4°C	∞

Table 16: Standard cycling conditions for sequencing reactions.

Temperature	Time	Cycles
96°C	1 min	1
96°C	10 sec	
50°C	5 sec	25
60°C	4 min	
4°C	∞	1

3.1.7 RNA isolation and sequencing

Cultured and infected DC were lysed with 3x volume of Trizol LS (Thermo Fisher Scientific). After adding 0.2 ml Chloroform per 1 ml sample and subsequent centrifugation at 13000*g 15 min at 4°C, RNA was collected from the aqueous phase. Further RNA purification was performed with the RNA Clean & Concentrator 25 kit (Zymo Research) following the manufacturer's protocol. The total RNA concentration was quantified by Qubit® Fluorometer (Invitrogen) and sample quality was verified by an Bioanalyzer (Agilent DNA 1000 Chip). For RNA sequencing from Ox-62 enriched DC, the NEBNext® Ultra II Directional RNA Library Prep Kit for Illumina® was used with 60% of suggested volumes by the manufacturer's protocol. About 600 ng total RNA were used for mRNA isolation with magnetic Oligo dT Beads $d(T)_{25}$ which bind to the poly-A tail of mRNA. After washing beads with RNA Binding buffer (2x), beads were incubated with RNA in a thermal cycler at 65°C for 5 minutes followed by cool down to 4°C with the heated lid set at ≥ 75°C to denature the RNA and facilitate binding of the mRNA to the beads. Samples were incubated another 5 minutes at RT to allow the mRNA to bind to the beads. To remove unbound RNA, tubes were placed on a magnetic rack until the solution cleared. Then the supernatant was discarded and samples washed with 120 µl Wash buffer. To elute the mRNA from the beads, the pellet was resuspended in Tris buffer and incubated in a thermal cycler with 80°C for 2 minutes, then held at 25°C with the heated lid set at ≥ 90°C. After further bead-binding as described above, the mRNA was fragmented with First Strand Synthesis Reaction buffer and Random Primer Mix (2x) in a thermal cycler with the heated lid set at 105°C as follows in Table 17:

Table 17: Elution and Fragmentation of mRNA.

Temperature	Time
94°C	15 min
4°C	∞

Samples were put on a magnetic rack and supernatant containing fragmented mRNA was collected for First Strand cDNA synthesis. NEBNext Strand Specificity Reagent and

NEBNext First Strand Synthesis Enzyme Mix were added to the fragmented RNA and incubated in a preheated thermal cycler with the heated lid set at ≥ 80°C as follows in Table 18:

Table 18: First Strand cDNA synthesis program.

Temperature	Time
25°C	10 min
42°C	15 min
70°C	15 min
4°C	∞

Immediately, Second Strand cDNA synthesis was performed with NEBNext Second Strand Synthesis Reaction Buffer with dUTP Mix (10x) and NEBNext Second Strand Synthesis Enzyme Mix in a thermal cycler for 1 h at 16°C with the heated lid set at ≤ 40°C. Double-stranded cDNA was then purified with SPRIselect Beads by incubation at RT for 5 min. Supernatant was removed On a magnetic rack and samples were washed with 80% ethanol twice. To repair DNA ends from sticky to blunt ends with dA-tails to prevent ligation (End Prep reaction), DNA was eluted from beads with 0.1x TE buffer (provided) and incubated with NEBNext Ultra II End Prep Reaction Buffer and NEBNext Ultra II End Prep Enzyme Mix in a thermal cycler with the heated lid set at ≥ 75°C as follows in Table 19:

Table 19: End Prep reaction program.

Temperature	Time
20°C	30 min
65°C	30 min
4°C	∞

To label the samples with individual Index numbers, adaptors were ligated with 5-fold dilution (because of 600 ng input RNA) in ice-cold Adaptor Dilution Buffer, NEBNext Ligation Enhancer and NEBNext Ultra II Ligation Master Mix. After incubation for 15 minutes at 20°C in a thermal cycler, USER Enzyme was added to the ligation mixture and incubated for another 15 minutes at 37°C with the heated lid set to ≥ 45°C. After this, purification of the Ligation Reaction was performed with SPRIselect Beads as described above. After eluting adaptor ligated DNA with 0.1x TE buffer, 1 µl was used for SYBRgreen qPCR to determine the number of PCR cycles enrichment. Enrichment PCR was conducted with NEBNext Ultra II Q5 Master Mix, Universal PCR Primer/i5 Primer and Index (X) Primer/i7 Primer in a thermal cycler with the heated lid set to 105°C using PCR cycling conditions listed in Table 20.

Table 20: PCR enrichment of Adaptor Ligated DNA.

Step	Temperature	Time	Cycles
Initial Denaturation	98°C	30 sec	1
Denaturation	98°C	10 sec	11
Annealing/Extension	65°C	75 sec	
Final Extension	65°C	5 min	1
Hold	4°C	∞	

A further purification of the PCR Reaction was performed with SPRIselect Beads as described above and library quality was assessed on a Bioanalyzer (Agilent DNA 1000 Chip). Pooled sequencing libraries were sequenced on an Illumina HiSeq 4000 device. After trimming the adapter sequence AGATCGGAAGAGCACACGT, about 18-30 million mappable reads per sample were obtained.

3.1.8 Detection of differentially expressed genes

RNA-Seq data were evaluated using the Snakemake-based tool SCORE (Wolf et al. 2020). SCORE uses a selection of tools for quantifying the expression of all transcripts within each given sample. Raw reads were initially trimmed, mapped to the current *Rattus norvegicus* reference genome (Rnor_6, https://www.ncbi.nlm.nih.gov/assembly/GCF_000001895.5) and quantified. Next, individual transcripts were analyzed for differential expression ($\alpha < 0.01$). SCORE identifies significantly differentially expressed genes (DEG) that were implemented to associated pathways of the Kyoto Encyclopedia of Genes and Genomes (KEGG) as well as gene ontologies (GO). Results were visualized in heatmaps by using R.

3.2 Protein biochemistry and flow cytometry

3.2.1 ELISA for vXCL1 detection

96-well flat-bottom MaxiSorp plates (Nunc) were coated with 100 µl of viral supernatant diluted in ELISA coating buffer and incubated overnight at 4°C. Unbound proteins were washed down 5 times with PBS. In order to cover free binding sites 200 µl of ELISA blocking buffer was added for 2 h, at RT and wells were washed twice with PBS. For vXCL1 detection 100 µl of RCMV-11 (final conc. 0.2 µg/ml, diluted in ELISA blocking buffer) was added and incubated at RT for 1 h. After washing five times with ELISA washing buffer, 100 µl of polyclonal anti-mouse immunoglobulin-horseradish peroxidase (HRP) (final conc. 0.2 µg/ml, diluted in ELISA blocking buffer) was added and incubated at RT for 1 h. Following further five washing steps with ELISA washing buffer plates were incubated with 50 µl of 3,3',5,5'-Tetramethylbenzidine (TMB) substrate solution (Thermo Fisher Scientific) for 10 min at RT.

The reaction was stopped by adding 50 µl of 1 M H_2SO_4 and absorbance was determined at OD 450 nm by using the FLUOstar Omega microplate reader.

3.2.2 Antibody coupling

A monoclonal antibody against RCMV-E IE1 was generated by Vanda Juranic Lisnic in the laboratory of Stipan Jonjic (University of Rijeka). To couple this mAb with the fluorophore A647, NaN_3 was removed by dialyzing 0.5 mg of 1 mg/ml concentrated antibody with the Slide-A-Lyzer Dialysis Cassettes with 10,000 MWCO (Thermo Fisher Scientific). After recovering from the dialysis cassette, the antibody was incubated for with 0.1 M $NaHCO_3$ and 0.1 mM A647 (Molar ratio = 15) for 1 h, at RT with gentle shaking every 10 min. The conjugated antibody was applied to a PD MiniTrap G-25 (GE Healthcare) column in order to remove unbound dye. The fluorophore-coupled antibody was eluted with PBS, protein concentration was measured by a NanoDrop spectrophotometer at 280 nm and 0.2% (w/v) BSA and 0.1% (w/v) NaN_3 were added.

3.2.3 Antigen staining with fluorophore-coupled antibodies

In order to measure cells by flow cytometry up to 10^7 cells were pelleted in a 96-well U-bottom microtiter plate at 400*g for 5 min at 4°C. To prevent unspecific binding by the antibody's Fc chain cells were incubated with 45.2 µg/ml of rat gamma globulin for 5 min on ice. Cells were stained with fluorophore-coupled antibodies in a total volume of 50 µl for 20 to 30 min on ice followed by two washing steps with FACS-PBS. Before measurement, 0.3 µM 4′,6-diamidino-2-phenylindole (DAPI) or 1 µg/ml propidium iodide (PI) were added as dead cell markers.

3.2.4 Fixable dead staining and intracellular staining

To exclude dead cells from flow cytometry analysis of fixed samples antibody-stained cells were washed with PBS and resuspended in 200 µl of 1.34 µM Pacific Orange (PacO) diluted in PBS. After 25 min incubation on ice, cells were washed with PBS followed by fixation with 2% (w/v) paraformaldehyde (PFA) for 20 min at RT in the dark. After fixation, cells were washed with PBS and FACS-PBS. For intracellular staining, cells were permeabilized with FACS-PBS containing 0.5% (w/v) saponin. Permeabilized cells were incubated 5 min on ice with rat gamma globulin followed by staining with either an unlabeled or fluorophore-coupled primary antibody. After 20 min incubation on ice in the dark, unbound antibodies were removed by washing once with Permeabilization buffer. In case of incubation with unlabeled primary antibody, incubation with the respective fluorophore-conjugated secondary antibody was performed for 15 min at RT. Prior to flow cytometric analysis cells were washed twice with Permeabilization buffer and resuspended in FACS-PBS.

3.2.5 Chemokine binding

To investigate the impact of XCL1 on XCR1-expressing DC, Ox-62-enriched spleen cells were incubated with different concentrations of the respective recombinant chemokines diluted in Chemotaxis medium for 4 h at 37°C. After incubation, cells were washed with FACS-PBS and stained with fluorophore-conjugated antibodies as described in section 3.2.3 followed by flow cytometry analysis.

3.2.6 Flow cytometry analysis

In order to identify DC, cells were labeled with fluorophore-coupled antibodies against CD3, CD45RA, MHCII, CD103, XCR1 and CD4. Cells were examined in FSC and SSC to gate the leukocyte population. Gating in FSC-Height (FSC-H) and FSC-Area (FSC-A) was needed to exclude cell doublets. To discriminate dead from viable cells, DAPI or PI was added before measurement. Then, T cells (CD3) and B cells (CD45RA) were excluded. MHCII is a marker for APC whereas CD103 is expressed exclusively on DC. These two markers allowed for the identification of DC. DC were further gated on XCR1, CD4, CD8α, CD11b/c, CD86, CD172a and CD54. To separate the two major DC subsets, cells were gated either on CD4 and XCR1 or CD4 and MHCII and referred to as $CD4^-$ and $CD4^+$ DC.

3.3 Virology

3.3.1 Virus infection

REF or DC were infected with RCMV-E or RCMV-B or recombinant viruses to generate virus stocks or to perform analytical experiments. REF were infected at a confluency of 70-80% in complete DMEM containing 2% FCS at a specific MOI. 1 h post infection virus containing supernatant was exchanged with complete DMEM containing 5% FCS. For *ex vivo* infection of DC, spleen cells were enriched with Ox-62 microbeads and infected with the respective virus in Chemotaxis medium at MOI 3 or 10.

3.3.2 Generation of high titer virus stocks

Several 15 cm dishes of REF were grown to a confluency of 70-80% and infected at a low MOI of 0.05 to 0.1 with DMEM containing 2% (v/v) FCS. After 5 to 6 days, when CPE was clearly visible, supernatants were collected and cell debris removed by centrifugation at 6000*g for 20 min at 4°C. The cell pellet was resuspended in 5 ml of supernatant and homogenized using a pre-cooled glass douncer followed by another centrifugation at 17000*g for 20 min at 4°C. To pellet the virus, supernatants were pooled and centrifuged at 27000*g for 3 h at 4°C. The virus-pellet was incubated in 5 ml PBS at 4°C overnight, before it

was homogenized with a pre-cooled glass douncer. To prepare the virus for animal experiments, the homogenized pellet was applied to a 15% (w/v) VSB sucrose cushion and virus was pelleted at 20000 rpm for 5 h at 4°C (SW32Ti rotor, Optima XL-90, Beckman Coulter). The virus pellet was dissolved in PBS and stored at -80°C. Viral titers were determined by plaque assay as described in 3.3.3.

3.3.3 Virus titration by plaque assay

To determine the titer of the generated virus stocks REF, grown to 70-80% confluency in 24-well plates, were infected with 200 µl of serial dilutions of a previously generated virus stock. After incubation at 37°C for 1 h, the infection process was stopped by adding 1 ml Plaque overlay medium followed by incubation for 7 days at 37°C and 5% CO_2. To stop viral replication, cells were fixed with 1% (v/v) PFA for 15 min at 37°C. Fixed cells were then stained with 1 ml Methylene blue staining solution for 30 min at 37°C. Plaque forming units (pfu) were counted and the viral titer was calculated by the mean value of eight replicates in pfu per ml.

3.3.4 Generation of RCMV-B Δ*vxcl1* virus

A RCMV-E Δ*vxcl1* with a Cre-Lox recombination cassette that had previously been generated was used to study the function of vXCL1 upon *ex vivo* infection. To create a RCMV-B *vxcl1* deletion mutant, CRISPR/Cas9 technology was employed. REF were grown to a confluency of 70-80% and transfected with 2 µg of three different vectors using PolyFect® Transfection Reagent (Qiagen). Vectors were kindly provided by Robert Jan Lebbink (UMC Utrecht), which encoded Cas9 and the guide RNA (gRNA) recognizing *vxcl1* of RCMV-B, as well as a puromycin and ampicillin resistance cassette. To successfully select transfected cells, 2.5 µg/ml puromycin was added to the cultivation medium after 30 h incubation at 37°C, followed by another 24 h incubation. Cells were then infected with RCMV-B at an MOI of 0.5 for 2 h in DMEM containing puromycin. After five days a CPE was visible and viral supernatant was serially diluted in 96-well plates for single plaque purification. Plates were screened under the light microscope to detect wells with a single plaque. Separate supernatants of single plaques were collected and incubated at 95°C for 5 min. Then, products of a first PCR were purified by using ExoSAP purification kit followed by the sequencing PCR (see section 3.1.6). After digital raw data were evaluated by using Geneious, promising mutants were grown and another limiting dilution was performed. Single plaques were verified by sequencing as described above.

3.4 Cell biology

3.4.1 Propagating and counting cells

REF were cultivated in complete DMEM at 37°C and 5% CO_2 and propagated with sterile media and buffers in a laminar airflow cabinet. Dead cells were discriminated by trypan blue staining and cell number of REF was determined with a Neubauer counting chamber. Organ derived cells were counted with MACSQuant 10 after DAPI staining.

3.4.2 Freezing and thawing cells

Freezing of REF was carried out by centrifugation at 1200 rpm for 5 min and resuspension in 90% (v/v) FCS and 10% (v/v) DMSO. Primary rat leukocytes were cooled down in RPMI on ice for 20 min followed by gentle resuspension in 1 volume FCS containing 20% (v/v) DMSO.

REF were thawed in a water bath and washed with 8 ml complete DMEM. After 5 min centrifugation at 1200 rpm, cell pellets were resuspended in complete DMEM and cells were seeded. Rat leukocytes were thawed in a 37°C water bath. To dilute the DMSO complete RPMI medium was added dropwise to the cells. After centrifugation at 380*g for 8 min at 4°C, cells were resuspended in complete RPMI, FACS- or MACS-PBS, respectively.

3.4.3 Preparation of single cell suspensions from spleens

Rat spleens were isolated and cut into smaller pieces. For single cell suspensions, spleens were homogenized using a gentleMACS dissociator (Miltenyi Biotec), program m_spleen_4.1. To get higher yields of DC, homogenates were digested with 500 µg/ml Collagenase D, 20 µg/ml DNaseI and 2% (v/v) FCS in RPMI 1640 for 25 min in a 37°C water bath shaking at 200 rpm. Digestion was halted by adding 10 mM EDTA for another 5 min under the same conditions. The cell suspension was filtered through a 100 µm nylon sieve (BD), centrifuged at 380*g for 8 min at 4°C, applied to NycoPrep® (PROGEN) or OptiPrep™ (PROGEN) density gradient centrifugation (density: 1.073 g/ml) at 1700*g for 10 min at 4°C without deceleration. Leukocytes were collected from the middle phase and washed twice with MACS-PBS.

3.4.4 Magnetically isolation of rat DC

In order to isolate $CD103^+$ cells from rat spleens, NycoPrep®/ Optiprep™ enriched spleen cells were incubated with Microbeads (Miltenyi Biotec) bearing antibody clones of Ox-62 according to the manufacturer's instructions. To prevent unspecific binding on Fc receptors cells were incubated with 45.2 µg/ml rat gamma globulin for 5 min on ice. Cells were applied to a MS column (Miltenyi Biotec) and magnetically labeled cells were eluted with MACS-PBS.

3.4.5 Isolation of leukocytes from salivary glands

After rats were sacrificed by an isoflurane overdose, mandibular, parotid and sublingual glands (in this work referred to as salivary glands) were dissected and stored in PBS. Adjacent lymph nodes were removed and salivary glands were homogenized using a gentleMACS dissociator (Miltenyi Biotec), program m_heart_01_01. To obtain single cell suspensions, the homogenized tissues were digested in RPMI containing 1 mg/ml Collagenase D, 0.1 mg/ml DNaseI and 10% (v/v) FCS at 37°C for 1 h while shaking. 5 mM $CaCl_2$ was added to enhance Collagenase D activity. Digestion was stopped by adding 10 mM EDTA for another 5 min under the same conditions. The suspension was filtered through a 70 µm and 30 µm nylon sieve and washed with MACS-PBS twice. After centrifugation at 380*g for 8 min at 4°C cells were applied to NycoPrep® density gradient centrifugation (density: 1.073 g/ml) at 1700*g for 10 min at 4°C without deceleration. Enriched leukocytes were collected from the middle phase, washed twice with MACS-PBS and resuspended in FACS-PBS. Cells were stained with several fluorophore-coupled antibodies as described in 3.2.3.

3.4.6 Preparation of single cell suspensions from lymph nodes

Salivary gland-embedded lymph nodes were isolated and fat was removed. To gain a single cell suspension, lymph nodes were dissected with micro-forceps in complete RPMI followed by a digestion with 2 mg/ml Collagenase D and 20 µg/ml DNaseI as described in section 3.4.3. After digestion cells were filtrated first through a 70 µm then 50 µm nylon sieve. Cells were stained with several fluorophore-coupled antibodies as described in section 3.2.3.

3.4.7 Collection of blood for cell enrichment

Blood was collected by cardiac puncture with a syringe filled with 5000 U/ml Heparin. For cell enrichment blood was applied to a Pancoll (PAN) gradient and centrifuged for 40 min at 800*g without deceleration at RT. The interphase containing leukocytes was recovered and washed with PBS. If necessary, an erythrocyte lysis with ACK-buffer was performed. Cells were stained with several fluorophore-coupled antibodies as described in section 3.2.3.

3.4.8 Chemotaxis assay

The influence of RCMV infection and recombinant chemokines on DC migration was examined by a 24-well 6.5 mm transwell system with a 5 µm pore size. 500 µl of recombinant rXCL1 were added into the bottom chamber of the transwell plate. As a control, Chemotaxis medium without chemokine was added to the well. 2 $*10^5$ to $5*10^5$ of previously stained Ox-62 enriched rat spleen cells were resuspended in 100 µl Chemotaxis medium and added to

the upper chamber of the transwell system. After incubation for 2.5 h at 37°C and 5% CO_2, cells that migrated into the lower chamber were analyzed by flow cytometry. Each sample was measured for 5 min at constant flow rate on a Fortessa flow cytometer or exactly 300 µl of each sample on MACSQuant 10 to count absolute numbers of migrated cells and input cells. The proportion of migrated cells was calculated as follows: number of migrated cells/number of input cells*100.

3.4.9 Stimulation of spleen cells with PMA and ionomycin

In order to investigate which cell subsets are expressing endogenous XCL1, spleens were minced and filtered through a 100 µm sieve followed by an erythrocyte lysis with ACK-buffer. $20*10^6$ cells were stimulated with 20 ng/ml Phorbol-12-myristat-13-acetat (PMA) and 1 µg/ml ionomycin in 10 ml for total of 5 h in the presence of brefeldin A for the last 3 h. Intracellular staining of rXCL1 was performed as described in section 3.2.4 with a commercially available polyclonal anti-rXCL1 antibody that was previously coupled to biotin. Detection was performed by using a streptavidin-APC conjugate followed by flow cytometry analysis.

3.5 Animal experiments

All animal experiments were performed in the RKI animal facility. Laboratory animal care and all experiments were carried out according to the German animal protection law (TierSchG) and the internationally recognized 3R principle (Refinement, Reduction, Replacement). Care and breeding of the rats were done by qualified animal keepers. Rats were kept in a 12 hours day/ night rhythm.

3.5.1 Animal infection and sample collection

To examine the role of XCR1 during RCMV-B infection 48 *Xcr1*$^{+/+}$ and 48 *Xcr1*$^{-/-}$ Sprague Dawley rats were i.p. infected with RCMV-B or PBS and analyzed at 3, 5, 16 and 90 dpi. Each test group contained 6 rats. For infection RCMV-B SG1 D12 passage 3 with $1*10^6$ pfu in 500 µl was used. In order to investigate the role of vXCL1, six 10-week-old Lewis rats were i.p. infected with RCMV-B wt SG1 D12 passage 3 or RCMV-B ∆*vxcl1* H3 passage 5, respectively, with $1*10^6$ pfu in 500 µl. Uninfected rats served as a negative control (Mock). All RCMV-B-infected and PBS-injected animals were monitored by qualified animal keepers.

On the respective days after infection rats were sacrificed with a lethal dose of Isofluran. Death was determined by monitoring the heartbeat. First, blood was collected as described in section 3.4.7. Then, lymph nodes, salivary glands, lung, liver and spleen were removed. For DNA analysis parts of the organs were directly frozen in liquid nitrogen.

3.5.2 Organ homogenization and titration

Salivary glands were homogenized in 1 ml DMEM 2% (v/v) FCS with a syringe plunger and a 70 µm Nylon sieve (BD). To dissociate cells the homogenates were manually processed through a precooled 5 ml glass douncer. Dilutions from 10^{-1} to 10^{-5} were titrated on REF (see section 3.3.3).

3.6 Statistics

For normally distributed data the parametric one-way analysis of variance (one-way ANOVA) was performed to compare the means of two or more samples. To measure the amount of variation between replicates a standard deviation (SD) or standard error of the mean (SEM) were calculated. For multiple comparisons between groups within one experiment post hoc tests were carried out. Whereas the Tukey's multiple comparison test was chosen to compare every mean with every other mean, the Dunnett's multiple comparison test was performed to compare every mean to a control mean. All statistics were calculated with GraphPad Prism 8 and were interpreted exploratory. Results with a high variance were presented as individual dots and the median.

4. Results

4.1 Analysis of XCR1 expression on DC and XCL1 expression on lymphocytes

4.1.1 Two major DC subsets are identified in rat spleens

To examine DC subsets, an enrichment protocol of these cells was established. First, spleens were digested (Digest) followed by a density gradient centrifugation (OptiPrep) that led to the exclusion of erythrocytes and smaller cell debris. Finally, DC were isolated with magnetically labeled beads (Ox-62) (Figure 7 A). Due to enrichment, the relative number of DC within the living cell population increased from 1% in the digest fraction to 7.6% in OptiPrep and 67.4% in Ox-62 enriched fraction (Figure 7 B). The enrichment had no influence on cell viability which remained at 88-92% (Figure 7 C). The analysis of surface protein expression revealed that spleen derived rat DC lack the expression of T and B cell lineage markers CD3 and CD45RA, respectively. After gating on CD4 and XCR1, two major DC subsets could be identified. After density centrifugation the frequency of $CD4^-$ $XCR1^+$ DC within the $CD103^+$ population was 30%, whereas $CD4^+$ $XCR1^-$ DC frequency was at 55%. After Ox-62 microbeads enrichment, the relative distribution of $CD4^-$ DC and $CD4^+$ DC changed to 54% and 37%, respectively.

Following the examination of further DC markers two distinct DC phenotypes could be identified: $MHCII^+$ $CD103^+$ $CD4^-$ $XCR1^+$ $CD11b/c^+$ $CD172a^{(+)}$ $CD54^+$ and $MHCII^+$ $CD103^+$ $CD4^+$ $XCR1^-$ $CD11b/c^+$ $CD172a^+$ $CD54^+$ DC (Figure 8). The two DC subsets shared expression of CD11b/c and CD54. While $CD4^+$ DC showed a high expression of the signal regulatory protein alpha (SIRPα/ CD172a), $CD4^-$ DC exhibited low expression. In contrast to murine DC, rat DC did not express CD8α. Apart from the two major DC subsets two other dim populations were visible, expressing higher amounts of MHCII ($CD4^+$ $MHCII^{++}$ and $CD4^-$ $MHCII^{++}$). The $CD4^-$ MHC^{++} population expressed lower XCR1 amounts. In addition, both MHC^{++} subsets showed higher CD86 expression (Figure 8).

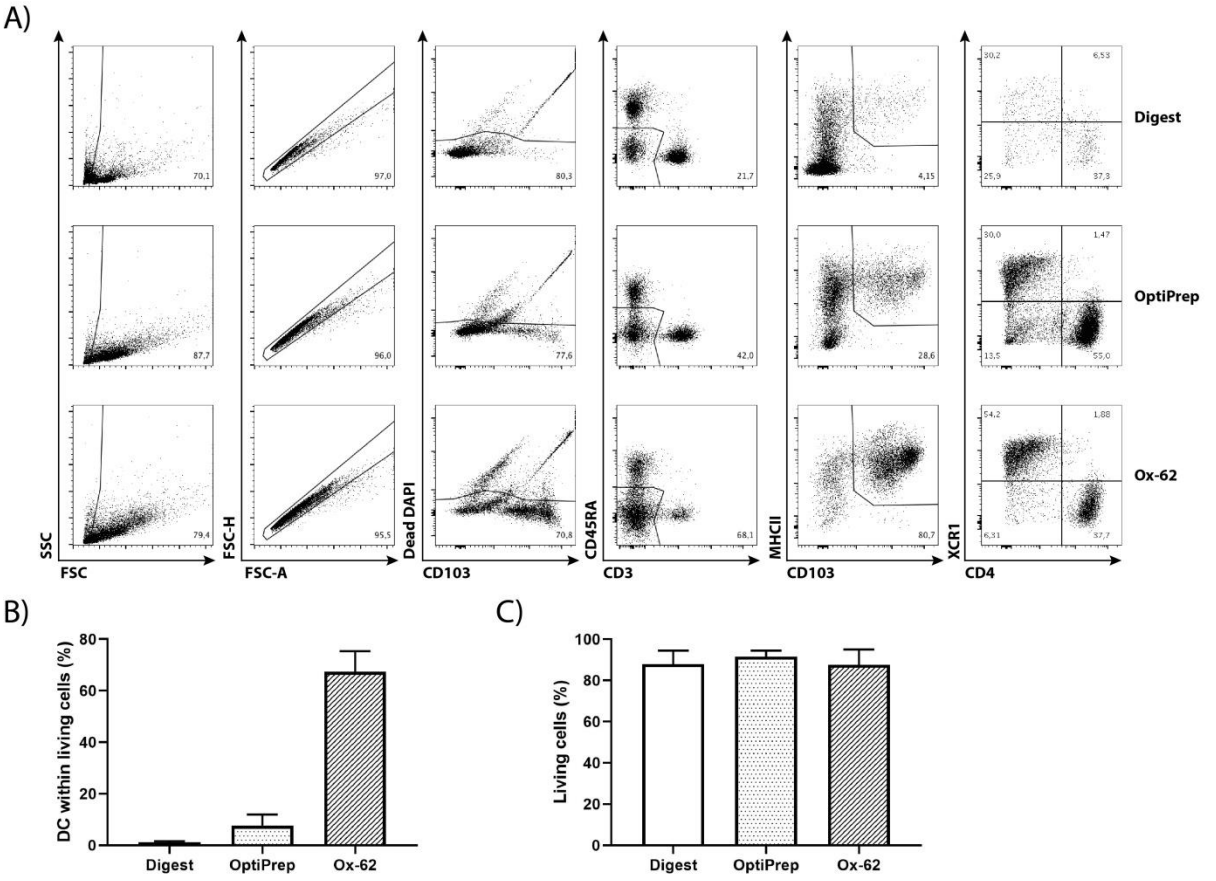

Figure 7: Isolation of DC from rat spleen. Spleens were mashed, digested and single cell suspensions were separated on a high density gradient (OptiPrep™). DC were isolated with Ox-62 magnetically labeled beads and finally stained with fluorophore-conjugated antibodies targeting CD3, CD45RA, CD103, MHCII, CD4 and XCR1. **A)** Gating strategy of cells after digest, OptiPrep and Ox-62 enrichment. Single cells were gated in FSC and SSC, dead cells, stained with DAPI, as well as T and B cells were excluded from the analysis. DC were identified by the expression of MHCII and CD103. Two major DC subsets were analyzed for XCR1 and CD4 expression. **B)** Frequency of DC population among living cells **C)** Viability of spleen cells after respective enrichment steps. Error bars represent mean ± SD, n = 4.

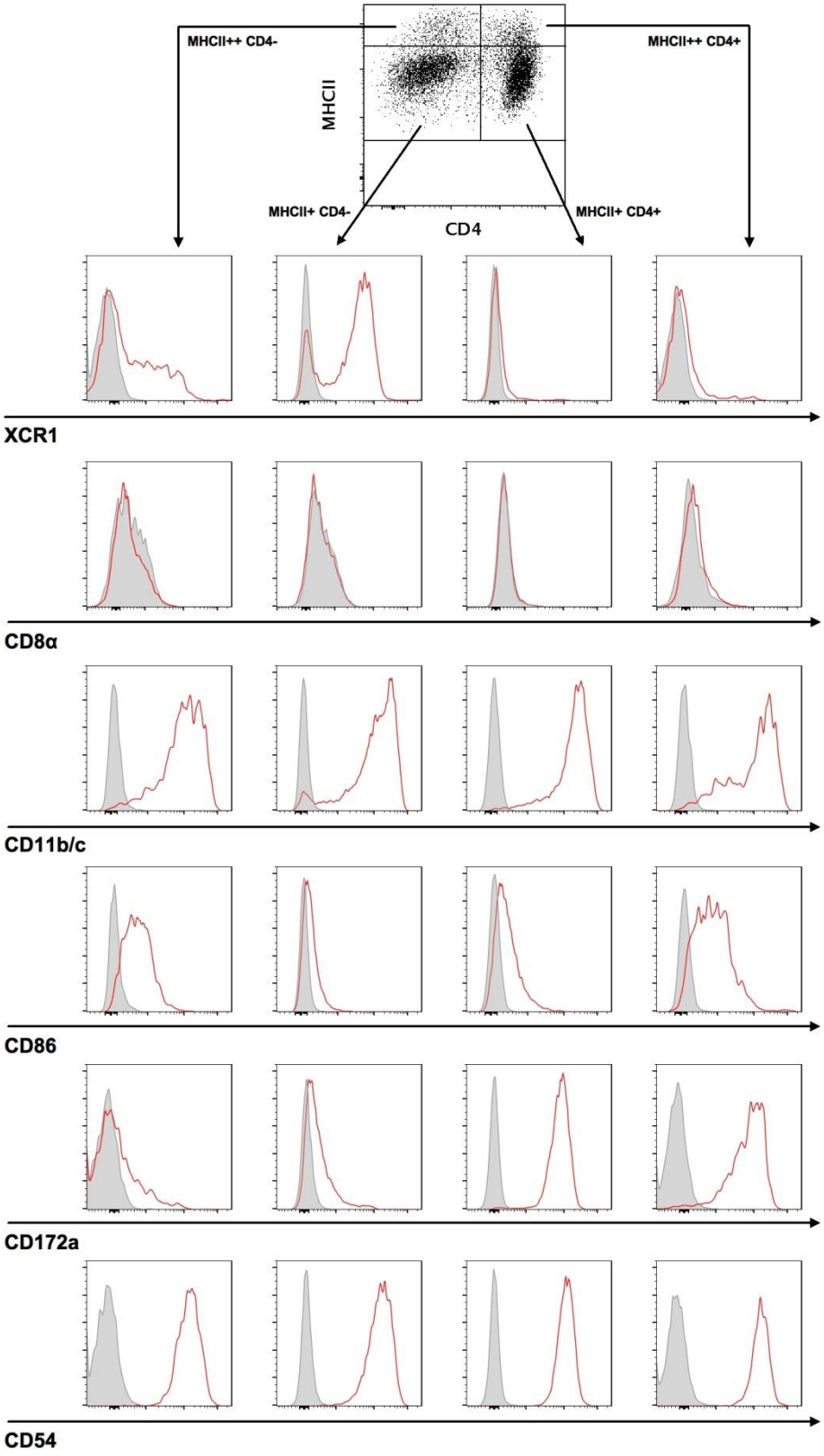

Figure 8: Two major DC subsets can be identified in rat spleens. Rat spleens were digested with Collagenase D and Dnase I followed by OptiPrep™ density centrifugation. DC were gated by excluding dead, $CD3^+$ and $CD45RA^+$ cells. Two major DC subsets were differentiated by the expression of CD4 (dotplot). $MHCII^{++}$ populations were gated separately. For each analyzed surface marker (red curve), a fluorescence minus one (FMO) control was implemented (grey curve).

4.1.2 Identification of XCR1 and XCL1 expression in *Xcr1*$^{+/+}$ and *Xcr1*$^{-/-}$ rats

To examine receptor function in the context of a RCMV infection, an *Xcr1* knockout Sprague Dawley rat was generated in collaboration with Michael Bader at the Max Delbrück Center using CRISPR/Cas technology (Bauer 2018). The transgenic animals showed a deletion of 169 bp in exon 2 of *Xcr1*. During heterozygous breeding, genotypes were verified by PCR with primers binding at positions 3204 and 3659 of *Xcr1*. *Xcr1*$^{+/+}$ rats showed a band at 456 bp, whereas *Xcr1*$^{-/-}$ rats had a product size of 287 bp. Heterozygous rats (*Xcr1*$^{+/-}$) showed two bands at respective heights (Figure 9 A). Analysis of XCR1 surface expression confirmed that the deletion of 169 bp in *Xcr1* led to a loss of the protein (Figure 9 B).

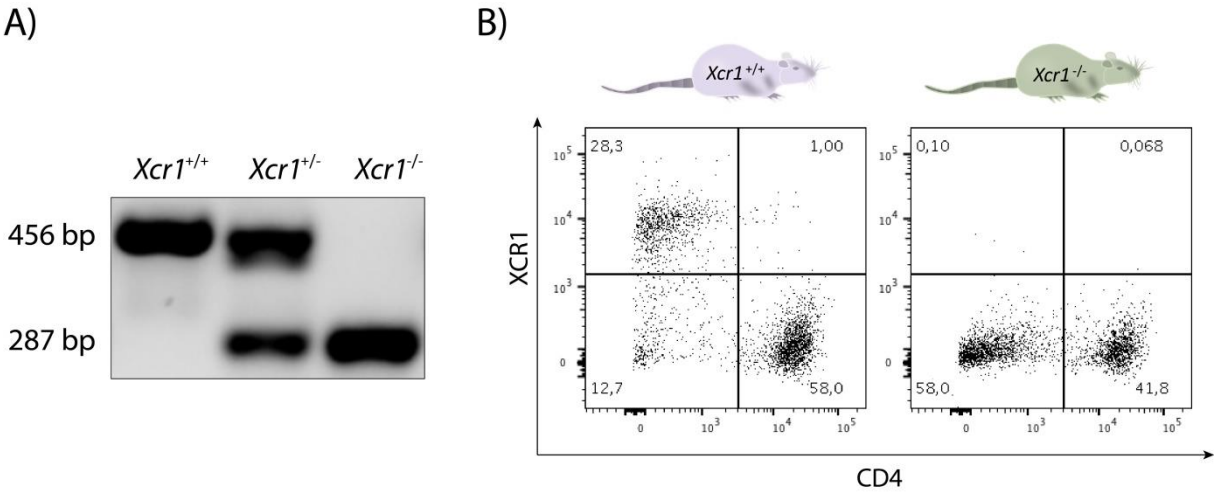

Figure 9: Genotyping and XCR1 expression in *Xcr1*$^{-/-}$ and *Xcr1*$^{+/+}$ rats. (A) Genotyping of *Xcr1*. PCR was performed with DNA obtained from ear biopsies. *Xcr1*$^{+/+}$ rats showed a product size of 456 bp and *Xcr1*$^{-/-}$ rats showed a product size of 287 bp. **B)** XCR1 expression on DC from *Xcr1*$^{+/+}$ and *Xcr1*$^{-/-}$ rats.

Furthermore, XCL1 production of splenic leukocytes was determined in *Xcr1*$^{+/+}$ and *Xcr1*$^{-/-}$ rats. For this purpose, spleen cells were isolated and stimulated with PMA and ionomycin followed by intracellular staining of XCL1. Gates were set on T cells, NKT cells, CD161^{+} and CD161^{++} NK cells (Figure 10 A). T cells were further gated on CD4^{+} and CD8^{+} T cells (gating not shown). Flow cytometry analysis revealed that without significant differences between *Xcr1*$^{+/+}$ and *Xcr1*$^{-/-}$ rats, about 20% of CD8^{+} T cells, 30% of CD161^{++} NK cells and 60% of NKT cells produced XCL1. Only 3% of CD4^{+} T cells expressed XCL1 (Figure 10 B). The CD161^{+} NK cell population almost completely disappeared after stimulation with PMA and ionomycin in *Xcr1*$^{+/+}$ as well as in *Xcr1*$^{-/-}$ rats and consequently was not included in the XCL1 expression analysis (Figure 10 C).

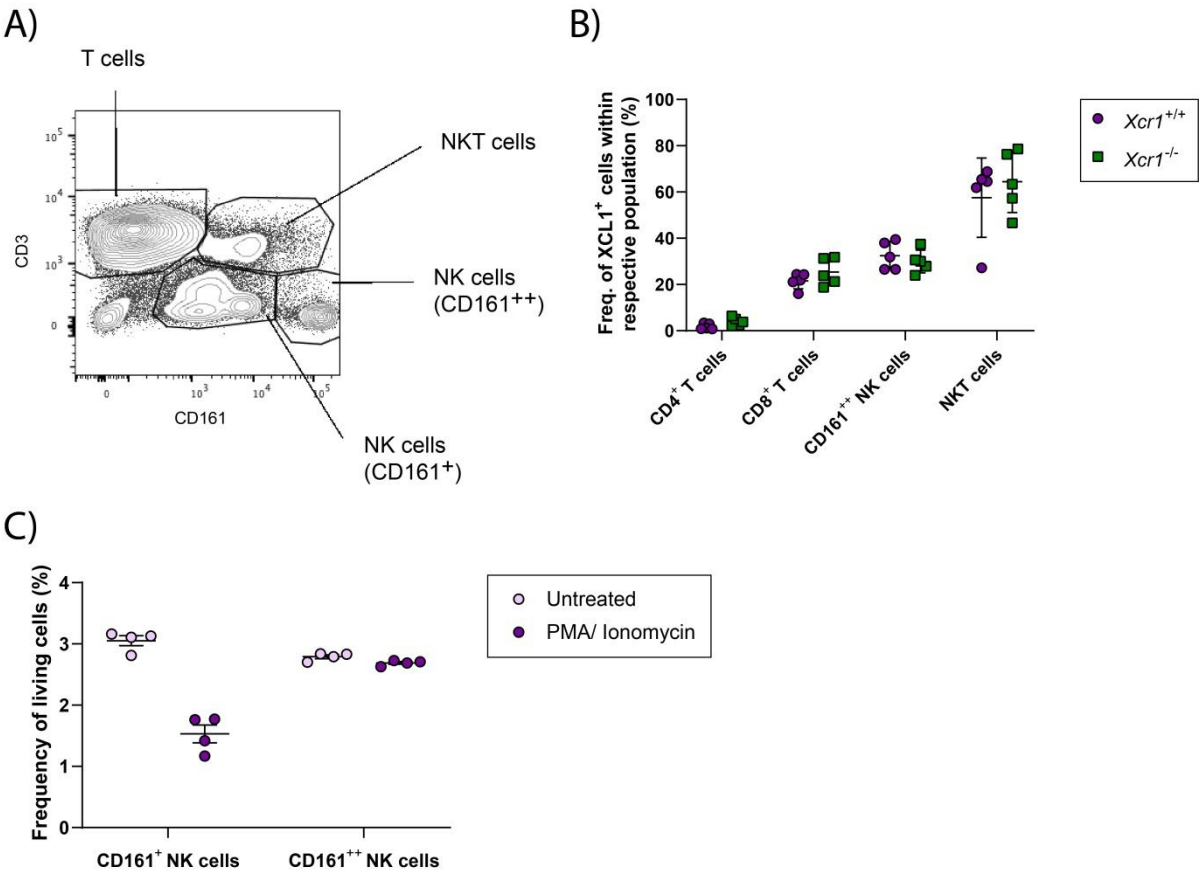

Figure 10: XCL1 expression of stimulated spleen cells from *Xcr1*$^{+/+}$ and *Xcr1*$^{-/-}$ rats. Isolated spleen cells were stimulated with 20 ng/ml PMA and 1 µg/ml ionomycin for 5 h followed by intracellular staining of XCL1. **A)** Cells were gated on T cells (CD3$^+$), NKT cells (CD3$^+$ CD161$^+$) and NK cells (CD161$^+$ and CD161^{++}). **B)** XCL1 expression in CD4$^+$ and CD8$^+$ T cells, NK cells (CD161^{++}) and NKT cells. **C)** Frequency of CD161$^+$ and CD161^{++} NK cells of *Xcr1*$^{+/+}$ rats as representative, with and without stimulation. Error bars represent mean ± SD, n = 4/5.

4.1.3 RCMV-B attracts DC from *Xcr1*$^{+/+}$ and *Xcr1*$^{-/-}$ rats

As it has been shown that RCMV-E encodes a chemokine that attracts XCR1$^+$ DC (Geyer et al. 2014), it was examined whether this population is also attracted by RCMV-B compared with the *Xcr1* knockout strain. Therefore, REF were infected with RCMV-B at an MOI of 10. 48 hpi DC were isolated from spleens of *Xcr1*$^{+/+}$ and *Xcr1*$^{-/-}$ rats and prepared for a chemotaxis assay using viral supernatants. To analyze background migration, supernatants of uninfected REF served as a control (Mock). DC (MHCII$^+$ CD103$^+$) were separated into two subsets according to the expression of CD4. As shown in Figure 11, 9-10.6% of CD4$^-$ DC from both *Xcr1*$^{+/+}$ and *Xcr1*$^{-/-}$ rats migrated towards mock-infected supernatants which was considered as background migration. In contrast, viral supernatant attracted 26.7% of CD4$^-$ DC from *Xcr1*$^{+/+}$ and 22.2% from *Xcr1*$^{-/-}$ rats (Figure 11 A). The *Xcr1* knockout strain exhibited slightly reduced but not complete loss of chemotactic activity towards RCMV-B. In contrast, CD4$^+$ DC were not attracted by viral supernatants, since the migration rate was comparable with the mock-infected control (Figure 11 B).

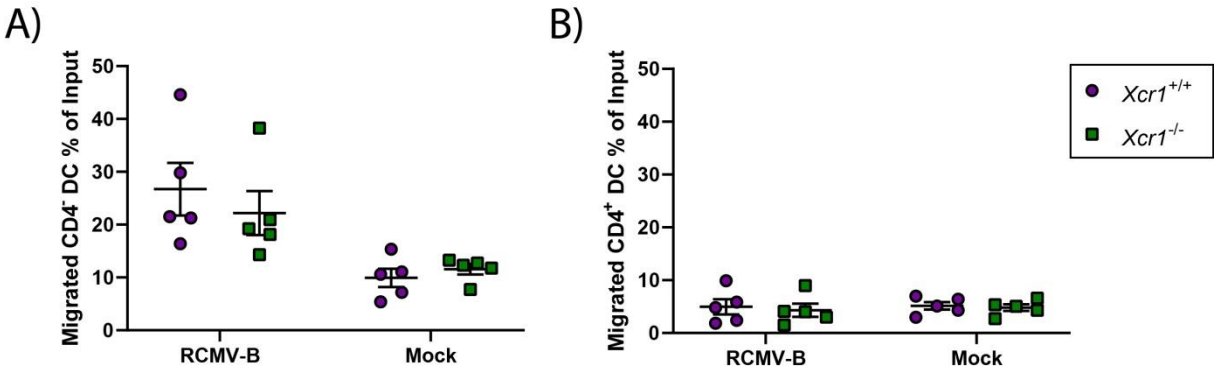

Figure 11: Chemotaxis of DC from *Xcr1*$^{+/+}$ and *Xcr1*$^{-/-}$ rats to supernatants of RCMV-B infected REF. REF were infected at an MOI of 10 for 48 h. Each transwell contained supernatant of RCMV-B infected or mock-infected REF in the lower chamber. 5*10^5 of Ox-62 enriched and stained DC were added to the upper chamber of a transwell system. After 2.5 h of incubation, cells that migrated to the lower chamber were analyzed by flow cytometry. **A)** Migration of CD4$^-$ DC. **B)** Migration of CD4$^+$ DC. Error bars represent mean ± SD, n = 5.

4.1.4 DC, T cells and B cells can be identified in salivary glands

To investigate the presence of DC and different lymphocytes in salivary glands, an organ digestion and cell isolation protocol was established. Submandibular and parotid glands (in this work referred to as salivary glands) were pooled and processed as described in section 3.4.5. Leukocytes were gated in FSC and SSC and dead cells were excluded from the analysis. B and T cells that were further divided in CD8$^+$ and CD4$^+$ subsets and DC were identified (Figure 12 A). The DC frequency increased from 0.2% to 0.6% of all living cells (Figure 12 C). The fluorescence minus one (FMO) control confirmed that the MHCII$^+$ CD103$^+$ events were no staining artefacts or auto fluorescent particles (Figure 12 B).

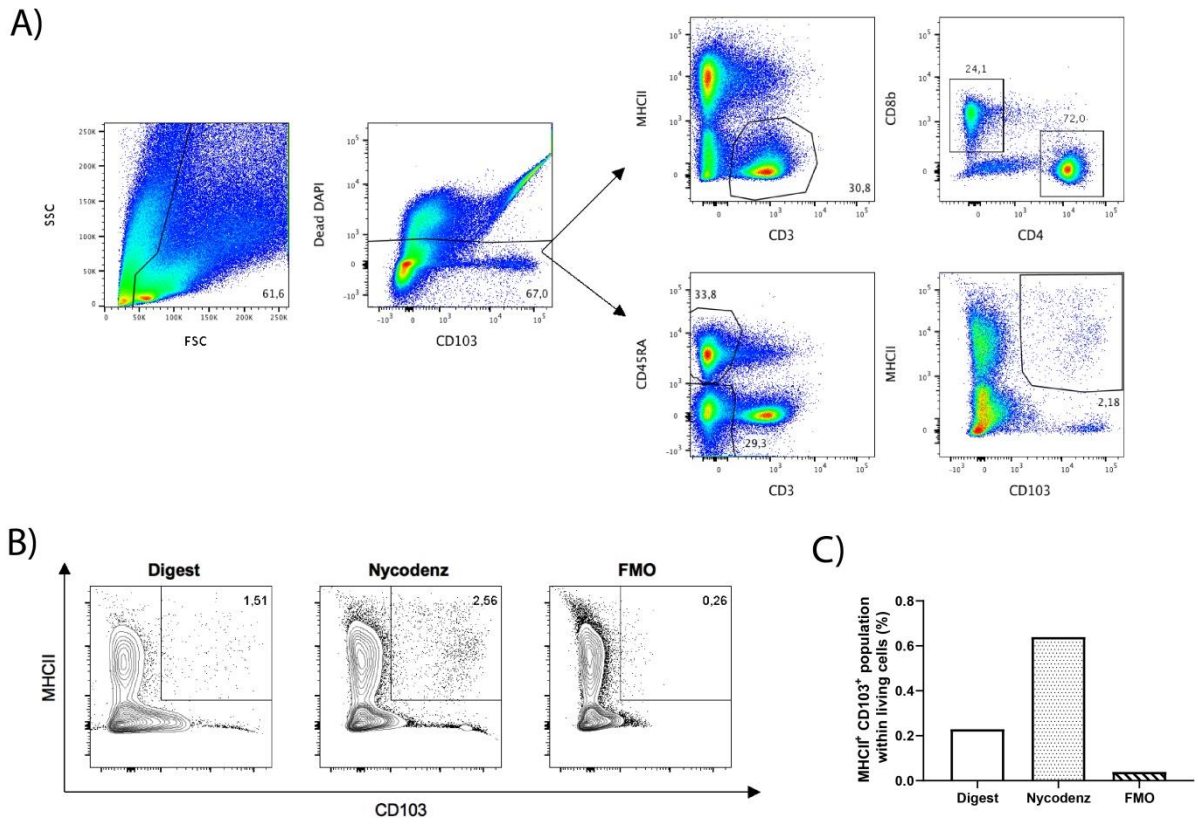

Figure 12: Identification of leukocytes in salivary glands. Submandibular and parotid glands from three SD rats were isolated, mashed, digested and enriched by using NycoPrep®. Several surface receptors were stained with fluorophore-coupled antibodies. **A)** Single cells were gated in FSC and SSC and dead cells stained with DAPI were excluded from the analysis. T cells ($CD3^+$) were divided into $CD4^+$ and $CD8^+$. B cells were gated according to CD45RA expression and DC were identified by the expression of MHCII and CD103. **B)** DC after digest and NycoPrep® enrichment. To exclude unspecific signal, a fluorescence minus one (FMO) control, without the antibody against CD103, was performed. **C)** Bar chart of DC frequency after digest and NycoPrep® enrichment.

4.2 *Ex vivo* infection of DC

4.2.1 RCMV-E infects and replicates in rat DC

In order to investigate whether RCMV replicates in DC, infection studies were carried out with splenic Ox-62 enriched cells. DC were infected at MOI 10 with recombinant RCMV-E carrying a *gfp*-cassette adjacent to *e32* for 8, 16, 24 and 48 h. To examine if viral replication occurs, UV-inactivation at 1 J/m^2 of recombinant virus was performed before infection. Mock-infected cells served as a negative control (Figure 13). Figure 13 A depicts the GFP signal, of $CD103^+$ $MHCII^+$ cells, which was at 23.5% 8 hpi and increased to 59.2% at 16 hpi, 73.8% at 24 hpi up to 87.9% at 48 hpi. Mock- and UV-infection showed no GFP signal. Dead cells were excluded from the analysis. Viability was decreasing in all Mock, RCMV-GFP and UV-infected samples from 70.4-83% 8 hpi to 32.8-60.2% 16 and 24 hpi and finally dropped to 20.4-39.4% 48 hpi (Figure 13 B). DC that were infected with UV-inactivated RCMV-E GFP showed lower viability rates at all time points compared to Mock and samples infected with

RCMV-E GFP. In contrast, infection with RCMV-E GFP showed small differences compared to Mock though cultivation of DC was limited to 48 h since viability decreased to 39.4%. Gating on DC as described above was impeded because RCMV-E infection led to changes in the DC phenotype. The expression of MHCII was reduced from 70% of all living cells to 20% at 48 hpi (Figure 13 C). Mock as well as UV-inactivated RCMV-E GFP had no influence on MHCII expression. In addition, a strong reduction of XCR1 surface expression was observed in infected as well as mock-infected DC. However, viral infection led to a more rapid reduction of XCR1 surface expression with 12% at 8 hpi, 1.7% at 16 hpi and 0.5-0.4% at 24 and 48 hpi (Figure 13 D) compared to Mock which was reduced from 32.5% at 8 hpi to 19.5% at 16 hpi, 5.5% at 24 hpi and dropped to the same level as in infected DC to 0.7% at 48 hpi. Infection with UV-inactivated virus showed the same trend as Mock but with lower expression rates.

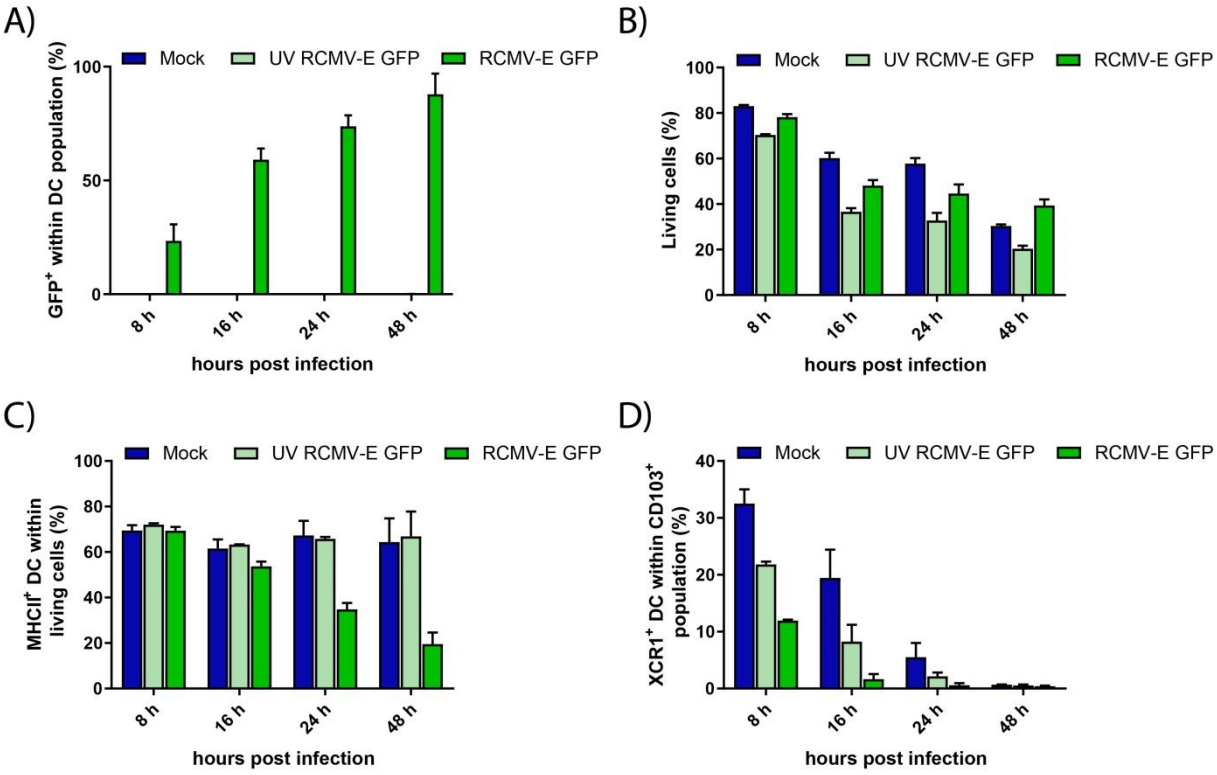

Figure 13: Infection of DC with RCMV-E GFP and UV-inactivated virus. Ox-62 enriched DC were infected with RCMV-E GFP and UV-inactivated RCMV-E GFP at an MOI of 10. Mock-infected cells served as a negative control. Expression of cell surface proteins was analyzed by flow cytometry after multi-color staining. Fixation was conducted with 2% (w/v) PFA. **A)** GFP signal in MHCII$^+$ CD103$^+$ DC. **B)** Cell viability was determined by staining cells with Pacific Orange (PacO) prior to fixation. **C)** MHCII expression within living cells. **D)** XCR1 expression within the CD103$^+$ population.

In order to confirm viral replication, intracellular expression of IE1 was detected after infection with both RCMV-E encoding *vxcl1* (wt) and a mutant virus lacking the viral chemokine (Δ*vxcl1*). Determination of IE1 expression at 8, 16 and 24 hpi confirmed the infection rates observed in RCMV-E GFP infected DC with no significant difference between RCMV-E wt

and RCMV-E Δ*vxcl1* (Figure 14 A). Here, viral infection did not affect cell viability (Figure 14 B).

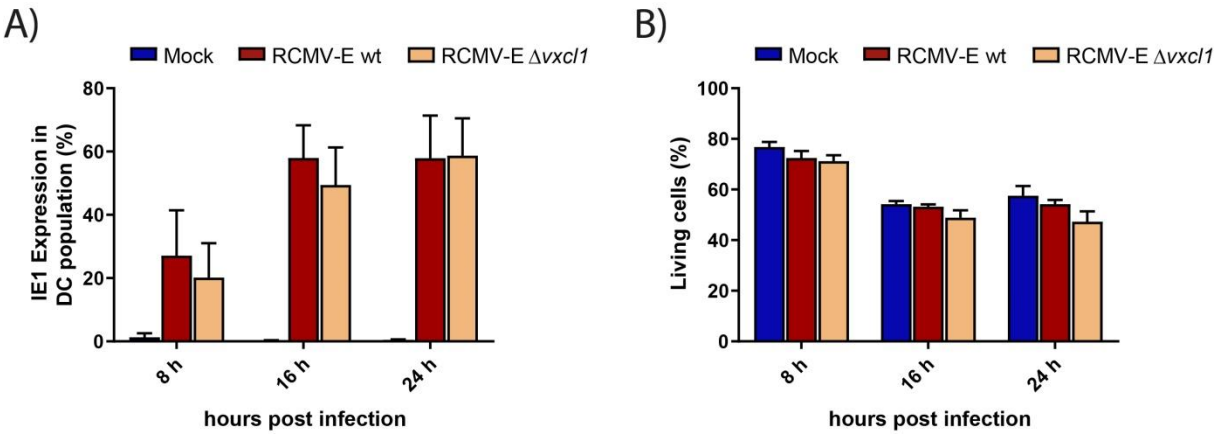

Figure 14: RCMV-E wt and RCMV-E Δ*vxcl1* infect splenic DC *ex vivo*. Ox-62 enriched DC were infected with RCMV-E wt and RCMV-E Δ*vxcl1* mutant at an MOI of 10. Mock-infected cells served as a negative control. At 8, 16 and 24 hpi intracellular IE1 was analyzed by flow cytometry after multi-color staining. Fixation was conducted with 2% (w/v) PFA and permeabilization with 0.5% (w/v) saponin. **A)** IE1 expression within the DC population. **B)** Viability of DC after infection. Error bars represent mean±SD, n = 3 independent experiments.

At 8 hpi the expression of XCR1 was significantly reduced by 42% in RCMV-E wt and by 32% in RCMV-E Δ*vxcl1* infected DC compared to mock-infected cells (Figure 15 A). At this time point the reduction of XCR1 was significantly higher in RCMV-E wt than in RCMV-E Δ*vxcl1* infected DC. Furthermore, it is shown that both viruses led to reduced MHCII expression, from 70% of all living cells to 20% at 16 hpi and to 15% at 24 hpi (Figure 15 B). Compared to MHCII expression in fresh isolated DC, MHCII was first upregulated after 8 h. MHCII was constantly upregulated in mock-infected cells but was notably reduced in RCMV-E infected cells (Figure 16). In addition, the expression of CD4 was reduced from 45% within the CD103$^+$ population to 13% at 16 hpi and 8% at 24 hpi in infected DC (Figure 15 C). Therefore, the DC subsets could be only differentiated until 8 hpi because of the reduction of MHCII, CD4 and XCR1 surface expression.

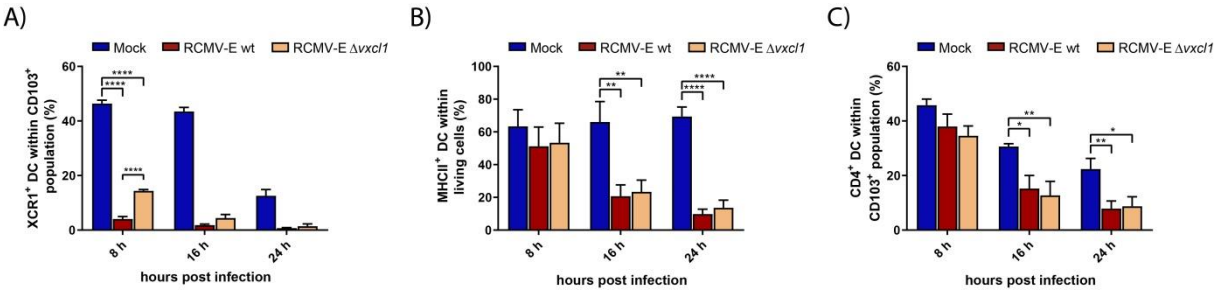

Figure 15: RCMV-E infection leads to changes in DC surface protein expression. Ox-62 enriched DC were infected with RCMV-E wt and RCMV-E Δ*vxcl1*. Mock-infected cells served as a negative control. Expression of cell surface proteins was analyzed by flow cytometry after multi-color staining. Fixation was conducted with 2% (w/v) PFA. **A)** XCR1 expression within CD103$^+$ cells. **B)** MHCII expression on DC within living cells. **C)** CD4 expression on DC. Error bars represent mean ± SD., n = 3 independent experiments. Data were analyzed by one-way ANOVA and Dunnett's multiple comparison test (* p<0.0332; ** p<0.0021; *** p<0.0002; **** p<0.00001).

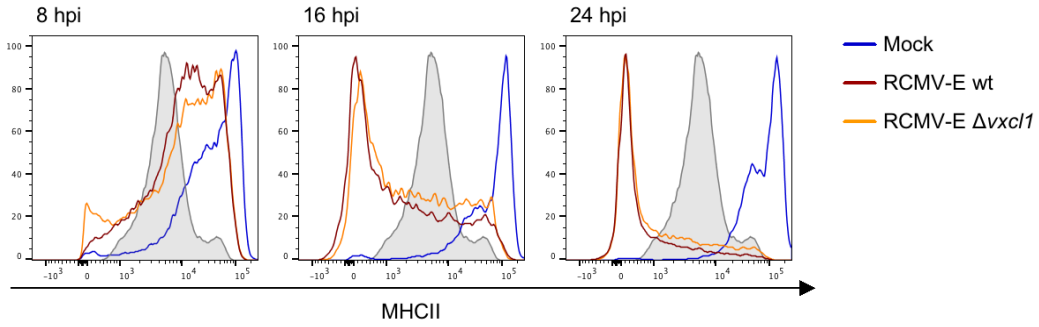

Figure 16: RCMV-E infection downregulates MHCII expression. Ox-62 enriched DC were infected with RCMV-E wt (red curve) and RCMV-E Δ*vxcl1* (yellow curve). Mock-infected cells served as a negative control (blue curve). Freshly isolated DC served as controls to demonstrate the initial state of expression (grey curve). Expression was analyzed by flow cytometry after multi-color staining. Fixation was conducted with 2% (w/v) PFA. One representative of 3 experiments is shown.

Since the investigation of GFP or IE1 expression does not imply viral replication, RCMV-E wt infected DC were analyzed with ultrathin section transmission electron microscopy (EM) at 24 hpi. EM analysis revealed cytoplasmic virus factories right next to deformed nuclei (Figure 17 A and B). Furthermore, mature viral particles could be visualized outside the cell (Figure 17 C). As replication and capsid formation is taking place in the nucleus, the identification of cytoplasmic virus factories indicated successful viral replication.

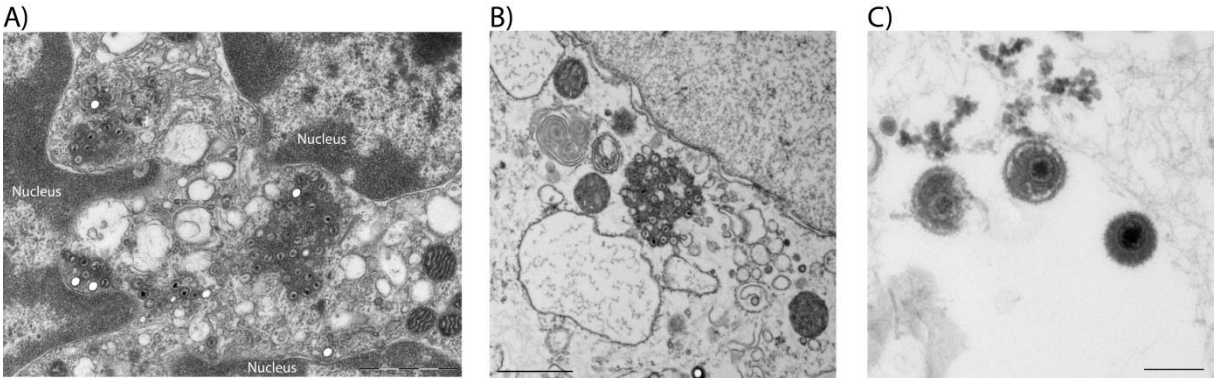

Figure 17: Ultrathin section transmission electron microscopy of RCMV-E infected DC. Ox-62 enriched DC were infected with RCMV-E wt at an MOI of 10. 24 hpi DC were fixed in 2.5% (w/v) glutaraldehyde and embedded in 3% (w/v) low melting agarose, followed by preparing sections with a size of 60-70 nm. Images were recorded using a Veleta CCD camera (EMSIS). **A)** Overview of cytoplasmic virus and deformed nuclei, **B)** a cytoplasmic virus factory including viral capsids after nuclear egress and **C)** mature viral particle of RCMV-E.

4.2.2 RCMV-E infection of DC alters their chemotactic activity

After verifying RCMV-E replication in DC, it was investigated whether RCMV-E infection affects the migration behavior of DC. To do so, Ox-62 enriched DC were infected with RCMV-E wt and RCMV-E Δ*vxcl1* for 4 h, followed by a transwell assay with 100 ng/ml recombinant rXCL1 in the bottom well for another 2.5 h. Mock-infected DC were analyzed as controls and no chemokine was added in the well (“No Chemokine” in the legend). As shown

in Figure 18 A, mock-infected CD4$^-$ DC migrated towards the host chemokine rXCL1 with a rate of 54% of input cells. In contrast, infection led to a significant, almost complete loss of chemotactic activity after both RCMV-E wt (to 8.4%) and RCMV-E Δ*vxcl1* (to 13.2%) infected DC (Figure 18 A). The reduction of chemotactic activity between both virus infections was not significant. Chemotaxis to the No Chemokine control ranged between 5-7.6% in all three samples. The CD4$^+$ DC subset that mainly lacked XCR1 hardly showed migration at a rate of 5-6%. Interestingly, mock-infected CD4$^+$ DC showed 14% migration towards rXCL1 (Figure 18 B).

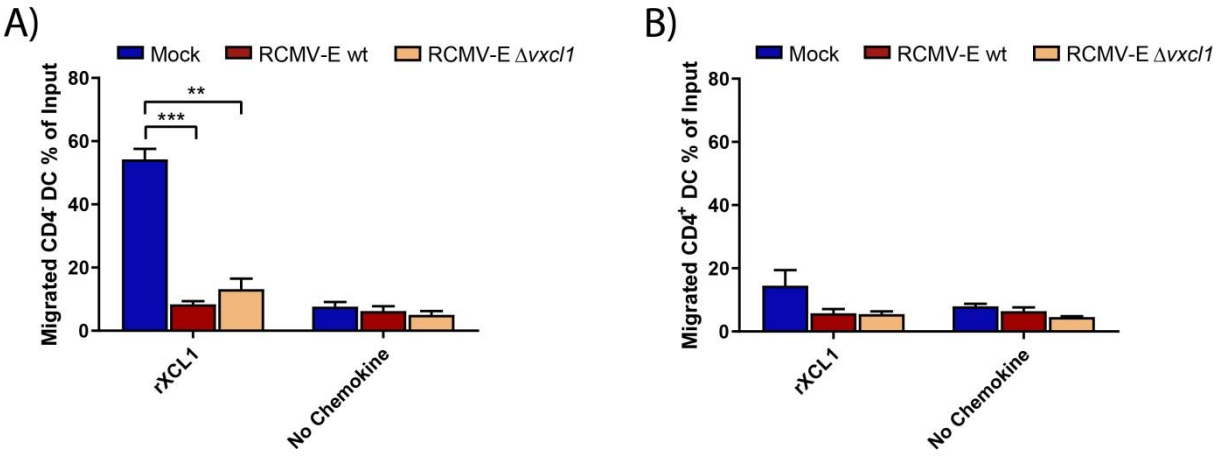

Figure 18: Chemotactic activity of RCMV-E infected DC towards rXCL1. Ox-62 enriched DC were infected with RCMV-E wt and RCMV-E Δ*vxcl1* with an MOI of 3 for 4 h at 37°C. Mock-infected cells served as negative control. After incubation the cell surface was stained with fluorophore-coupled antibodies. In order to investigate chemotactic activity, $2*10^5$ of the incubated and stained DC were added to the upper chamber of a transwell system. Each transwell contained either 100 ng/ml rXCL1 or no chemokine in the lower chamber. After 2.5 h of incubation, cells that migrated to the lower chamber were analyzed by flow cytometry. **A)** Migrated CD4$^-$ DC, **B)** Migrated CD4$^+$ DC. Two independent replicates were carried out in technical duplicates (n = 2). Error bars represent mean ± SD. Data were analyzed by one-way ANOVA and Dunnett's multiple comparison test (* p<0.0332; ** p<0.0021; *** p<0.0002; **** p<0.00001).

4.2.3 RCMV-E infection leads to changes in the DC transcriptome profile

To gain deeper insights in DC gene expression after RCMV-E infection, the DC transcriptome profile was analyzed by using a RNA sequencing technique. In this analysis, two aspects were determined: First, changes of transcribed genes in enriched DC after cultivation (Mock) and second, changes after infection with RCMV-E wt, RCMV-E Δ*vxcl1* and RCMV-E UV inactivated wt (here referred to as UV). In order to obtain a relatively high number of infected DC without decreased viability, DC were infected with a MOI of 3 for 24 h. To demonstrate DEG, RNA sequencing data were normalized on freshly isolated uncultivated DC, resulting in diagrams that depict fold changes. Figure 19 shows Venn-diagrams that give an overview of the quantity of DEG. Figure 19 A indicates that 1513 genes were upregulated considering Mock, RCMV-E wt, RCMV-E Δ*vxcl1* and UV. These samples shared 688 upregulated genes. Circles without any overlap represent genes that

were exclusively upregulated in the respective group, e.g., 13 in RCMV-E wt and 15 genes in RCMV-E Δ*vxcl1* infected DC (Figure 19 A). Figure 19 B shows that in total 2160 genes were downregulated. Mock, RCMV-E wt, RCMV-E Δ*vxcl1* and UV shared 869 downregulated genes. To get a better overview of the similarity between the test groups a heatmap of all DEG was generated with red colored upregulated and blue colored downregulated genes (Supplement 2). Automated clustering revealed that RCMV-E wt and RCMV-E Δ*vxcl1* induced similar transcriptomic changes. The same applied for RCMV-E UV and Mock, indicating that not-replicating virus induced a similar phenotype as in mock-infected DC.

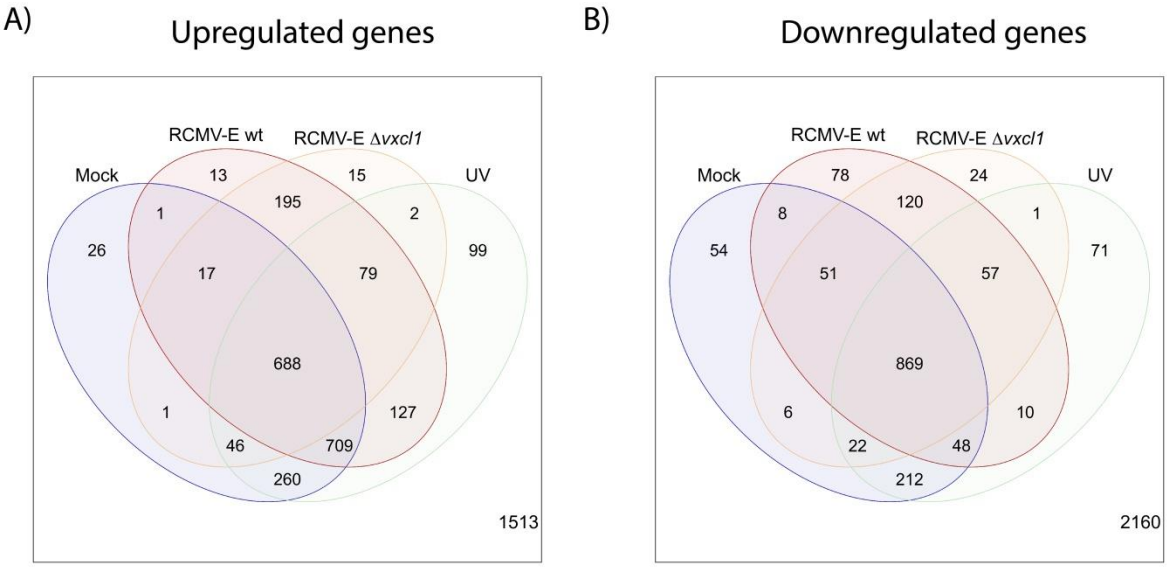

Figure 19: Regulated genes in RCMV-E infected DC. Ox-62 enriched DC were infected with RCMV-E wt, UV-inactivated RCMV-E and RCMV-E Δ*vxcl1*. Mock-infected cells served as negative control. Gene expression was normalized to uncultivated DC. **A)** Venn-diagram of upregulated genes. **B)** Venn-diagram of downregulated genes. Differentially expressed genes predicted by SCORE with a fold change > 4, $p \leq 0.05$, n = 3.

To further analyze what type of genes are differentially expressed, the DEG list was integrated in the KEGG. Genes were mapped by pathways on molecular interactions, reaction and relation networks. KEGG creates a list of pathways where DEG are clustered. Using these overviews, DEG of interest were picked and clustered in a more detailed heatmap (Supplement 3). In addition, genes that are not categorized in KEGG were manually picked (Figure 20). The heatmap in Figure 20 depicts genes associated with antigen presentation that are differently transcribed in infected and mock-infected DC. On the one hand, *Rab27a*, *Rac2* and the Tap gene *Tap2* were downregulated in infected DC but upregulated in Mock and UV samples (Figure 20). On the other hand, *Calr*, *Pdia3* and *Sec22b* were stronger upregulated in infected than in mock-infected DC (Supplement 4). *Ccl17* was strongly downregulated in infected but massively upregulated in uninfected DC (Supplement 4). *Ccl2, Ifnb1* and *Ifng* are three of the few genes that were upregulated in all three infection settings but not in the Mock sample (Supplement 3, Supplement 4). *Ccl6* was

stronger downregulated in infected than in mock- or UV-infected DC (Supplement 4). The maturation markers *Cd86*, *Cd80*, *Cd40* and *Ccr7* were upregulated during cultivation at 37°C. This upregulation was hampered by the infection with RCMV-E wt and RCMV-E Δ*vxcl1*. Compared with RCMV-E wt *Ccr7* and *Cd40* were less impeded by the infection with RCMV-E Δ*vxcl1* (Figure 20). Genes related to migration were upregulated in all groups, including PI3K as well as Akt. However, this upregulation was stronger in mock-infected DC (Supplement 4).

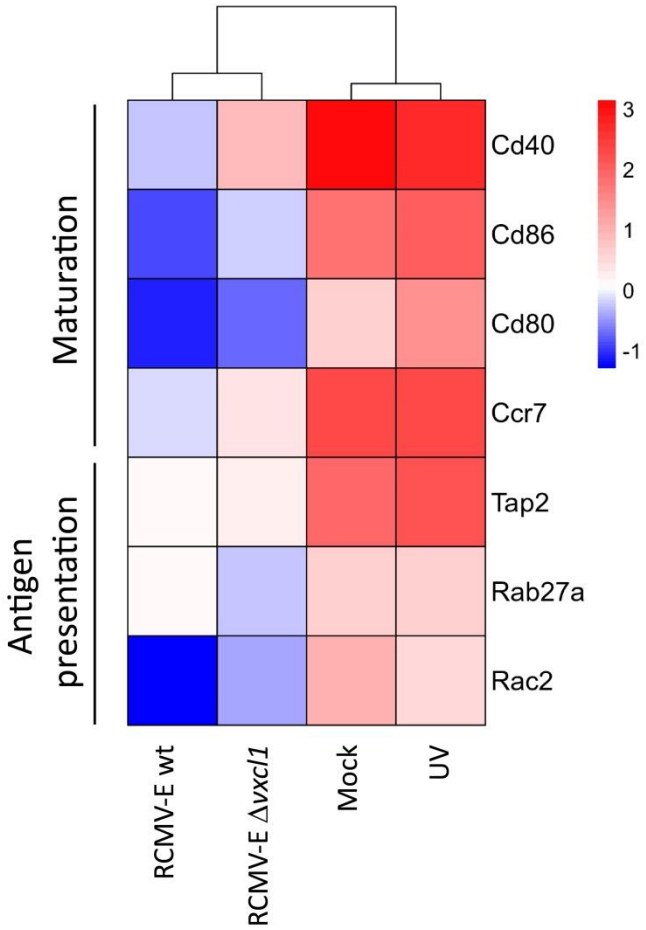

Figure 20: Heatmap of DEG of interest. Ox-62 enriched DC were infected with RCMV-E wt, UV-inactivated RCMV-E and RCMV-E Δ*vxcl1* for 24 h (MOI 3). Mock-infected cells served as a negative control. Expressed genes were normalized to uncultivated DC. Upregulated genes are shown in red, downregulated genes are depicted in blue. Differentially expressed genes were predicted by SCORE with a fold change > 4, $p \leq 0.05$, $n = 3$.

4.3 rXCL1 and vXCL1 interact with XCR1$^+$ DC

4.3.1 rXCL1 and RCMV-B and -E encoded vXCL1 share sequence similarities

To further determine the homology of rXCL1 and vXCL1, sequence alignment was performed and XCL1 from human, mouse, rat was compared to vXCL1 of RCMV-E and RCMV-B. In rats XCL1 is the only known member of the γ-chemokines that binds solely XCR1. Comparison of the amino acid (AA) sequences between different species revealed highly

conserved parts, including the protein core, but also little variable parts regarding the N-terminus and high variable sites regarding the C-terminus (Figure 21 A). XCL1 of *Mus musculus*, *Homo sapiens* and *Rattus norvegicus* consist of 114 AA. RCMV-B and RCMV-E are the only known viruses encoding a XCL1 homolog, in this work referred to as vXCL1 E and vXCL1 B, respectively. While vXCL1 B comprises 114 AA as its host, vXCL1 E consists of 115 AA. Both vXCL1 variants contain two AA gaps at positions 7 and 8 while having three additional AA at positions 98, 99 and 100 (Figure 21 A). Comparing the AA sequence of XCL1 from *Rattus norvegicus* (rXCL1) with vXCL1 E or vXCL1 B, similarity was 63.2% and 65.5%, respectively. vXCL1 B and vXCL1 E shared 83.3% similarity (Figure 21 B).

A)

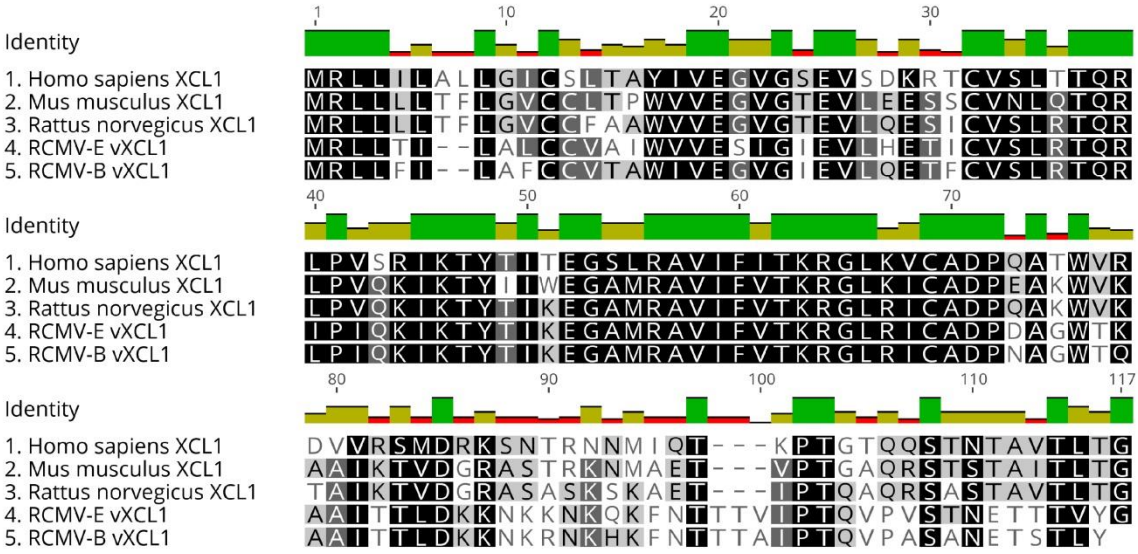

B)

XCL1	Homo sapiens	Mus musculus	Rattus norvegicus	RCMV-E	RCMV-B
Homo sapiens		60.5%	57.0%	45.3%	50.0%
Mus musculus	60.5%		82.5%	56.4%	57.8%
Rattus norvegicus	57.0%	82.5%		63.2%	65.5%
RCMV-E	45.3%	56.4%	63.2%		83.3%
RCMV-B	50.0%	57.8%	65.5%	83.3%	

Figure 21: Protein alignment of XCL1 from different species and vXCL1 encoded by RCMV-E and RCMV-B. A) Amino acid (AA) sequence from *Homo sapiens* (NC_000001.11), *Mus musculus* (NM_008510), *Rattus norvegicus* (NC_005112.4), RCMV-E (NC_019559), and RCMV–B (KP202868). Identical AA are indicated by black background and similar AA by gray background. White background indicates no similarity in AA sequence. **B)** Distance matrix for depicted protein sequences generated by Geneious.

4.3.2 rXCL1 and vXCL1 affect XCR1 surface expression

To investigate whether vXCL1 and rXCL1 have a different impact on XCR1$^+$ DC, Ox-62 enriched splenocytes of Sprague Dawley rats were incubated with different concentrations of recombinant Strep-tagged rXCL1, vXCL1 E and vXCL1 B at 37°C for 4 h. After incubation,

cells were stained with fluorophore-coupled antibodies to determine the DC phenotype. Incubation with either 0,5 or 25 ng/ml of recombinant chemokines revealed that 25-30% of all DC expressed XCR1 without any difference between rXCL1 and the vXCL1 variants (Figure 22). 50 ng/ml of both vXCL1 variants slightly reduced the XCR1 surface expression. This reduction was strengthened after incubating with 100 ng/ml of vXCL1. In contrast, a comparable reduced XCR1 expression was only observed after incubation with 250 ng/ml of rXCL1. With higher amounts of chemokine, the receptor disappeared further from the cell surface. At a concentration of 500 ng/ml, XCR1 expression was reduced to 19.9% after incubation with rXCL1 and to 12.4% after incubation with vXCL1 E and vXCL1 B (Figure 22).

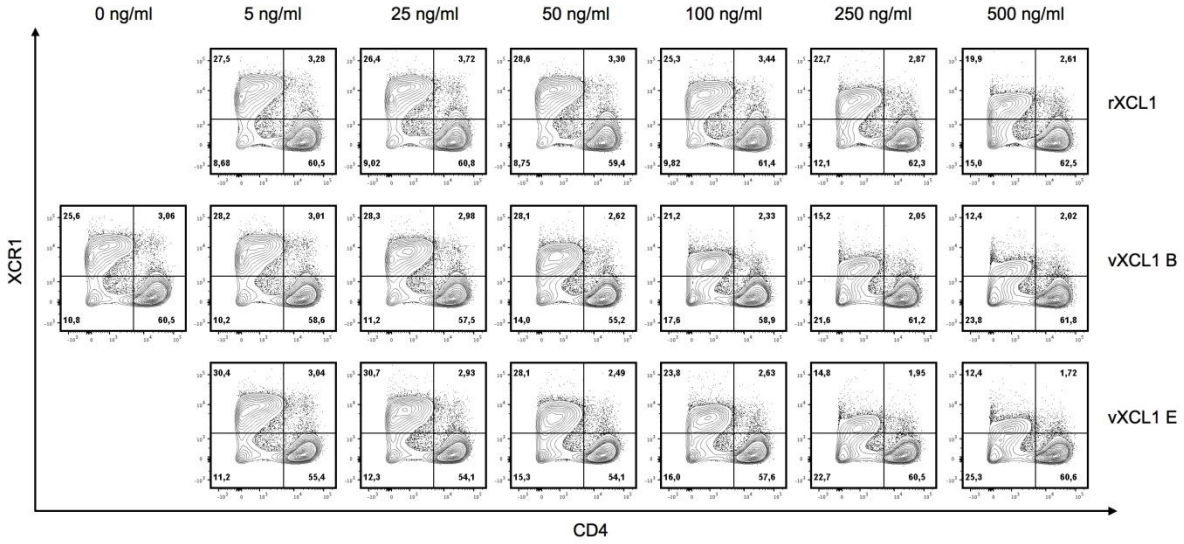

Figure 22: XCR1 cell surface expression on CD4$^-$ DC after incubation with recombinant chemokines. 2*10^5 Ox-62 enriched splenic DC were incubated for 4 h with 0, 5, 25, 50, 100, 250 or 500 ng/ml of recombinant rXCL1, vXCL1 E and vXCL1 B, respectively. DC (CD3$^-$ CD45RA$^-$ MHCII$^+$ CD103$^+$) were analyzed by flow cytometry after multicolor-staining. Dead cells were excluded by DAPI staining prior to measurement. One of three independent experiments are shown.

4.3.3 Prior incubation of DC with rXCL1 and vXCL1 impairs chemotactic migration towards rXCL1

Since XCL1 binding led to a reduced XCR1 surface expression, the chemotactic activity of DC to endogenous rXCL1 was investigated following a previous incubation with recombinant chemokine rXCL1 and vXCL1. Splenic DC of Lewis rats were isolated with Ox-62 beads and incubated with 500 ng/ml of rXCL1 and vXCL1 E, respectively, for 4 h at 37°C followed by a chemotaxis assay towards rXCL1. The input control showed that XCR1 disappeared from the surface due to incubation with the respective chemokines (Figure 23 A). A ligand-independent reduction of XCR1 was observed as well which led to a low migration rate of 7.4%. The control with no chemokine in the bottom well showed that there was unspecific migration of 2.5%. The incubation with the recombinant chemokines led to a significant

reduction of migratory potential from 7.4% (Untreated) to 4% (rXCL1) and 2.8% (vXCL1), respectively, which represented the rate of unspecific migration (Figure 23 B).

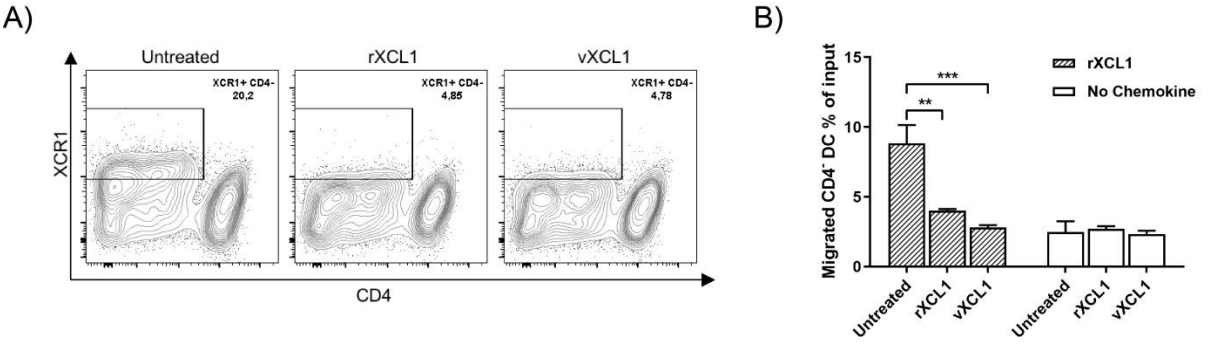

Figure 23: Chemotactic activity of CD4$^-$ XCR1$^+$ DC after incubation with rXCL1 and vXCL1. Ox-62 enriched splenic DC were incubated with 500 ng/ml rXCL1 or vXCL1, respectively, for 4 h at 37°C. Cells incubated without chemokine served as a control (Untreated). After incubation the cell surface was stained with fluorophore-coupled antibodies. In order to investigate chemotactic activity, $2*10^5$ of the incubated and stained DC were added to the upper chamber of a transwell. Each transwell contained 100 ng/ml rXCL1 or no chemokine in the lower chamber. After 2.5 h of incubation cells that migrated to the lower chamber were analyzed by flow cytometry. **A)** XCR1 surface expression after 4 h incubation at 37°C. **B)** Migrated CD4$^-$ DC relative to the input cell number. Error bars represent mean ± s.e.m., n = 2 independent experiments were carried out in duplicates. Data were analyzed by one-way ANOVA and Dunnett's multiple comparison test (**, $p < 0.005$; ***, $p < 0.0005$).

4.4 *In vivo* infection of *Xcr1*$^{+/+}$ and *Xcr1*$^{-/-}$ rats with RCMV-B

4.4.1 Viral spread of RCMV-B in *Xcr1*$^{+/+}$ and *Xcr1*$^{-/-}$ rats

The RCMV-E strain, that was used in above described *ex vivo* infection experiments (4.2), could not be successfully isolated from salivary glands 16 days after i.p. infection. Therefore, it was decided to perform the *in vivo* experiments with RCMV-B which is the second isolate classified as MuHV-8.

To investigate whether XCR1 plays a role in viral dissemination 10-week old *Xcr1*$^{+/+}$ and *Xcr1*$^{-/-}$ Sprague Dawley rats were infected i.p. with $1*10^6$ pfu RCMV-B wt. As a control 1 ml PBS (Mock) was injected i.p. After 3, 5, 16 and 90 dpi salivary glands, liver, lung and spleen were collected for virus detection by TaqMan qPCR. To determine RCMV-B, a probe targeting *gB* was utilized. For a defined copy number of the gene of interest, a standard with 10^0 -10^7 copies was used. To normalize the samples, copy numbers of *gB* were divided by copy numbers of *c-myc*.

The highest amount of RCMV-B *gB* was detected in spleen, lung and liver at 5 dpi (Figure 24). The median *gB*/*c-myc* ratio in spleen was 0.33 and 0.28 in *Xcr1*$^{+/+}$ and *Xcr1*$^{-/-}$ rats, respectively. At 3, 16 and 90 dpi *gb* was hardly detectable in spleen (ratio < 0.004) (Figure 24 A). The highest ratio in lung was also detected at 5 dpi though ratios were lower compared to those in spleen. Interestingly, 5 dpi the *gB*/*c-myc* ratio in the lung was ten fold higher (0.03)

in *Xcr1*$^{+/+}$ than in *Xcr1*$^{-/-}$ (0.004) rats. At 16 dpi, the ratio in the lung decreased to 0.007 and 0.002 in *Xcr1*$^{+/+}$ and *Xcr1*$^{-/-}$ rats, respectively (Figure 24 B). In liver, median ratios were similar to lung with 0.011 and 0.016 *Xcr1*$^{+/+}$ and *Xcr1*$^{-/-}$ rats at 5 dpi, respectively (Figure 24 C). In salivary glands the highest viral load was detected at 16 dpi where the median ratio was 0.3 and 0.6 in *Xcr1*$^{+/+}$ and *Xcr1*$^{-/-}$ rats, respectively. Although the median was lower in *Xcr1*$^{+/+}$ rats, it has to be considered that two *Xcr1*$^{+/+}$ rats showed a massively higher *gB*/*c-myc* ratio with 7.6 (rat 28) and 9.3 (rat 30), whereas two of the *Xcr1*$^{-/-}$ rats showed an extremely low *gB/c-myc* ratio with 0.02 and 0.005 (rat 62; Figure 24 D). These findings could be confirmed by plaque assay (Figure 25). The median of pfu/ml was $8.1*10^4$ and $5.1*10^4$ in *Xcr1*$^{+/+}$ and *Xcr1*$^{-/-}$ rats, respectively. Rat 28 that showed a *gB/c-myc* ratio of 7.6 exhibited $7.3*10^5$ pfu/salivary gland, rat 30 had a *gB/c-myc* ratio of 9.3 and $4.1*10^6$ pfu/salivary gland. Further, rat 62 indicated a *gB/c-myc* ratio of 0.005 and $1.6*10^3$ pfu/salivary gland. At 90 dpi, low ratios in salivary glands of both *Xcr1*$^{+/+}$ and *Xcr1*$^{-/-}$ rats could be determined (Figure 24 D).

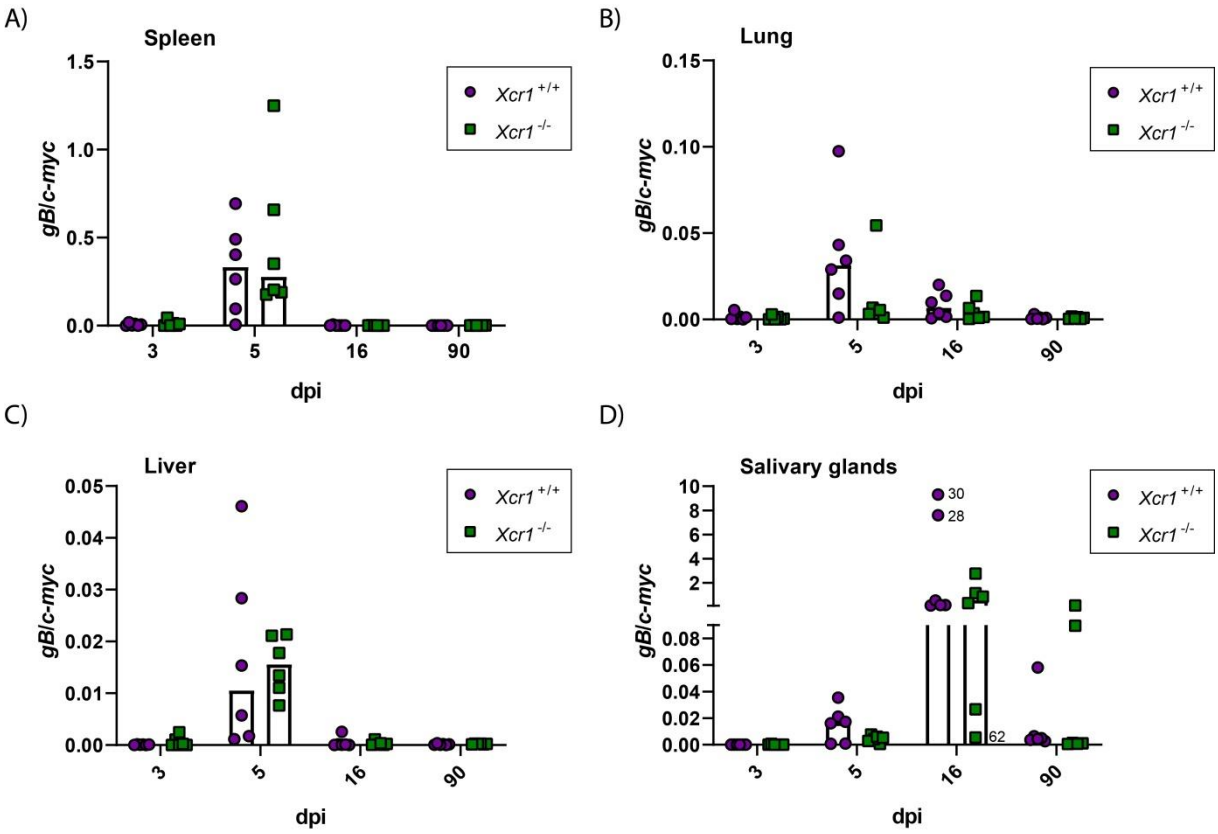

Figure 24: Detection of viral *gB* DNA after infection of *Xcr1*$^{+/+}$ and *Xcr1*$^{-/-}$ rats with RCMV-B. 10-week-old male Sprague Dawley rats were infected with $1*10^6$ pfu of RCMV-B wt. After 3, 5, 16 and 90 dpi, spleens **(A)**, lungs **(B)**, livers **(C)** and salivary glands **(D)** were collected and DNA was isolated, followed by TaqMan-qPCR with specific primers and probes targeting the viral gene *gB* and the host gene *c-myc*. Relative copy numbers of *gB* were normalized to the housekeeping gene *c-myc*. Results were obtained from 6 biological replicates in technical duplicates. Numbers represents the individual rat 28, 30 and 62. Bars represent the median.

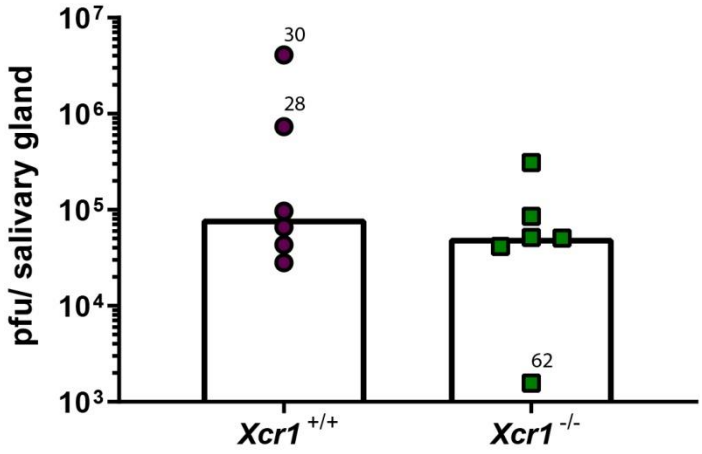

Figure 25: Titration of salivary glands of *Xcr1*$^{+/+}$ and *Xcr1*$^{-/-}$ rats at 16 dpi. 10-week-old male Sprague Dawley rats were infected with 1*10^6 pfu of RCMV-B. 16 days post infection the left salivary gland was homogenized, diluted and put on REF. After 1 h cells were covered with Overlay-medium and one week later pfu were counted. Results were obtained from 6 biological replicates in technical duplicates. Numbers represent individual rat 28, 30 and 62. Bars represent the median.

4.4.2 Frequencies of leukocytes after infection with RCMV-B wt

Following the investigation of RCMV-B wt dissemination in *Xcr1*$^{+/+}$ and *Xcr1*$^{-/-}$ rats, frequencies of DC, B cells, T cells, NK cells and NKT cells were determined in blood, lymph nodes, salivary glands and spleens at 3, 5, 16 and 90 dpi. Supplement 2 depicts dot blots and the gating strategy for the different cell populations within the respective organs (Supplement 5). Only significant differences between infected and mock-infected as well as *Xcr1*$^{+/+}$ and *Xcr1*$^{-/-}$ rats are described. An overview about all cell frequencies of all organs and timepoints are summarized in the supplements (Supplement 6-11).

4.4.2.1 Three days post infection

In blood and lymph nodes *Xcr1*$^{+/+}$ and *Xcr1*$^{-/-}$ rats the frequency of CD8$^+$ T cells was slightly decreased after infection (Figure 26 A and B). In lymph nodes of *Xcr1*$^{+/+}$ rats the amount of DC was higher after infection compared to Mock. In lymph nodes of infected *Xcr1*$^{-/-}$ rats the frequency of DC was increased as well but was significantly lower than in infected *Xcr1*$^{+/+}$ rats (Figure 26 C).

In spleens the number of CD8$^+$ T cells was significantly increased in infected *Xcr1*$^{-/-}$ from 21% to 32% and not significantly increased in *Xcr1*$^{+/+}$ rats from 19% to 22 (Figure 26 D). On the contrary, the frequency of CD4$^+$ T cells was reduced in infected *Xcr1*$^{-/-}$ rats but not in *Xcr1*$^{+/+}$ rats (Figure 26 E). The amount of NK cells was increased in the spleen of infected *Xcr1*$^{-/-}$ rats but not in *Xcr1*$^{+/+}$ rats compared to the respective mock-infected animals (Figure 26 F). The number of NKT cells in spleens was elevated in both *Xcr1*$^{-/-}$ and *Xcr1*$^{+/+}$ rats after infection. The amount of B cells slightly dropped after infection of *Xcr1*$^{+/+}$ and *Xcr1*$^{-/-}$ rats (Figure 26 H).

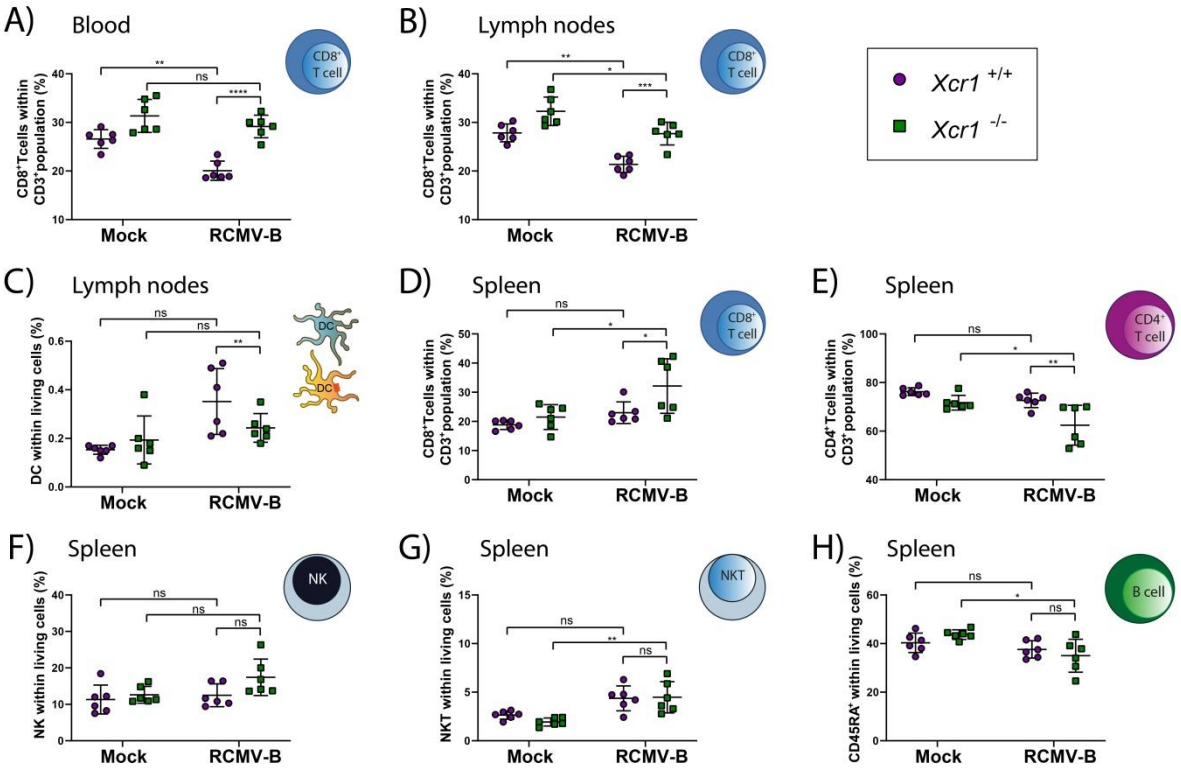

Figure 26: Frequency of leukocytes in RCMV-B and Mock infected *Xcr1*$^{+/+}$ and *Xcr1*$^{-/-}$ rats at 3 dpi. 10-week-old male Sprague Dawley rats were infected with 1*10^6 pfu of RCMV-B or 500 µl PBS (Mock) for 3 days. Leukocytes were isolated from blood, lymph nodes and spleen. After surface staining, cells were gated on DC, CD8$^+$ and CD4$^+$ T cells, B cells, NK and NKT cells. **A)** Frequency of CD8$^+$ T cells within the CD3$^+$ population in blood. **B)** Frequency of CD8$^+$ T cells within the CD3$^+$ population in lymph nodes. **C)** Frequency of DC within living cells in lymph nodes. Orange: CD4$^-$ DC, turquois: CD4$^+$ DC **D)** Frequency of CD8$^+$ T cells within the CD3$^+$ population in spleen. **E)** Frequency of CD4$^+$ T cells within the CD3$^+$ population in spleen. **F)** Frequency of NK cells within living cells in spleen. **G)** Frequency of NKT cells within living cells in spleen. **H)** Frequency of B cells within living cells in spleen. Error bars represent mean ± SD, n = 6 rats. Data were analyzed by one-way ANOVA and Tukey's multiple comparison test (ns = not significant; * p<0.0332; ** p<0.0021; *** p<0.0002; **** p<0.00001).

4.4.2.2 Five days post infection

After five days of infection, higher frequencies of NKT cells could be detected in the blood and lymph nodes of *Xcr1*$^{+/+}$ and *Xcr1*$^{-/-}$ rats after infection (Figure 27 A and C). In lymph nodes an increased rate of NK cells could be detected as well after infection (Figure 27 B).

In spleen several changes in cell frequency were observed. DC frequency was lower in both infected *Xcr1*$^{+/+}$ and *Xcr1*$^{-/-}$ rats compared to Mock (Figure 27 C). The number of NK cells was increased in infected *Xcr1*$^{-/-}$ rats compared to Mock. In infected *Xcr1*$^{+/+}$ rats the NK cell rate increased not as high as in infected *Xcr1*$^{-/-}$ rats (Figure 27 F). Like their counterpart, NKT cell frequency was significantly higher in spleens of infected rats (Figure 27 G). Furthermore, the frequency of B cells was significantly decreased in *Xcr1*$^{+/+}$ and *Xcr1*$^{-/-}$ rats after infection (Figure 27 H).

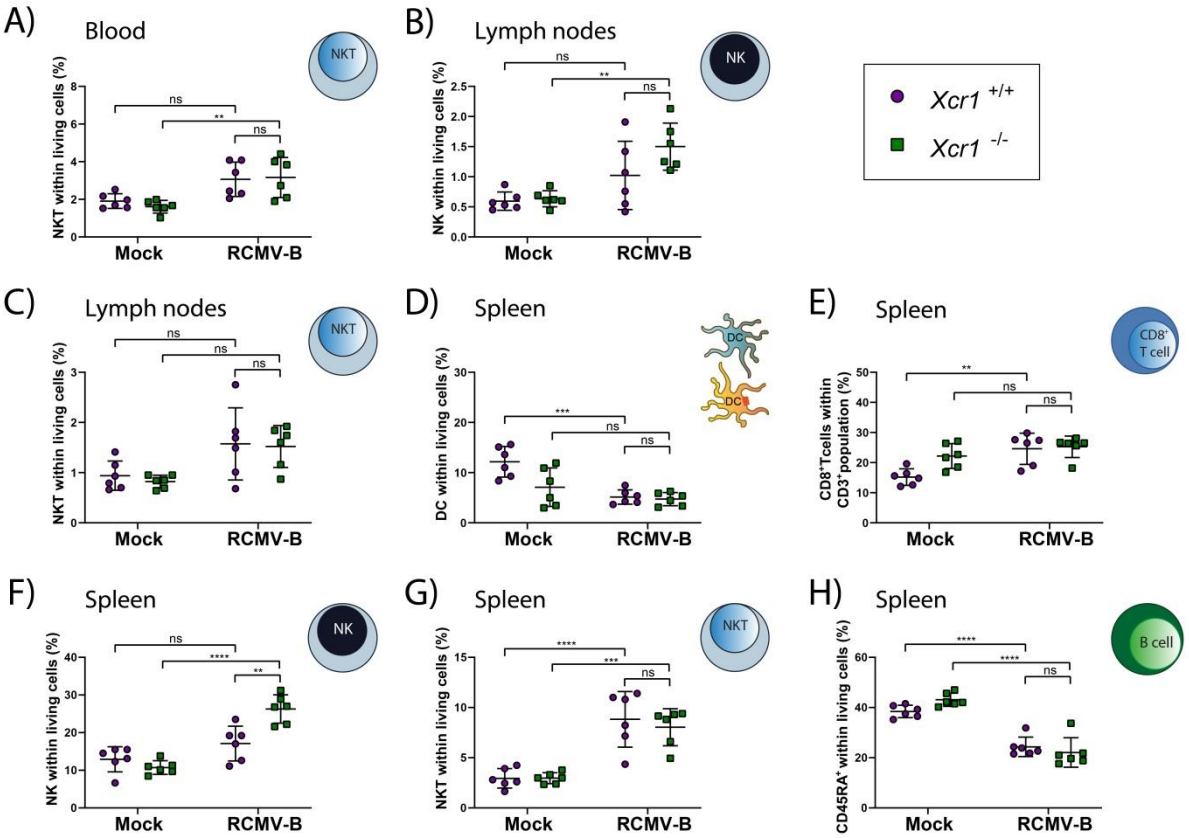

Figure 27: Frequency of leukocytes in RCMV-B and Mock infected *Xcr1*$^{+/+}$ and *Xcr1*$^{-/-}$ rats at 5 dpi. 10-weeks-old male Sprague Dawley rats were infected with 1*10^6 pfu of RCMV-B or 500 µl PBS (Mock) for 5 days. Leukocytes were isolated from blood, lymph nodes and spleen. After surface staining, cells were gated on DC, CD8$^+$ T cells, B cells, NK and NKT cells. **A)** Frequency of NKT cells within living cells in blood. **B)** Frequency of NK cells within living cells in lymph nodes. **C)** Frequency of NKT cells within living cells in lymph nodes. **D)** Frequency DC within living cells in spleen. Orange: CD4$^-$ DC, turquois: CD4$^+$ DC **E)** Frequency of CD8$^+$ T cells within the CD3$^+$ population in spleen. **F)** Frequency of NK cells within living cells in spleen. **G)** Frequency of NKT cells within living cells in spleen. **H)** Frequency of B cells within living cells in spleen. Error bars represent mean ± SD, n = 6 rats. Data were analyzed by one-way ANOVA and Tukey's multiple comparison test (ns = not significant; * p<0.0332; ** p<0.0021; *** p<0.0002; **** p<0.00001).

4.4.2.3 Sixteen days post infection

After 16 days of infection, significant changes of cell frequencies were observed in salivary glands. There, the frequency of CD8$^+$ T cells was increased to 60% and 58% in infected *Xcr1*$^{+/+}$ and *Xcr1*$^{-/-}$ rats, respectively, compared to Mock with 21% and 11% (Figure 28 A). DC frequency was 5.2 times higher in infected *Xcr1*$^{+/+}$ rats (0.81%) and only 3.7 times higher in *Xcr1*$^{-/-}$ rats (0.33%) (Figure 28 B). The increased number of DC in salivary glands and the difference between both genotypes was more noticeable in the representative dot plots in Figure 29 that shows 2724 events in infected *Xcr1*$^{+/+}$ rats and 1150 events in infected *Xcr1*$^{-/-}$ rats (event number is the mean of all 6 replicates). The NK cell frequency was increased in salivary glands of infected *Xcr1*$^{+/+}$ rats, whereas infected *Xcr1*$^{-/-}$ rats showed no significant elevated NK cell frequency (Figure 28 C). In addition, the NKT cell frequency escalated in salivary glands of infected *Xcr1*$^{+/+}$ and *Xcr1*$^{-/-}$ rats and was significantly higher in infected *Xcr1*$^{+/+}$ rats than in infected *Xcr1*$^{-/-}$ rats (Figure 28 D).

In blood of infected *Xcr1*$^{+/+}$ rats a higher amount of NKT cells was observed compared to Mock. The elevated NKT cell frequency in blood of infected *Xcr1*$^{-/-}$ rats was significantly lower than in *Xcr1*$^{+/+}$ rats (Figure 28 E). In lymph nodes, the NKT cell frequency was increased in both infected *Xcr1*$^{+/+}$ and *Xcr1*$^{-/-}$ rats (Figure 28 F). In spleen the DC frequency was still reduced after infection (Figure 28 G).

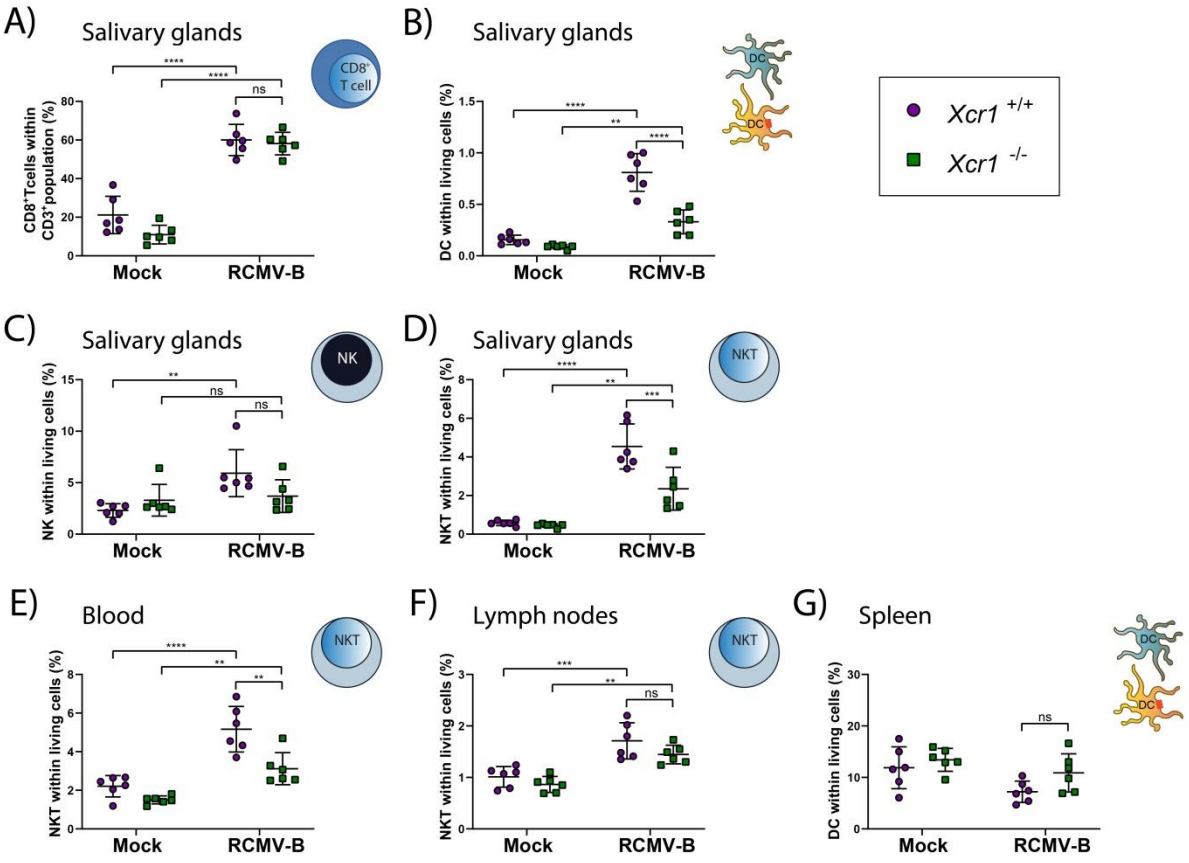

Figure 28: Frequency of leukocytes in RCMV-B and Mock infected *Xcr1*$^{+/+}$ and *Xcr1*$^{-/-}$ rats at 16 dpi. 10-week-old male Sprague Dawley rats were infected with 1*10^6 pfu of RCMV-B or 500 µl PBS (Mock) for 16 days. Leukocytes were isolated from blood, lymph nodes, salivary glands and spleen. After surface staining, cells were gated on DC, CD8$^+$ T cells, NK and NKT cells. **A)** Frequency of CD8$^+$ T cells within the CD3$^+$ population in salivary glands. **B)** Frequency DC within living cells in salivary glands. Orange: CD4$^-$ DC, turquois: CD4$^+$ DC **C)** Frequency of NK cells within living cells in salivary glands. **D)** Frequency of NKT cells within living cells in salivary glands. **E)** Frequency of NKT cells within living cells in blood. **F)** Frequency of NKT cells within living cells in lymph nodes. **G)** Frequency DC within living cells in spleen. Error bars represent mean ± SD, n = 6 rats. Data were analyzed by one-way ANOVA and Tukey's multiple comparison test (ns = not significant; * p<0.0332; ** p<0.0021; *** p<0.0002; **** p<0.00001).

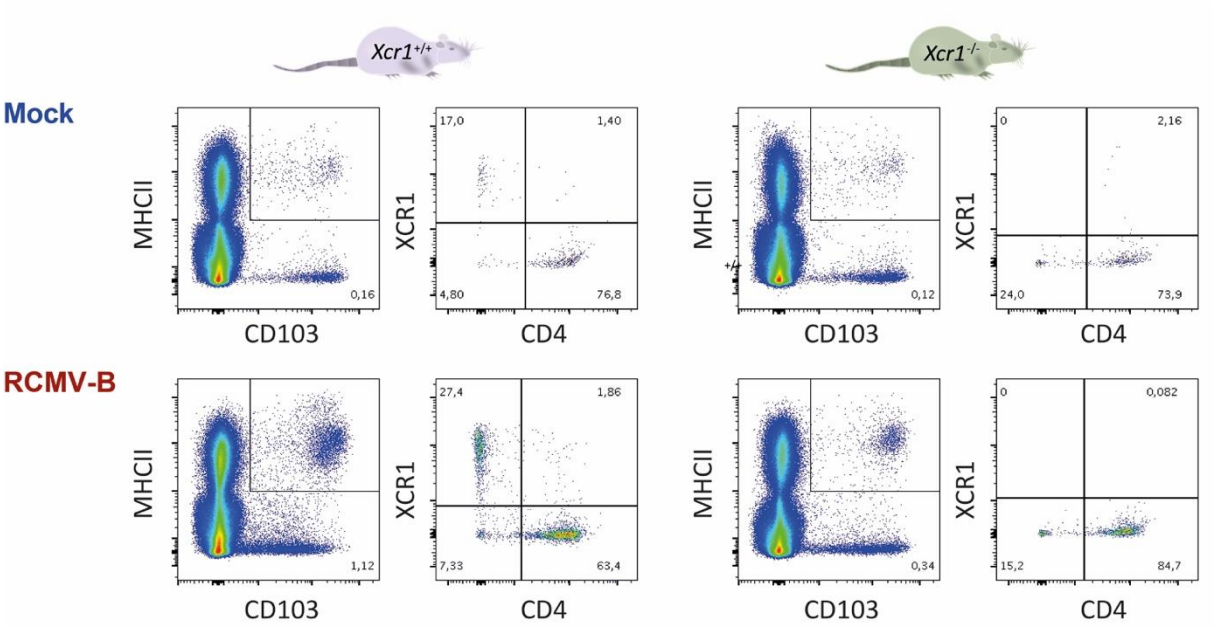

Figure 29: Dotplot of DC population within living cells at 16 dpi. 10-week-old male Sprague Dawley rats were infected with $1*10^6$ pfu of RCMV-B or 500 µl PBS (Mock) for 16 days. Leukocytes were isolated from salivary glands. After surface staining, cells were analyzed for $MHCII^+$ and $CD103^+$ expression and further gated on CD4 and XCR1 to analyze both DC subsets. Dotplot represents one of 6 biological replicates.

4.4.2.4 Ninety days post infection

After 90 days of infection most of the cell frequencies were balanced and comparable to mock-infected rats. However, in salivary glands of infected *Xcr1*$^{+/+}$ rats a maintained increased $CD8^+$ T cell frequency was determined. Interestingly, this was not the case for infected *Xcr1*$^{-/-}$ rats (Figure 30 A). Furthermore, the frequency of NKT cells in salivary glands was still higher after 90 days of infection in both *Xcr1*$^{+/+}$ rats and *Xcr1*$^{-/-}$ rats (Figure 30 B). In spleens the DC rate was, as observed for the other time points, still lower after infection (Figure 30 C).

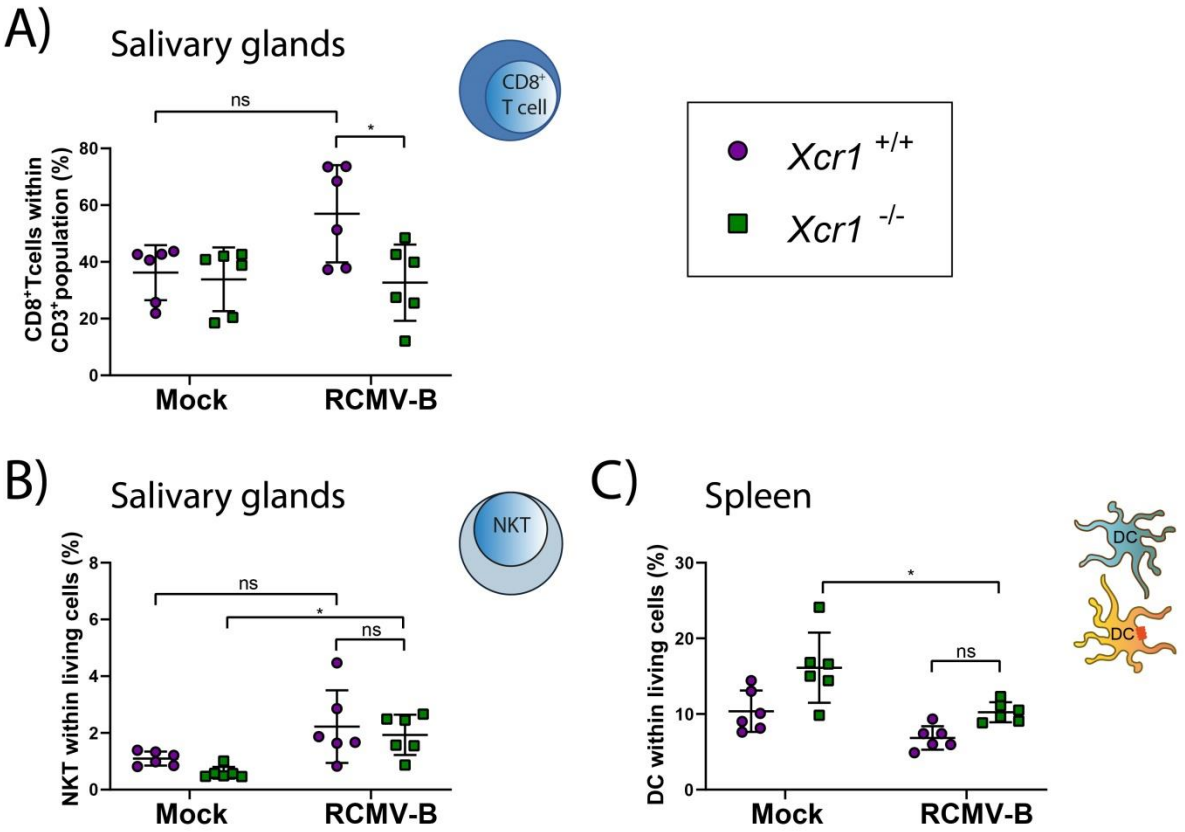

Figure 30: Frequency of leukocytes in RCMV-B and Mock infected *Xcr1*$^{+/+}$ and *Xcr1*$^{-/-}$ rats at 90 dpi. 10-week-old male Sprague Dawley rats were infected with 1*10^6 pfu of RCMV-B or 500 µl PBS (Mock) for 90 days. Leukocytes were isolated from salivary glands and spleen. After surface staining, cells were gated on DC, CD8$^+$ T cells and NKT cells. **A)** Frequency of CD8$^+$ T cells within the CD3$^+$ population in salivary glands. **B)** Frequency of NKT cells within living cells in salivary glands. **C)** Frequency DC within living cells in salivary glands. Orange: CD4$^-$ DC, turquois: CD4$^+$ DC Error bars represent mean ± SD, n = 6 rats. Data were analyzed by one-way ANOVA and Tukey's multiple comparison test (ns = not significant; * p<0.0332; ** p<0.0021; *** p<0.0002; **** p<0.00001).

4.5 Generation of a RCMV-B *vxcl1* deletion mutant

In order to perform functional analysis on RCMV-B vXCL1, a RCMV-B *vxcl1* deletion mutant was generated with the genetic engineering technique CRISPR/Cas. A vector containing Cas9 and primer sequences that recognize *vxcl1* of RCMV-B was provided by Robert Jan Lebbink (UMC Utrecht). Following limiting dilution promising mutants were cultivated and diluted again for plaque purification followed by another sequencing screening. The chosen mutant was characterized by a cytosine insertion at position 161 in *vxcl1*, resulting in a frameshift with a premature stop-codon (Figure 31 A). To verify that vXCL1 lacks translation supernatants of infected REF with different clones of the second limited dilution were tested by ELISA (Figure 31 B). Compared with positive controls including a RCMV-B stock and a supernatant of RCMV-B wt infected REF, the selected mutants had the same absorbance value as supernatants of mock-infected cells. For additional confirmation that the introduced premature stop-codon leads to a premature termination of translation, vXCL1 was measured

in REF infected with RCMV-B wt and RCMV-B Δ*vxcl1* for 24 h by intracellular staining and flow cytometry. 3 h prior to fixation cells were treated with brefeldin A to inhibit vesicular transport. RCMV-B Δ*vxcl1* showed a dim signal for vXCL1 compared to mock-infected cells, but lower than RCMV-B wt (Figure 31 C).

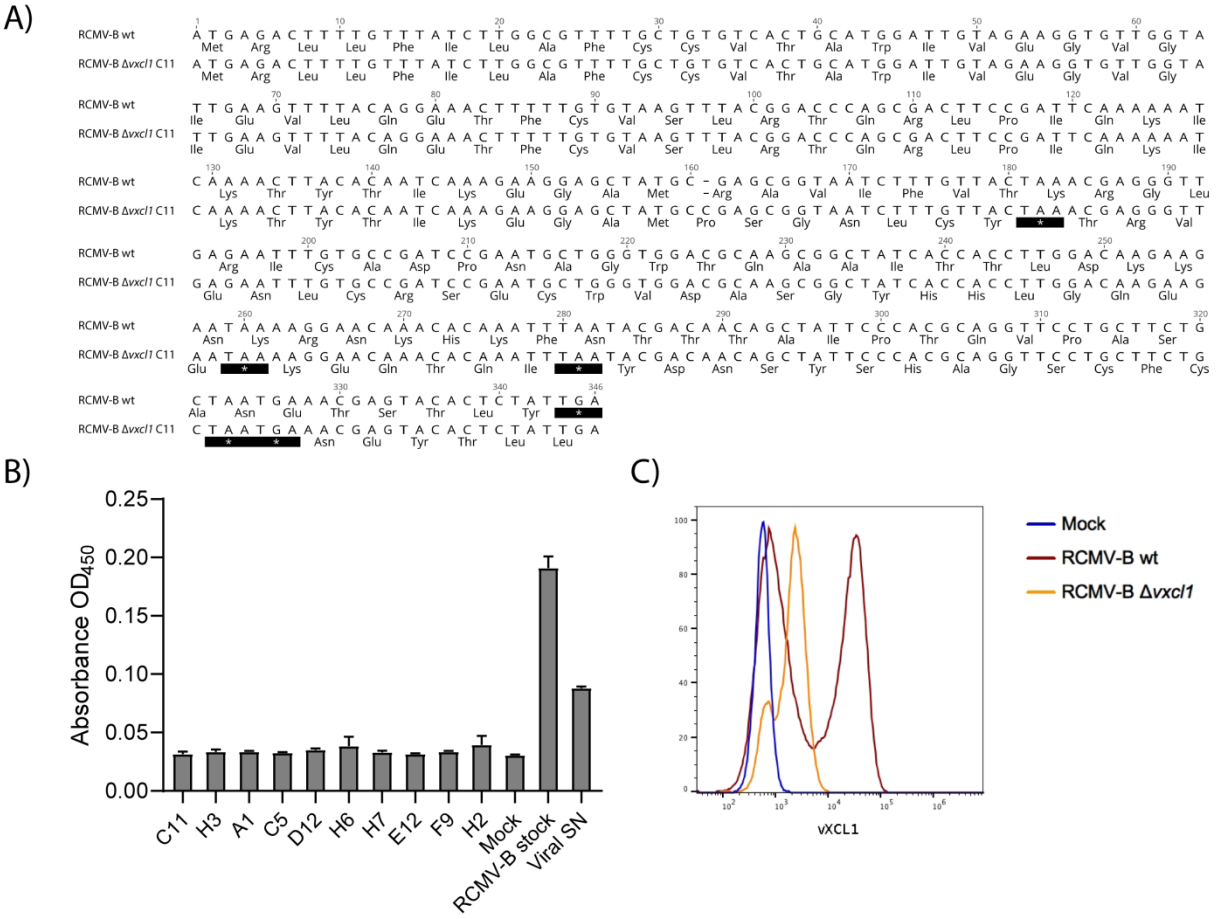

Figure 31: CRISPR/Cas generated RCMV-B Δ*vxcl1*. REF were transfected with CRISPR/Cas vectors and infected with RCMV-B wt. After double plaque purification, single plaques were sequenced and characterized. **A)** Sequence alignment of *vxcl1* from RCMV-B wt and RCMV-B Δ*vxcl1* clone C11. **B)** Supernatants (SN) of single plaques were tested in ELISA with mock-infected SN as a negative and viral SN as well as RCMV-B stock as positive controls. **C)** Intracellular staining of vXCL1 in infected REF (MOI 5, 24 hpi) with RCMV-B wt and RCMV-B Δ*vxcl1* C11.

4.6 *In vivo* infection of wildtype rats with RCMV-B wt and RCMV-B Δ*vxcl1*

4.6.1 Viral dissemination

To examine the function of vXCL1 *in vivo* and to address whether vXCL1 is used for viral dissemination, 9-week-old Lewis rats (*Xcr1*$^{+/+}$) were infected i.p. with 1*10^6 pfu of RCMV-B wt and RCMV-B Δ*vxcl1*, respectively. 16 dpi, salivary glands, liver, lung and spleen were collected for virus detection by TaqMan qPCR. The *gB/c-myc* ratio was very low (<0.001) in spleen, liver and lung of both RCMV-B wt and RCMV-B Δ*vxcl1* infected rats. The median of

RCMV-B wt was 13 fold higher than the median of RCMV-B Δ*vxcl1* in spleen, 11 fold higher in liver and 7 fold higher in the lung (Figure 32 A). In salivary glands the ratio of RCMV-B Δ*vxcl1* was low with a median of 0.001. In comparison, the median ratio of RCMV-B wt was 170 times higher (Figure 32 B). These results correspond to the plaque assay of homogenized salivary glands. Here, RCMV-B wt showed $8.2*10^3$ pfu/salivary gland, whereas for RCMV-B Δ*vxcl1* only $1.9*10^2$ pfu/salivary gland could be detected (Figure 32 C).

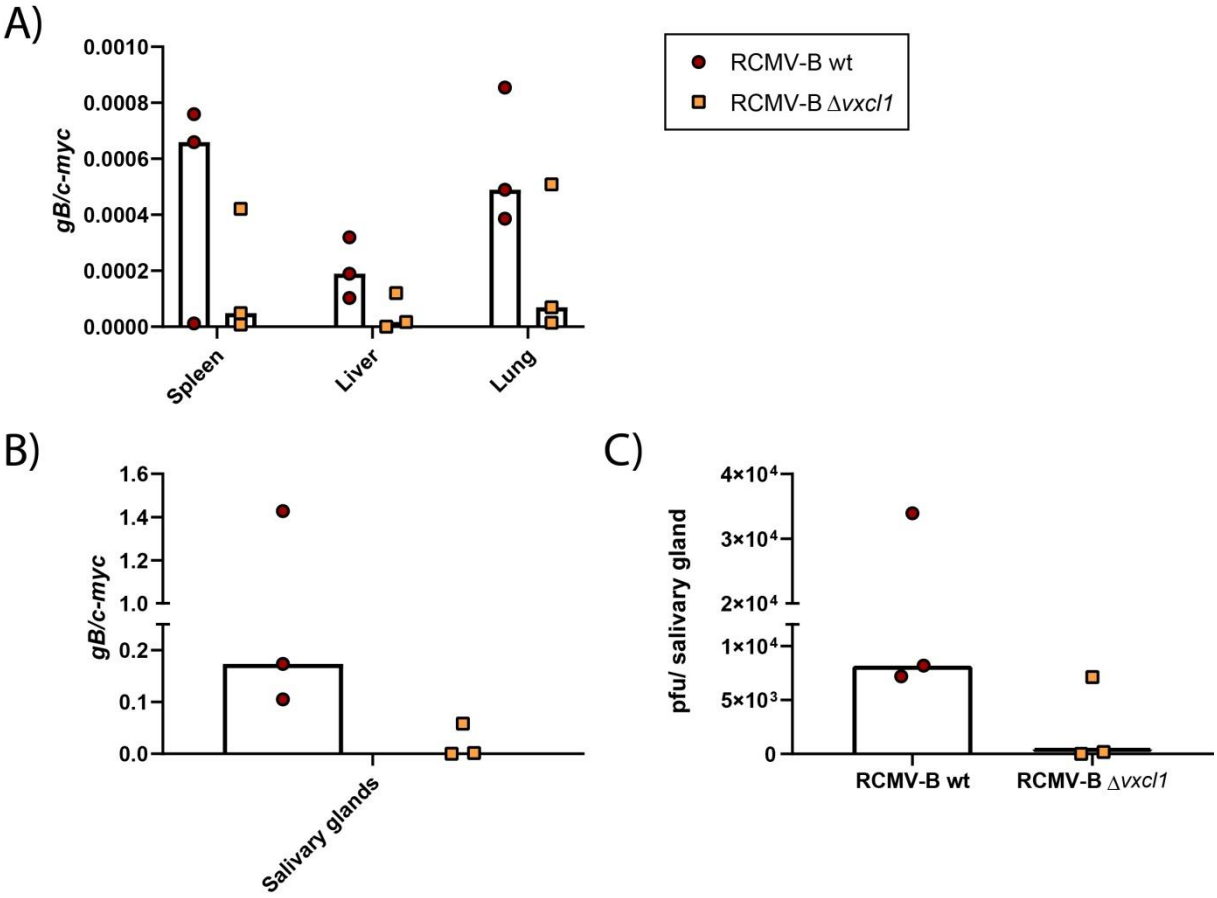

Figure 32: Detection of viral *gB* DNA after infection with RCMV-B wt and RCMV-B Δ*vxcl1*. 9-week-old male Lewis rats were infected with $1*10^6$ pfu of RCMV-B wt or RCMV-B Δ*vxcl1*, respectively. After 16 dpi, spleen, lung, liver **(A)** and salivary glands **(B)** were collected and DNA was isolated, followed by TaqMan-qPCR with specific primers and probes targeting the viral gene *gB* and host gene *c-myc*. Relative copy numbers of *gB* were normalized to the housekeeping gene *c-myc*. **C)** The left salivary gland was homogenized and diluted on REF. After 1 h cells were covered with Overlay-medium and one week later pfu were counted. Results were obtained from 3 biological replicates in technical duplicates. Bars represent the median.

4.6.2 Frequencies of leukocytes after RCMV-B wt and RCMV-B Δ*vxcl1* infection

To further investigate whether the deletion of vXCL1 has an impact on the migratory behavior of leukocytes, DC, T cells and B cells, NK cells as well as NKT cells were analyzed in blood, lymph nodes, salivary glands and spleen.

4.6.2.1 Dendritic cells

The highest DC frequency ranging from 5-6% was determined in spleen from mock- and RCMV-B Δ*vxcl1* infected animals. In comparison, the DC frequency in the spleen of RCMV-B wt infected rats was lower (3.9%, Figure 33 A).

In blood and lymph nodes there was no significant difference in DC frequency between mock-, RCMV-B wt and RCMV-B Δ*vxcl1* infected rats. In salivary glands the frequency was significantly increased from 0.08% (Mock), to 0.3% in RCMV-B wt and 0.15% in RCMV-B Δ*vxcl1* infected rats. Here, the increase in DC frequency was significantly higher in RCMV-B wt compared to RCMV-B Δ*vxcl1* infected rats (Figure 33 A).

4.6.2.2 T cells

The frequency of $CD8^+$ T cells was significantly increased to 3.1% in salivary glands of RCMV-B wt infected rats compared to Mock with 0.18% and RCMV-B Δ*vxcl1* infected rats with only 0.7% (Figure 33 B). In spleen the frequency was 2.5 higher in RCMV-B wt and 2 times higher in RCMV-B Δ*vxcl1* infected rats. In blood and lymph nodes there was no notable difference between the three groups. Infection with both virus variants did not change the frequency of $CD4^+$ T cells compared to Mock (Figure 33 C).

4.6.2.3 NK and NKT cells

NK cells were differentiated into a CD161 high ($CD161^{++}$) and low ($CD161^+$) expressing population. RCMV-B infection had no influence on the frequency of $CD161^+$ NK cells. In contrast, the $CD161^{++}$ NK population was strongly influenced by the infection.

In blood the $CD161^{++}$ frequency escalated from 3.3% (Mock) to 7.2% in RCMV-B wt and to 5.5% in RCMV-B Δ*vxcl1* infected rats (Figure 33 E). In salivary glands the frequency was increased from 0.4% (Mock) to 2% in RCMV-B wt and 0.96% in RCMV-B Δ*vxcl1* infected rats. In spleen the $CD161^{++}$ frequency doubled after infection with RCMV-B wt and RCMV-B Δ*vxcl1*.

NKT cells were as well affected by the infection. In blood the frequency of NKT cells was 2.3 and 1.75 times higher in RCMV-B wt and RCMV-B Δ*vxcl1* infected rats, respectively (Figure 33 G). In salivary glands the NKT cell frequency went up to 2.1% in RCMV-B wt infected rats which is higher than in RCMV-B Δ*vxcl1* infected rats with 0.8% and Mock with 0.3%. In spleen the rate of NKT cells increased by the factor of 2.7 and 2.2 in RCMV-B wt and RCMV-B Δ*vxcl1* infected rats, respectively.

4.6.2.4 B cells

Also B cells were influenced by RCMV-B infection. The frequency of B cells was reduced in lymph nodes by the factor of 1.6 and 1.3 in RCMV-B wt and RCMV-B Δ*vxcl1* infected rats, respectively. In spleen the reduction of B cells was more notable. There, the frequency decreased from 44.5% to 19.7% in RCMV-B wt and 26.5% in RCMV-B Δ*vxcl1* infected rats (Figure 33 F).

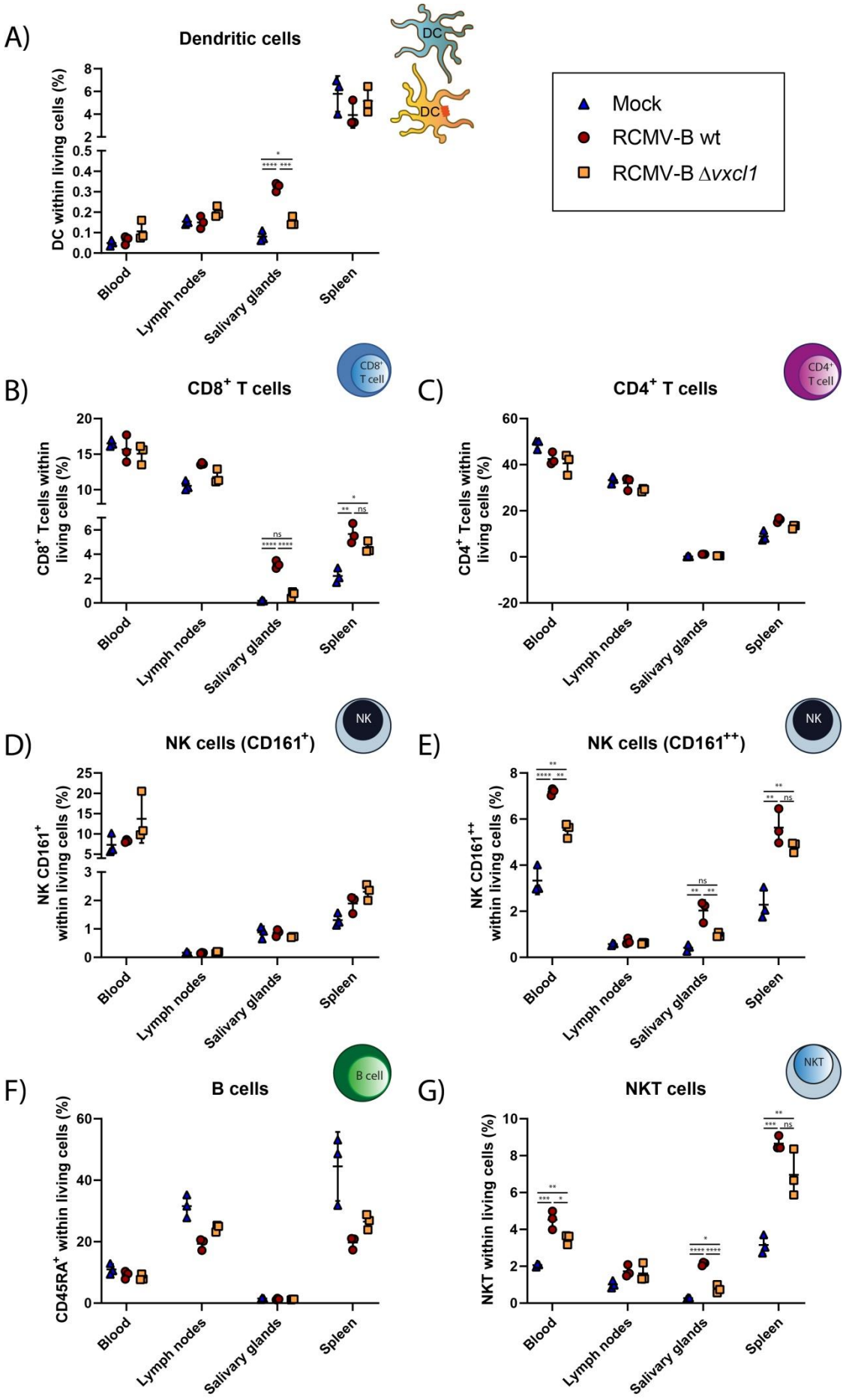
A)
Dendritic cells
DC
DC
DC within living cells (%)
Blood
Lymph nodes
Salivary glands
Spleen
Mock
RCMV-B wt
RCMV-B Δvxcl1
B)
CD8+ T cells
CD8+ T cell
CD8+ Tcells within living cells (%)
C)
CD4+ T cells
CD4+ T cell
CD4+ Tcells within living cells (%)
D)
NK cells (CD161+)
NK
NK CD161+ within living cells (%)
E)
NK cells (CD161++)
NK
NK CD161++ within living cells (%)
F)
B cells
B cell
CD45RA+ within living cells (%)
G)
NKT cells
NKT
NKT within living cells (%)

Figure 33: Frequencies of cell populations after infection with RCMV-B wt and RCMV-B Δ*vxcl1*. 9-week-old male Lewis rats were infected with $1*10^6$ pfu of RCMV-B wt or RCMV-B Δ*vxcl1*, respectively. Leukocytes were isolated from blood, lymph nodes, salivary glands and spleen. After surface staining, cells were gated to analyze dendritic cells **(A)**, $CD8^+$ T cells **(B)**, $CD4^+$ T cells **(C)**, B cells **(D)**, NK $CD161^+$ **(E)**, NK $CD161^{++}$ **(F)** and NKT cells **(G)**. Frequency within living cells is shown. Error bars represent mean ± SD, n = 3 rats. Data were analyzed by one-way ANOVA and Tukey's multiple comparison test (ns = not significant; * p<0.0332; ** p<0.0021; *** p<0.0002; **** p<0.00001).

5. Discussion

5.1 Identification of splenic rat DC subsets

DC play a crucial role in recognizing pathogens, presenting antigens and inducing immune responses. To manage these different functions DC comprise phenotypically and locally distinct subsets. The observation that DC with apparently similar functions have distinct phenotypes in lymphoid tissues versus to those in peripheral organs, complicates the classification of DC. Another complicating issue is that markers of a particular cell subset are not consistent across species (Guilliams et al. 2014, Gurka et al. 2015). According to the DC nomenclature proposed in 2014, mouse and human conventional DC (cDC) are divided into two types (cDC1 and cDC2), both originated from a common DC precursor (Guilliams et al. 2014, Naik et al. 2007). To include immature rat DC into that classification, the surface expression of different markers was investigated subsequently after enrichment. As in all mammals, rat DC lack the expression of T and B cell lineage markers. Two major DC subsets were determined: MHCII^{+} CD103^{+} CD4^{-} XCR1^{+} CD11b/c^{+} CD172a$^{(+)}$ CD54^{+} and MHCII^{+} CD103^{+} CD4^{+} XCR1^{-} CD11b/c^{+} CD172a^{+} CD54^{+} DC. A recent suggestion revealed that mouse cDC can be universally subdivided into XCR1^{+} and CD172a^{+} (SIRPα) DC (Gurka et al. 2015). In rats, however, the expression of CD4 allows the separation of the two major subsets (Liu et al. 1998). The CD4^{+} rat DC co-express CD172a and CD4^{-} DC express XCR1 (Figure 8). XCR1 is described in mouse and human as a marker for Type 1 and cross-presenting cDC (Crozat et al. 2010, Dorner et al. 2009). Cross-presenting murine DC are further characterized by the expression of CD8. In contrast, CD8 is not expressed on cross-presenting human DC and was not expressed on spleen derived rat DC (Shortman and Liu 2002, Vremec et al. 2000). Nevertheless, CD4^{-} rat DC are thought to be the equivalent to murine CD8^{+} DC (Hubert et al. 2006, Yrlid and Macpherson 2003). The expression of XCR1 on CD4^{-} DC and CD172a on CD4^{+} DC supports the idea, to classify rat CD4^{-} DC as cDC1 and CD4^{+} DC as cDC2.

In addition another two dim populations were identified with higher expression of MHCII and CD86. CD86 is a costimulatory molecule that interacts with CD28 on T cells, leading to T cell activation and tolerance. Since CD86 plays a role in antigen presentation, it is considered as a DC maturation marker (Greenwald et al. 2005, Lenschow et al. 1996). Furthermore, the MHCII^{++} CD4^{-} DC subset showed lower XCR1 expression. Reduced XCR1 expression was previously observed in mouse upon DC activation (Gurka et al. 2015). The higher CD86 and MHCII expression and the reduction of XCR1 indicate that DC become activated during the isolation and enrichment procedure.

Another interesting observation was made concerning the ratio between both DC subsets. After density centrifugation the frequency of $CD4^-$ $XCR1^+$ DC within the $CD103^+$ population was 30%, whereas the $CD4^+$ $XCR1^-$ DC frequency was 55% (Figure 7). Since DC frequencies can differ between rat strains, the comparison between species is not useful (Hubert et al. 2006). However, the relative distribution of $CD4^-$ DC and $CD4^+$ DC changed after Ox-62 microbead enrichment to 54% and 37%, respectively. Investigation of the flow through after positive selection revealed a loss of $CD4^+$ DC (data not shown). Interestingly, $CD4^-$ DC were shown to have higher expression of CD103 (Supplement 1). Despite experiments using higher amounts of microbeads the loss of the $CD4^+$ subpopulation could not be prevented. This leads to the assumption that most of the Ox-62 microbeads were bound by $CD4^-$ DC.

5.2 XCL1 is secreted by $CD161^{++}$ NK cells, NKT cells and $CD8^+$ T cells

Upon stimulation, leukocytes secrete chemokines to attract effector cells, including DC and T cells, to the site of inflammation. To complement the knowledge about the expression of the only known γ-chemokine on single cell level, XCL1 production was investigated in rats. After 5 h stimulation with ionomycin and PMA, about 20% of $CD8^+$ T cells produced XCL1. In comparison, the frequency measured in mouse was between 25% and 40% (Dorner et al. 2003). In accordance to mouse, the frequency of $CD4^+$ T cells expressing XCL1 was 3% in rats. The identification of NK cell populations was impeded, since the stimulation altered the CD161 expression. Here, the $CD3^-$ $CD161^+$ population almost completely disappeared after stimulation and, thus, could not be included in the XCL1 expression analysis. However, the frequency of XCL1 producing $CD161^{++}$ NK cells was 34% which was just the half of the frequency that was measured in BALB/c and C57BL/6 mice (Dorner et al. 2003). There are no published single cell data about XCL1 expression in NKT cells obtained from spleen. In rat spleen, however, these cells were identified as the highest XCL1 producer after stimulation with ionomycin and PMA (Figure 10). These data correspond to recent published invariant NKT cells from liver that expressed as well higher amounts of XCL1 than adaptive T cells and NK cells (Woo et al. 2018).

As already discussed for DC classification, the comparisons between species might be not useful for a better understanding of the function of rat XCL1. The different expression values between species may have several reasons, like the age of the animals or the procedure of cell isolation. Nevertheless, the most interesting issue is that leukocytes expressing XCL1 share a cytotoxic ability across species. NK cells and NKT cells represent actors of the innate immune response. Early upon infection with MCMV and Listeria NK cells were shown to release XCL1 and a set of other cytokines, including MIP-1α, MIP-1β, RANTES and IFN-γ

(Dorner et al. 2002, Dorner et al. 2004, Dorner et al. 2003). On the site of adaptive immune response, $CD8^+$ T cells dominantly secreted XCL1. This underlines the idea that DC, controlled by the XCL1-XCR1 axis, are a communication platform between innate and adaptive immune response. In addition, $XCR1^+$ DC may be the ideal communication partner for $CD8^+$ T cells, since they cross-present antigens and induce a proliferative monoclonal antigen specific T cell clone that combats pathogen infected cells (Kroczek and Henn 2012).

5.3 RCMV interference with DC

5.3.1 RCMV attracts and productively infects splenic DC *ex vivo*

DC are attracted by innate and adaptive immune cells to the site of infection to take up antigens that will be presented by MHCI or MHCII to $CD8^+$ or $CD4^+$ T cells, respectively. This migratory potential could be exploited by RCMV. On the one hand, DC could be infected and used as distribution vehicles to access other organs or cells. On the other hand, the virus could remain in DC and subvert antigen presentation to escape the immune response (Banchereau et al. 2000).

RCMV-E and RCMV-B are unique in encoding the γ-chemokine homolog vXCL1 which solely chemoattracts $XCR1^+$ DC (Bauer et al. 2020, Geyer et al. 2015, Geyer et al. 2014). Interestingly, when XCR1 is knocked out, the $CD4^-$ DC population was still attracted by RCMV-B supernatant, though with reduced frequency (Figure 11). Since chemokines are promiscuous, binding to more than one receptor (Thiele and Rosenkilde 2014), one assumption would be that vXCL1 binds to another chemokine receptor. Actually, DC chemotaxis could be mediated by several chemokine receptors, like CCR1, CCR2, CCR5, CCR6, CXCR1 and CXCR2 (Sozzani et al. 2001). However, binding studies demonstrated that recombinant rXCL1 and vXCL1 did not bind to $CD4^-$ DC from *Xcr1*$^{-/-}$ rats which proves that XCR1 is the only receptor for XCL1 (Bauer 2018). These findings suggest that RCMV encodes other chemokines that attract $CD4^-$ DC.

Chemokine mimicry is a common phenomenon among herpesviruses. Except for HCMV UL130 and Herpes simplex virus 2 gL that are described as C type chemokine hybrids (Malkowska et al. 2013, Wyrwicz and Rychlewski 2007), MuHV-8 vXCL1 is the only known C type chemokine (Geyer et al. 2014). HCMV UL130 acts as a membrane anchored ligand and is part of a cell-entry pentameric complex. This complex, additionally composed of gH, gL, UL131 and UL128, is essential for the infection of leukocytes, endothelial cells and epithelial cells (Gerna et al. 2005, Wang and Shenk 2005). A functional homolog to UL128 was identified in MCMV, m131/m129 (MCK-2), that promotes infection as part of a trimeric gH/gL/MCK-2 complex (Wagner et al. 2013). RCMV-E encoded e131/e129 (ECK-2) has the

same genomic organization as MCK-2 which consists of two syntenic ORF (Voigt et al. 2005). Hence, it is suggested that ECK-2 executes the same function as MCK-2. It was reported that MCK-2 deficient virus establishes a lower viral burden in mouse salivary glands which is the central reservoir for viral latency and transmission (Jordan et al. 2011). Consequently, MCK-2 is necessary for the infection of salivary glands but was dispensable for the infection of other organs (Fleming et al. 1999, Jordan et al. 2011). Furthermore, MCK-2 was shown to mobilize and recruit myeloid progenitor cells to facilitate viral dissemination (Noda et al. 2006). To date no specific receptor has been identified but recent studies revealed that MCK-2 is an atypical viral chemokine that binds to glycosaminoglycans (Pontejo and Murphy 2017). On this basis it appears possible that $CD4^-$ DC of *Xcr1*$^{-/-}$ rats were attracted by ECK-2. Additionally, CMV infected fibroblasts could secrete endogenous chemokines, including CCL5 (Michelson et al. 1997) that may induce DC migration. By contrast, the $CD4^+$ DC subset of both *Xcr1*$^{+/+}$ and *Xcr1*$^{-/-}$ rats was not attracted by supernatants of RCMV-B infected REF (Figure 11). Thus, it appears that RCMV, by encoding *vxcl1,* has the intention to only attract $CD4^-$ $XCR1^+$ DC. If one assumes that this population equals the cDC1 subset of Guilliam's nomenclature, it might be possible that RCMV-E evolved a strategy to directly interact with potentially cross-presenting DC which could result in a distracted antigen specific cytotoxic immune response.

The interaction with DC function is a strategy used by a number of viruses to elude the immune system. Whereas the infection with measles virus abrogates the ability of DC to stimulate the proliferation of naïve allogeneic $CD4^+$ T cells (Grosjean et al. 1997), HIV uses DC for dissemination (Wu and KewalRamani 2006). For HIV it might be more beneficial to not replicate in DC until they reach their T helper subset in which they efficiently replicate (Granelli-Piperno et al. 1999). In contrast to HIV, successful RCMV-E replication could be shown in both $CD4^-$ and $CD4^+$ DC. Since it is known that MCMV and HCMV infect DC, it was not surprising that RCMV behaves as its orthologs (Andrews et al. 2001, Jahn et al. 1999, Moutaftsi et al. 2002). RCMV-E replication was demonstrated by the identification of cytoplasmic virus factories by electron microscopy (Figure 17). Since RCMV has a broad cell tropism it was possible that both DC populations could be infected *in vitro* even though only $CD4^-$ DC were attracted by RCMV-B. Regardless of infection, the viability of DC decreased after 24 h. It is known that full matured DC die by apoptosis after interaction with other lymphocytes (Hou and Van Parijs 2004). By using DC for its own advantage RCMV might be under pressure to maintain DC viability. This was already described for MCMV that protects DC from apoptosis (Andoniou et al. 2004). However, *ex vivo* RCMV-E infection did not increase the life span of DC (Figure 14).

5.3.2 RCMV-E infection affects DC maturation and migratory ability towards rXCL1

To elucidate the relevance of RCMV infection with respect to DC function, the expression of surface proteins was investigated. After 8 hpi a transient increase of MHCII was observed which remained in mock-infected DC but decreased in DC infected with RCMV-E 16 hpi (Figure 16). In MCMV studies an upregulation was also observed for MHCI, CD40, CD54 and CD86 (Andrews et al. 2001). Additionally, UV-inactivated RCMV-E did not influence the downregulation of MHCII 16 hpi (Figure 13). Due to these findings it appears possible that the initial activation of MHCII 8 hpi was a consequence of the normal DC response to a pathogen. However, unlike other pathogens, replicating RCMV-E was able to subvert this activation, resulting in a downregulation of MHCII expression. vXCL1 had no influence on surface protein expression since RCMV-E Δ*vxcl1* showed the same effects as RCMV-E wt.

To get further insights into the relevance of vXCL1, the DC transcription profile after infection with RCMV-E wt, RCMV-E Δ*vxcl1* and UV-inactivated RCMV-E was investigated 24 hpi. Due to the annotated genome of *Rattus norvegicus* published in 2014, the transcriptome of rat DC could be analyzed by using RNA sequencing technique. This innovative technique enables the examination of molecular processes within DC during RCMV-E infection or incubation at 37°C without infection. As described above, no specific stimulus was necessary to activate DC since they become activated by the enrichment procedure. Because of this unspecific activation, freshly isolated DC with an immature phenotype were used as an input control to normalize the data. RNA sequencing revealed that incubation at 37°C (Mock) activates expression of the maturation markers CD40, CD80 and CD86, thereby proving that the isolation procedure indeed leads to DC maturation. The activation of CD40, CD80 and CD86 was impaired after infection with RCMV-E. As UV-inactivated RCMV-E had no inhibitory effect on DC maturation markers, it can be concluded that viral replication is necessary to subvert DC activation and consequently to prevent DC maturation.

A slight difference was observed between RCMV-E wt and RCMV-E Δ*vxcl1* concerning the expression of CD40 which was not completely inhibited by RCMV-E Δ*vxcl1* (Figure 20). CD40 is a member of the tumor necrosis factor receptor (TNF-R) family which activation is one of the critical signals that allows full maturation of DC. CD40 activation leads to several signal transduction pathways resulting in enhanced cell survival, cytokine secretion (IL-6, IL-12, IL10 etc.) and finally T cell activation (Banchereau and Steinman 1998, van Kooten and Banchereau 2000). The fact that the presence of vXCL1 inhibits the CD40 expression suggests that signal transduction via XCR1 could have an inhibitory effect on CD40 transcription.

During incubation at 37°C another maturation marker, CCR7, was upregulated. CCR7 upregulation is critical for the guiding of migratory maturing DC to the local draining lymph nodes, where CCR7 ligands, including CCL19 and CCL21, are secreted. As soon as DC reach the lymphoid organs, antigens are presented to T cells (Braun et al. 2011, Förster et al. 1999, Sozzani et al. 1998). Furthermore, CCR7 regulates the organization of the actin cytoskeleton, enabling migration and dendritic extension which may enhance the “capturing” of T cells for antigen presentation (Sánchez-Sánchez et al. 2006, Yanagawa and Onoé 2002). Interestingly, RCMV-E wt prevented the upregulation of CCR7 and this inhibition of CCR7 upregulation was less efficient in RCMV-E Δ*vxcl1* infected DC (Figure 20). Little is known about the transcriptional regulation of CCR7 though a positive regulation by NF-κB was described earlier (Mathas et al. 2002). Binding of vXCL1 to XCR1 would activate GPCR-adopted signaling proteins including Src family tyrosine kinases and components of the ERK1/2 and JNK3 MAP kinases (Luttrell and Lefkowitz 2002). In the cell signaling network these kinases are involved in the activation of NF-κB that regulates transcription of several cellular proteins involved in cytokine production, cellular growth and differentiation, cell survival, migration and apoptosis (Grandage et al. 2005, Kopp and Ghosh 1995, Van Antwerp et al. 1998). It appears likely that CCR7 is only one of many factors controlled by NF-κB. Inhibiting the expression of CCR7 would mean that RCMV-E prevents the migration and consequently the activation of T cells which reside in lymph nodes. Similar effects were reported for HHV-8 and HCMV that have inhibitory effects on CCR7 expression and thus subvert DC migration capacity (Cirone et al. 2012, Moutaftsi et al. 2004).

Furthermore, expression of XCR1 was significantly reduced after infection with RCMV-E wt and RCMV-E Δ*vxcl1* although the absence of vXCL1 resulted in slower receptor internalization (Figure 15). Additionally, XCR1 expression after RCMV-E UV infection was reduced as well but not as rapid as in RCMV-E wt infected cells (Figure 13). This observation suggests that replicating and inactive virus had an influence on XCR1 internalization. The increased expression of IFN-β and IFN-γ after infection with RCMV-E UV underlines the assumption that DC were stimulated by the viral particle itself (Supplement 3). It is possible that proteins from the virion surface, such as ECK-2, or tegument proteins play a notable role in that activation. Since XCR1 disappeared from the cell surface, RCMV-E wt and RCMV-E Δ*vxcl1* infected DC were not able to migrate towards recombinant rXCL1 (Figure 18).

Apart from maturation and migration markers, genes related to antigen cross-presentation were influenced by RCMV-E. Rab27 and Rac2 were upregulated upon cultivation but downregulated after RCMV-E wt and RCMV-E Δ*vxcl1* infection. Both proteins are involved in the process of phagosomal protein degradation described for antigen cross-presentation. Whereas Rab27 regulates phagosomal pH and the recruitment of the NADPH oxidase 2

(NOX2), Rac2 regulates the assembly of NOX2 to the cytosolic subunits to the phagosome (Jancic et al. 2007, Savina et al. 2009). NOX2 prevents acidification of phagosomes, limiting antigen degradation and supporting cross-presentation. The absence of Rab27 and Rac2 leads to decreased phagosomal pH resulting in enhanced proteolysis of phagocytosed antigens and thus impaired cross-presentation (Jancic et al. 2007, Mantegazza et al. 2008). Besides Rab27 and Rac2, which participate in cross-presentation, expression of Tap2 was reduced by RCMV-E wt and RCMV-E Δ*vxcl1* (Figure 20). Tap proteins deliver peptides to the ER, the place where antigens are loaded onto MHCI molecules (Suh et al. 1994).

Due to these findings, it appears that RCMV functionally paralyzes DC by hampering maturation and migration to the lymphoid tissue. Furthermore, RCMV may prevent antigen presentation, especially cross-presentation.

5.4 rXCL1 and vXCL1 induce internalization of XCR1 and hamper chemotactic activity towards rXCL1

The XCL1-XCR1 axis appears to be an attractive target for viruses since many of them evolved the ability to exploit the interaction between the γ-chemokine and its respective GPCR. Kaposi sarcoma-associated herpesvirus (KSHV) encodes two β-chemokines, vCCL-2 that acts as an antagonist and vCCL-3 that has an agonistic function on XCR1 (Lüttichau 2008, Lüttichau et al. 2007, Nicholas 2007). Furthermore, HHV-6 encodes the β-chemokine receptor U51A that interacts with XCL1 (Catusse et al. 2008). RCMV-E/ -B evolved a unique strategy to interfere with the XCL1-XCR1 axis. The vXCL1 analogs of RCMV-E and RCMV-B share an amino acid identity of 83.3%. Rat XCL1 (rXCL1) is 63.2% and 65.5% identical to RCMV-E (vXCL1 E) and RCMV-B (vXCL1 B), respectively, and differs at the N-terminus which is implicated in receptor binding and activation (Clark-Lewis et al. 1995). Indeed, previous studies revealed that vXCL1 and rXCL1 compete for XCR1 (Geyer et al. 2014). It was shown that vXCL1, compared to host rXCL1, attracts slightly higher numbers of $XCR1^+$ $CD4^-$ DC and stronger activates XCR1 (Bauer et al. 2020). Upon chemokine binding and activation GPCR internalize, a process called desensitization. It was observed that both vXCL1 variants led to a stronger reduction of XCR1 surface expression compared to rXCL1 (Figure 22). This observation supports the hypothesis that vXCL1 is a better agonist than rXCL1. Similar results have been reported for KSHV vCCL-3, a selective XCR1 agonist, whose activating potency was 10fold higher than human XCL1 (Lüttichau et al. 2007).

Chemokine receptor activation is described by a two-step mechanism. In the first step, the chemokine binds to the receptor without inducing activation. This step requires the positively charged chemokine core which binds to the negatively charged receptor domain (Thiele and Rosenkilde 2014). In the second step, receptor activation is induced which is suggested to

be facilitated by the flexible chemokine N-terminus. The core that is important for receptor binding is highly conserved in the vXCL1 variants as well as in rXCL1. In contrast, the N-terminus that induces receptor activation exhibits variable sites (Figure 21). Nevertheless, the most striking difference between the XCL1 homologs is the high variable C-terminus with two additional threonines in both vXCL1 variants that exhibit glycosylation sites. This posttranslational modification might have an impact on receptor affinity and receptor activation (Geyer et al. 2014, Mortier et al. 2011). Years ago it was suggested that the C-terminal α-helix of the cell-derived factor 1 binds glycosaminoglycans which enhanced the biological activity of the N-terminus (Luo et al. 1999). Since it was described for MCK-2 to bind glycosaminoglycans (Pontejo and Murphy 2017), this might also apply to vXCL1. To investigate the impact of the high variable C-terminus, studies with trimmed C-termini have to be performed, followed by comparative activation analysis with rXCL1.

Modifications in sequence and structure of viral homologs have likely arose during co-evolution to perfectly adapt to their hosts. This adaptation possibly leads to a higher species specificity compared to host chemokines. Indeed, it was demonstrated recently that rXCL1 crossed the species barrier by activating the human XCR1, whereas vXCL1 solely activates rat XCR1 (Bauer et al. 2020).

The disappearance of XCR1 from the DC surface after ligand-binding could impede the communication with immune cells expressing endogenous XCL1, including NK cells, NKT cells and $CD8^+$ T cells. After preincubation with vXCL1 the chemotactic activity of $CD4^-$ DC towards recombinant rXCL1 was abolished. As discussed before, cultured DC become activated which results in ligand-independent XCR1 internalization. Hence, the chemotactic activity of untreated DC towards rXCL1 was reduced as well (Figure 23). Internalization of XCR1 appears to be a part of the DC maturation process. Matured DC change their function from patrolling and taking up antigens and are recruited directly to lymphoid organs where antigens are presented to T cells (Alloatti et al. 2016). To successfully complete antigen presentation, XCR1 expression has to be reduced, otherwise DC would be attracted to another site of inflammation. In the context of vXCL1, $XCR1^+$ rat DC, assumed to cross-present antigens, would be attracted to the site of RCMV infection. RCMV infection induces functional paralysis of DC, possibly resulting in impaired antigen presentation. This strategy might be key to exclude cross-presenting DC from immune cell communication and misdirecting them to the advantage of the virus.

5.5 Infection of *Xcr1*$^{-/-}$ and *Xcr1*$^{+/+}$ rats

5.5.1 XCR1 is dispensable for RCMV-B spread

70 years ago, Frank Fenner *et al.* were the first to describe virus dissemination on the basis of Mousepox infection. They proposed a two-step dissemination model with a primary viremia in liver and spleen followed by secondary viremia causing dissemination throughout the body (Fenner 1949). This model of dissemination got widely accepted for many viruses, including CMV with salivary glands being secondary infection sites (Collins et al. 1994). i.p. infection with RCMV-B revealed high titers in liver and spleen 5 dpi (Figure 24) which was in line with i.p. infected MCMV and RCMV-M (Bruggeman et al. 1985, Collins et al. 1994). However, recent studies demonstrated that the colonization of spleen and liver appears only after i.p. or i.v. injection that do not represent natural routes of CMV infection but occur as a result of the interception of cell-free virions by local macrophages (Farrell et al. 2017, Frederico et al. 2014). In contrast, an olfactory inoculation with MCMV which parallels a natural CMV infection route was shown to omit infection of liver and spleen (Farrell et al. 2019, Sacher et al. 2011). Moreover it was shown that MCMV reaches salivary glands via DC after both i.p. and olfactory infection (Farrell et al. 2019). This suggests that the virus directly attracts DC to the site of infection regardless of the infection route.

Since RCMV-E and RCMV-B exclusively attract XCR1^{+} DC it remained to be investigated whether XCR1 is necessary for viral spread. In accordance to i.p. infection with MCMV, RCMV-M and RCMV-E, viral DNA of RCMV-B was identified in liver and spleen 5 dpi (Figure 24) (Bruggeman et al. 1985, Collins et al. 1994, Sandford et al. 2001). Interestingly, at that time point more gB copies could be detected in lung and salivary glands of *Xcr1*$^{+/+}$ rats, suggesting that XCR1 has an impact on the pace of RCMV-B spread (Figure 24).16 dpi viral DNA as well as infectious RCMV-B could be determined in salivary glands with no significant difference between *Xcr1*$^{-/-}$ and *Xcr1*$^{+/+}$ rats. However, two *Xcr1*$^{+/+}$ rats had greater viral titers whereas two *Xcr1*$^{-/-}$ rats showed much lower titers (Figure 25). Considering that CMV disseminates through blood (Collins et al. 1994), the high RCMV-B titers in salivary glands were probably supported by a high rate of blood flow through the glands which is achieved by an abundant capillary supply (Lü and Jacobson 2007). Since these experiments provides only indications for XCR1 being necessary for RCMV to reach the salivary glands, this issue needs further investigations with larger test groups.

5.5.2 RCMV-B infection leads to migration of DC, B cells, CD8$^+$ T cells, NK and NKT cells in primary infected organs

In order to get an overview of immune cell migration during RCMV-B infection and to determine the role of XCR1 in immune cell communication, cells from innate and adaptive immune system were analyzed in blood, spleen, lymph nodes and salivary glands at different time points post infection. Whereas virus detection failed at 3 dpi, a response could be determined on the cellular level (Figure 26). In spleen, the place of primary infection, higher frequencies of NK cells, NKT cells and CD8$^+$ T cells were observed. In addition, the frequency of CD8$^+$ T cells was reduced in lymph nodes while the frequency of DC was slightly elevated. This leads to the presumption that the innate immune system recognized the virus in a very early phase, followed by activation of the adaptive immune system in lymph nodes which led to the migration of CD8$^+$ T cells to the site of infection. This kind of bridging is facilitated by DC (Banchereau et al. 2000). According to the elevated viral load in spleen, frequencies of NK cells and NKT cells were increased as well two days later. In contrast, DC and B cell frequency was reduced in spleen. Since activated B cells generated in spleen migrate to the bone marrow this could lead to a reduced frequency of B cells in spleen after infection and might indicate that adaptive immunity is activated by 5 dpi. Furthermore, antigen-bearing DC could leave the spleen to migrate to lymph nodes where ingested antigens are presented. Surprisingly, higher amounts of NK and NKT cells were detected in lymph nodes, leading to the presumption that RCMV colonizes these organs as well. Indeed, Farrell *et al.* demonstrated that MCMV-infected DC reach the blood via lymph nodes (Farrell et al. 2017). Moreover, it has been suggested that the main location of NK-DC interactions might be sites of inflammation and lymph nodes (Cooper et al. 2004). Unfortunately, lymph nodes from *Xcr1*$^{+/+}$ and *Xcr1*$^{-/-}$ rats were not investigated for RCMV infection.

5.5.3 RCMV-B infection leads to increased frequency of DC, CD8$^+$ T cells, NK cells and NKT cells in the salivary glands

After 16 dpi RCMV-B was detected in salivary glands. Salivary glands represent a very attractive site for the virus to become latent since reactivation would pour out virions into the saliva followed by smear transmission, even though no oral target cells have been identified to date (Farrell et al. 2019). Besides the determination of viral titers, the immune cells that migrated to salivary glands after infection were examined. As expected, higher amounts of NK cells and NKT cells were found. Compared to *Xcr1*$^{-/-}$ rats, more NK cells and NKT cells were found in salivary glands and blood of *Xcr1*$^{+/+}$ rats. Mostly interesting was that also the frequency of DC was higher in *Xcr1*$^{+/+}$ salivary glands which corresponded to the chemotaxis assay performed *ex vivo* in which DC isolated from *Xcr1*$^{-/-}$ rats migrated in lower numbers

(Figure 11). This again raised the question whether there is another chemokine or chemokine receptor encoded by RCMV that attracts DC to the site of infection. Furthermore, strong elevated amounts of $CD8^+$ T cells were determined in salivary glands. NK cells, NKT cells as well as $CD8^+$ T cells were shown to produce XCL1 after stimulation *ex vivo* (Figure 10). Therefore, these cells might reach the salivary glands first where they secrete XCL1 to attract $XCR1^+$ DC. This scenario could explain why the attraction of DC in *Xcr1*$^{-/-}$ rats was not as successful as in *Xcr1*$^{+/+}$ rats (Figure 29). Paradoxically, the absence of XCR1 influences the migration of NK cells and NKT cells to the salivary glands as well. In contrast, the frequency of $CD8^+$ T cells has trebled after infection, regardless of XCR1 expression. The rapidity with which viral spread and immune cell migration occurs makes intermediate events hard to capture. To gain a more complete picture of the immunological processes caused by RCMV-B, time points should be chosen in a 24 h rhythm.

Furthermore, only in *Xcr1*$^{+/+}$ rats the frequency of $CD8^+$ T cells remained elevated at 90 dpi (Figure 30). In MCMV infected mice, primed $CD8^+$ T cells could be isolated from salivary glands. Nevertheless, in spite of the adaptive cytotoxic immune response, MCMV could not be eliminated from the host (Campbell et al. 2008). These data correspond to our findings, since still low ratios of RCMV-B DNA could be determined after 90 dpi (Figure 24).

In contrast to $CD8^+$ T cells, the amount of $CD4^+$ T cells remained unchanged during infection (Supplement 11). However, $CD4^+$ T cells are known to play a role in clearing replicating MCMV in later phases of infection (Cavanaugh et al. 2003, Holtappels et al. 2008, Jonjić et al. 1990).

Taken together, XCR1 seems to impact the pace of viral dissemination and plays a role in the attraction of cytotoxic innate immune cells and the maintenance of cytotoxic adaptive immune cells in the salivary glands.

5.6 vXCL1 plays a pivotal role in RCMV-B dissemination and immune cell migration

To examine the role of vXCL1 on viral dissemination, a *vxcl1* deletion mutant of RCMV-B was generated to perform functional analysis of vXCL1 *in vivo*. The deletion mutant contains an insertion of cytosine at position 161 of *b156.5* (*vxcl1*) which leads to a frameshift and a premature stop codon. Whereas *vxcl1* mRNA is transcribed in RCMV-B ∆*vxcl1* (data not shown), no vXCL1 protein is being secreted (Figure 31). Interestingly, vXCL1 could still be intracellularly shown in RCMV-B ∆*vxcl1* infected REF (Figure 31), suggesting that the antibody recognizes an epitope among the first 60 amino acids which are still produced. Since vXCL1 could be detected neither with Western Blot nor ELISA in supernatants of

RCMV-B Δ*vxcl1* infected REF, it can be concluded that the shortened protein is not secreted and is likely degraded by the cellular proteasome. In addition, loss of function was confirmed by chemotaxis assay where supernatants of RCMV-B Δ*vxcl1* infected REF were unable to attract XCR1$^+$ DC (Kelch 2020).

To analyze the function of vXCL1 *in vivo*, Lewis rats were infected with RCMV-B wt and RCMV-B Δ*vxcl1*. To monitor viral access to the salivary glands, animals were analyzed at 16 dpi. In contrast to XCR1-deleted animals where RCMV-B infection had no influence on viral DNA loads, the absence of vXCL1 showed greatly reduced viral DNA loads in spleen, liver, lung and especially salivary glands. Titration of salivary glands on REF revealed that RCMV-B Δ*vxcl1* scarcely formed plaques (Figure 32). Therefore, it can be assumed that the virus did not reach the salivary glands. *Ex vivo* reactivation experiments at 16 dpi underlined these findings and demonstrated that RCMV-B wt could be reactivated already 4-6 days post organ removal whereby RCMV-B Δ*vxcl1* reactivated first after 15-28 days (Kelch 2020). Possibly, the deletion mutant could have been defeated by the innate and adaptive immune cells at an earlier time point. Indeed, in spleen elevated frequencies of NK cells, NKT cells and CD8$^+$ T cells were determined (Figure 33). However, the number of these cell populations in the spleen of RCMV-B Δ*vxcl1* infected rats was lower. This supports the idea that the absence of vXCL1 hampers viral transport to the spleen. Alternatively, if replicating virus had been successfully cleared by immune cells, the immune response could have been abated after 16 days of infection. Those questions remain to be investigated.

In line with data obtained from infection experiments in *Xcr1*$^{-/-}$ rats the frequency of NK cells and NKT cells was significantly less elevated in salivary glands of RCMV-B Δ*vxcl1* compared to RCMV-B wt infected *Xcr1*$^{+/+}$ rats. However, whereas the absence of XCR1 had no significant influence on viral load in salivary glands, the lower frequency of NK cells and NKT cells was accompanied with lower titers of RCMV-B Δ*vxcl1*. According to data obtained from infected *Xrcr1*$^{-/-}$ rats, the absence of vXCL1 resulted in reduced DC migration to salivary glands of infected rats. Thus, vXCL1-XCR1 communication appears to be necessary for DC to migrate to the salivary glands after RCMV-B infection. Furthermore, the lower frequency of DC was consistent with lower RCMV-B Δ*vxcl1* titers. It was striking that the migration of CD8$^+$ T cells to the salivary glands was almost undetectable when vXCL1 was not present. This stands in contrast to results obtained with the XCR1 knockout rat where no reduced CD8$^+$ T cell migration was observed. T cells become attracted by several chemokines, including CCL5 (RANTES) (Hidi et al. 2000) that are produced by monocyte-derived DC and NKT cells in inflamed tissue (Faunce and Stein-Streilein 2002, Zhu et al. 2000). On the basis of the low RCMV-B Δ*vxcl1* titers, it can be assumed that T cell migration requires infectious particles.

The lower frequencies of immune cells in salivary glands of RCMV-B Δ*vxcl1* infected rats appear to be a consequence of impaired viral dissemination due to the absence of vXCL1.

In conclusion, vXCL1 is indispensable for successful dissemination of RCMV-B. However, the mechanism resulting in failure of viral dissemination needs further investigation. Three possibilities can be imagined: 1) vXCL1 is needed to attract DC which are used to reach the spleen; 2) vXCL1 attracts DC to the spleen and RCMV infects them for productive amplification; 3) Viral replication occurs in other cells of the spleen which secrete vXCL1 attracting DC. Attracted DC could become infected by RCMV and be used as a transport vehicle to reach the salivary glands.

Besides all these indications, it still remains to be examined whether RCMV uses DC as a transport vehicle to reach salivary glands. Unfortunately, the detection of IE1 in salivary gland DC failed (data not shown). However, if RCMV reaches salivary glands using XCR1$^+$ DC as a vehicle, the question arises how DC become manipulated by RCMV to reach the site of secondary infection. What are the molecular mechanisms to misdirect a cell? The capacity of DC to migrate first to the site of infection and then to the draining lymph nodes is crucial for their function. Basically, cell recruitment occurs in response to stimuli like type 1 IFN and chemokines that interact with specific chemokine receptors (Biron et al. 1999). Immature DC express receptors including XCR1, CCR1, CCR2 and CCR5 which enable migration to inflamed tissue where XCL1, CCL5/RANTES, CCL4, CCL3 and CCL2 are secreted (Dorner et al. 2004, Frascaroli et al. 2006). Upon DC maturation the inflammation-associated chemokine receptors (CCR1, CCR5 and CCR6) are downregulated whereas CCR7-mediated migration to the lymph nodes is upregulated (Sallusto et al. 1999). The RCMV-E-induced inhibition of CCR7 upregulation is one possibility how migration routes of DC could be changed. In that regard, HCMV was shown to downregulate CCR1 and CCR5 in infected DC which suggests another strategy to influence DC migration (Varani et al. 2005).

5.7 Proposed model of RCMV interference with the XCL1-XCR1 axis *in vivo*

Many data have been published on CMV infection, dissemination and immune evasion strategies (Farrell et al. 2019, Miller-Kittrell and Sparer 2009, Mocarski et al. 2013). However, RCMV-E and RCMV-B are the only known viruses to encode the γ-chemokine homolog vXCL1 (Geyer et al. 2014). Thus, RCMV-B and RCMV-E evolved an exclusive strategy to explicitly interact with XCR1$^+$ DC that are the only known cells to cross-present antigen (Bachem et al. 2010, Bachem et al. 2012). The data presented in this work are divided in an *ex vivo* and *in vivo* part, thus connections between these parts are only speculative.

In *ex vivo* experiments it was demonstrated that RCMV-B chemoattracts solely CD4$^-$ DC. At first glance, it might not be beneficial for the virus to attract a powerful antigen presenting cell subset. However, in *ex vivo* infections it was revealed that RCMV-E is able to infect and successfully replicate in DC. RCMV-E infection induced downregulation of maturation markers and changed the migration behavior towards rXCL1. Furthermore, genes related to antigen presentation were downregulated. These findings are in line with studies of MCMV infected DC (Andrews et al. 2001). vXCL1 had no influence on the infection and replication *ex vivo*, suggesting that vXCL1 exerts exclusively an *in vivo* function that cannot be investigated *ex vivo*. Nevertheless, RNA sequencing of infected DC revealed slight differences between RCMV-E wt and RCMV-E Δ*vxcl1* in the expression of several genes including CD40 and CCR7. The activation of XCR1 and the following signaling cascade might be involved in the regulation of the respective genes.

Since CD4$^-$ DC of *Xcr1*$^{-/-}$ rats were still attracted by supernatants of RCMV-B-infected REF the question arose whether there might be another viral chemokine that influences this respective cell population. To investigate XCR1 and vXCL1 independently, *Xcr1*$^{-/-}$ rats were infected with RCMV-B wt and wild type rats were infected with a RCMV-B *vxcl1* deletion mutant. Whereas deletion of XCR1 has an impact on the pace of RCMV dissemination, the absence of vXCL1 led to an almost completely prevention of dissemination. This underlines the idea, that vXCL1 might act through another surface-protein or –molecule expressed on CD4$^-$ DC. To date there is no evidence that vXCL1 has another interaction partner, though it is known for viruses to encode promiscuous chemokines as well as chemokine binding proteins (Murphy 2001, Thiele and Rosenkilde 2014). The HCMV chemokine binding protein pUL21.5 binds CCL5/RANTES, blocking the interaction with its cellular receptor (Wang et al. 2004). The question whether vXCL1 has another interaction partner, including host chemokines, requires further investigations.

MCMV does not encode *vxcl1*, but it was demonstrated that M33, a viral chemokine receptor, and MCK-2 ensure infection of DC and myeloid progenitor cells, respectively, and delivery of viral particles to salivary glands (Farrell et al. 2019, Jordan et al. 2011, Noda et al. 2006). The HCMV homolog UL33 was shown to heterodimerize with CCR5 and CXCR4 which facilitates the interaction with DC (Tadagaki et al. 2012). Since disrupting the GPCR homolog of RCMV-M (R33) also reduces infection of salivary glands (Beisser et al. 1998b), a conserved function can be assumed for RCMV-E E33 and RCMV-B B33. However, Farrell et al. did not exclude that random DC migration could also initiate salivary gland infection (Farrell et al. 2017, Farrell et al. 2019). An infection of randomly migrated DC would be unlikely for RCMV-E and RCMV-B since they encode a chemokine that exclusively attracts XCR1$^+$ DC.

Most of investigated CMV species are known to infect many other cells than DC including granulocytes, monocytes and endothelial cells (Revello and Gerna 2010) which were all shown to facilitate CMV dissemination (Sacher et al. 2011, van der Strate et al. 2003). Since CMV has a broad cell tropism, it is possible that CMV uses more than one cell population to reach their shedding site. However, this would mean that CMV must have an accurate time management to evade the immune responses.

In terms of viral time management, a model is proposed of how RCMV-B and immune cells could interact with each other. Early post infection high numbers of innate immune cells (NK cells and NKT cells) were found at sites of RCMV-B infection. The attraction to the site of infection could have been mediated by resident DC and other cell types that produce cytokines and chemokines as a response to infection (Cooper et al. 2004, Lande et al. 2003). During infection activated NK cells produce a number of cytokines and chemokines that attract patrolling DC to the inflamed tissue (Moretta 2002). These chemokines include XCL1 that attracts $XCR1^+$ DC. During RCMV infection, $XCR1^+$ DC could be attracted by vXCL1 before DC encounter NK cell-secreted XCL1. After becoming infected, DC chemotaxis could have been induced by different chemokines including CCL4, CCL5, CCL22 (Cooper et al. 2001, Robertson 2002). RCMV could then reprogram DC by suppressing the transcription of chemokine receptors, e.g., CCR7 which would prevent migration to lymph nodes and activate other receptors that support migration to salivary glands. Following the infection of salivary glands by DC one could assume that $CD8^+$ T cells, previously primed in the lymph nodes, reach the site of secondary infection. In addition, migration and maybe even the priming of $CD8^+$ T cells was driven by high viral titers. When RCMV-B Δ*vxcl1* dissemination was reduced, $CD8^+$ T cells were hardly detected in salivary glands. In contrast, the frequency of $CD8^+$ T cells was only slightly reduced in spleen after RCMV-B Δ*vxcl1* infection (Figure 33), leading to the assumption that the deletion mutant was cleared by recruited CTL in the spleen. Interestingly, although primed $CD8^+$ T cells could be found in MCMV-infected salivary glands, the virus could not be cleared from the tissue and MCMV became latent (Campbell et al. 2008). These findings correspond to RCMV-B wt whose DNA was still detectable at 90 dpi (Figure 24). Unfortunately, it still cannot be definitely answered how CMV hides from the immune response.

In conclusion, the proposed model in Figure 34 demonstrates that migration of immune cells to infection sites is temporally separated. It is suggested that RCMV-B vXCL1 attracts $XCR1^+$ DC before the latter become attracted by NK cell-secreted XCL1. As part of the second phase of infection, eventually infected DC become enticed by NK cells and NKT cells in salivary glands. Finally, primed $CD8^+$ T cells get lured to the site of secondary infection. In the case of a RCMV-B Δ*vxcl1* infection, viral dissemination was hampered resulting in a

reduced recruitment of immune cells to the salivary glands. This model suggests that vXCL1 plays a crucial role for DC attraction and dissemination to the salivary glands.

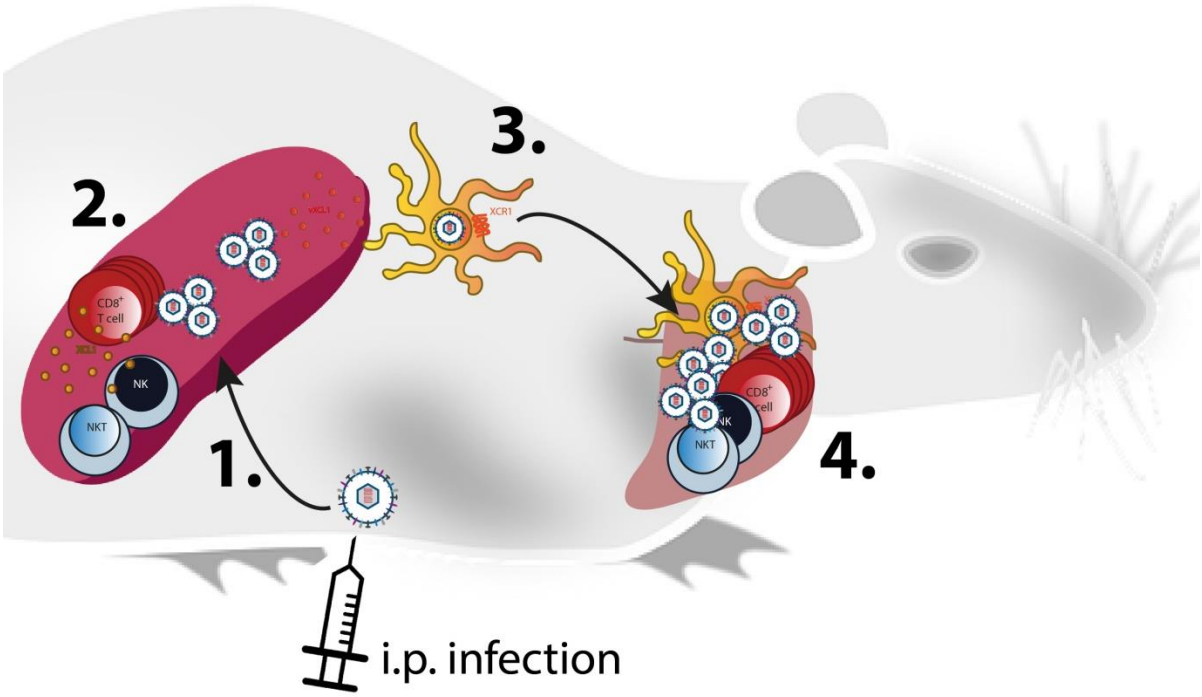

Figure 34: Proposed model of the interplay between RCMV and immune cells. 1. Following an i.p. infection RCMV disseminates to the spleen (primary infection). **2.** XCR1$^+$ DC are attracted by vXCL1 before NK cells, NKT cells and CD8$^+$ T cells co-localize with RCMV in the spleen and secrete XCL1. **3.** Infected XCR1$^+$ DC are used as a transport vehicle to reach the salivary glands. **4.** NK cells and NKT cells are recruited to infected salivary glands. Infected DC reach salivary glands followed by the attraction of primed CD8$^+$ T cells. Although innate and adaptive immune cells are alarmed, RCMV replication is not halted and the virus achieves latency.

5.8 Conclusion

The two MuHV-8 isolates RCMV-B and RCMV-E are the only known viruses that encode the γ-chemokine vXCL1 (Geyer et al. 2014). Since CMV is strict species-specific, rats were used as an animal model to analyze RCMV infection and vXCL1 functionality. However, most of immunological studies were conducted in the mouse model. Comparisons between species have to be made with caution since cell phenotypes and functions differ for similar occurring cell populations (Yrlid and Macpherson 2003). The same applies to comparisons between CMV species (Rölle and Olweus 2009). Due to millions of years of co-evolution the immune response has adjusted to immune-modulating viruses. It is speculated that MCMV and RCMV originated from a common progenitor but evolved differently during the separation of mouse and rats millions of years ago. Therefore, it is obvious that both virus species evolved different strategies to subvert their host's immune response. Nevertheless, both species appear to target DC (Farrell et al. 2017, Geyer et al. 2014). Actually, DC can be infected by a wide range of viruses, even in the absence of a specific receptor. It is proposed that this is

rather a strategy by the host, promoting antiviral cytotoxic T cell response (Freigang et al. 2005). However, during the long-lasting co-evolution CMV evolved many strategies to subvert this response. The “cat-and-rat” game between the immune response and CMV could improve evading mechanisms of the virus. On the contrary, it could induce the development of new immune response strategies to fight the virus. This would mean that the evolution of our immune system is driven by viruses like CMV.

6. Summary

To date, the two Rat Cytomegalovirus (RCMV) isolates RCMV-England (RCMV-E) and RCMV-Berlin (RCMV-B) are the only known viruses that encode a homolog of XCL1, a γ-chemokine adopted by viral piracy to interfere with the host's chemokine network. Like its host homolog, vXCL1 exclusively attracts dendritic cells (DC) that express the XC chemokine receptor 1 (XCR1).

In this work, it was investigated whether RCMV misuses the XCL1-XCR1 axis to infect DC in order to disseminate within the host. Initially, rat DC phenotyping revealed two major DC populations, $XCR1^+$ $CD4^-$ DC and $XCR1^-$ $CD4^+$. It could be shown that supernatants of RCMV-infected rat embryonic fibroblasts solely attracted the $XCR1^+$ $CD4^-$ population. Moreover, RCMV was able to infect and replicate in DC.

Due to digestion of the spleen and leukocyte enrichment DC became activated leading to full maturation 24 h after cell isolation. During infection, RCMV inhibited the upregulation of several maturation markers including CD40, CD86 and CCR7 and also led to reduced expression of MHCII, CD4 and XCR1. Regardless of vXCL1, RCMV appears to paralyze DC functionality by downregulating maturation genes.

In order to analyze the role of XCR1 and vXCL1 function *in vivo*, $Xcr1^{+/+}$ and $Xcr1^{-/-}$ rats were infected with RCMV-B wt and RCMV-B Δ*vxcl1*. Whereas the XCR1 expression level had an influence on the pace of RCMV-B wt dissemination to the salivary glands, the absence of vXCL1 led to a strong decrease in viral spread. DC migration to the salivary glands was dependent on vXCL1 as well as XCR1 and was markedly reduced when vXCL1 and XCR1 were not present. During infection, $CD8^+$ T cells were recruited to the salivary glands, however, this migration was missing when $Xcr1^{+/+}$ rats were infected with RCMV-B Δ*vxcl1*.

In conclusion, RCMV has the ability to infect DC regardless of vXCL1 expression. RCMV uses vXCL1 to attract $XCR1^+$ DC which appears to be important for viral dissemination to the salivary glands.

7. Zusammenfassung

Bis heute sind die beiden Ratten-Cytomegalovirus (RCMV)-Isolate RCMV-England (RCMV-E) und RCMV-Berlin (RCMV-B) die einzig bekannten Viren, die ein Homolog von XCL1 kodieren, einem γ-Chemokin, das vom Virus kopiert wurde um das Chemokin-Netzwerk des Wirts zu beeinträchtigen. Wie das Wirtshomolog lockt vXCL1 ausschließlich dendritische Zellen (DC) an, die den XC-Chemokinrezeptor 1 (XCR1) exprimieren.

In dieser Arbeit wurde untersucht, inwieweit RCMV die XCL1-XCR1-Achse nutzt, um DC zu infizieren und sich im Wirt auszubreiten. Durch die Phänotypisierung von Ratten-DC konnten zwei Hauptpopulationen identifiziert werden, $XCR1^+$ $CD4^-$ und $XCR1^-$ $CD4^+$ DC. Es konnte gezeigt werden, dass Überstände von RCMV-infizierten embryonalen Rattenfibroblasten ausschließlich die $XCR1^+$ $CD4^-$ Population anlocken. Darüber hinaus konnte nachgewiesen werden, dass RCMV DC infiziert und in diesen repliziert.

Durch den Verdau der Milz und die Leukozyten Anreicherung wurden die DC aktiviert, was zu einer vollständigen Reifung 24 h nach der Zell Isolierung führte. Während der Infektion inhibierte RCMV die Hochregulation mehrerer Reifungsmarker, einschließlich CD40, CD86 und CCR7 und führte zu einer verringerten Expression von MHCII, CD4 und XCR1. Unabhängig von vXCL1 scheint RCMV die DC-Funktionalität durch das Herunterregulieren von Reifungsgenen zu lähmen.

Um die Rolle von XCR1 und die Funktion von vXCL1 *in vivo* zu analysieren, wurden *Xcr1*$^{+/+}$ und *Xcr1*$^{-/-}$ Ratten mit RCMV-B wt und RCMV-B Δ*vxcl1* infiziert. Während das XCR1-Expressionsniveau einen Einfluss auf die Geschwindigkeit der RCMV-Verbreitung in den Speicheldrüsen hatte, führte das Fehlen von vXCL1 zu einer starken Abnahme der Virusausbreitung. Die DC-Migration in die Speicheldrüsen war sowohl von vXCL1 als auch von XCR1 abhängig und war deutlich reduziert, wenn vXCL1 und XCR1 nicht vorhanden waren. Während der Infektion wurden $CD8^+$ T-Zellen in die Speicheldrüsen rekrutiert. Diese Migration blieb jedoch aus, wenn *Xcr1*$^{+/+}$ Ratten mit RCMV-B Δ*vxcl1* infiziert wurden.

Zusammenfassend besitzt RCMV die Fähigkeit DC unabhängig von der vXCL1-Expression zu infizieren. RCMV verwendet vXCL1, um $XCR1^+$ DC anzulocken, was entscheidend für die Virusausbreitung in die Speicheldrüsen zu sein scheint.

8. Bibliography

Alcami A. 2003. Viral mimicry of cytokines, chemokines and their receptors. Nature Reviews Immunology 3:36-50.

Alloatti A, Kotsias F, Magalhaes JG, Amigorena S. 2016. Dendritic cell maturation and cross-presentation: timing matters! Immunological Reviews 272:97-108.

Andoniou CE, Andrews DM, Manzur M, Ricciardi-Castagnoli P, Degli-Esposti MA. 2004. A novel checkpoint in the Bcl-2–regulated apoptotic pathway revealed by murine cytomegalovirus infection of dendritic cells. The Journal of Cell Biology 166:827-837.

Andrews DM, Andoniou CE, Granucci F, Ricciardi-Castagnoli P, Degli-Esposti MA. 2001. Infection of dendritic cells by murine cytomegalovirus induces functional paralysis. Nature Immunology 2:1077-1084.

Austyn JM. 1996. New insights into the mobilization and phagocytic activity of dendritic cells. Journal of Experimental Medicine 183:1287-1292.

Bachem A, Güttler S, Hartung E, Ebstein F, Schaefer M, Tannert A, Salama A, Movassaghi K, Opitz C, Mages HW. 2010. Superior antigen cross-presentation and XCR1 expression define human CD11c+ CD141+ cells as homologues of mouse CD8+ dendritic cells. Journal of Experimental Medicine 207:1273-1281.

Bachem A, Hartung E, Güttler S, Mora A, Zhou X, Hegemann A, Plantinga M, Mazzini E, Stoitzner P, Gurka S. 2012. Expression of XCR1 characterizes the Batf3-dependent lineage of dendritic cells capable of antigen cross-presentation. Frontiers in Immunology 3:214.

Bacon K, Baggiolini M, Broxmeyer H, Horuk R, Lindley I, Mantovani A, Matsushima K, Murphy P, Nomiyama H, Oppenheim J. 2003. Chemokine/chemokine receptor nomenclature. Cytokine 21:48-49.

Banchereau J, Briere F, Caux C, Davoust J, Lebecque S, Liu Y-J, Pulendran B, Palucka K. 2000. Immunobiology of dendritic cells. Annual Review of Immunology 18:767-811.

Banchereau J, Steinman RM. 1998. Dendritic cells and the control of immunity. Nature 392:245-252.

Bauer A. 2018. Functional analysis of the interaction between Rat Cytomegalovirus-encoded vXCL1 and XCR1+ dendritic cells. Doctoral Thesis. Freie Universität Berlin.

Bauer A, Madela J, Berg C, Daugvilaite V, Gurka S, Mages HW, Kroczek RA, Rosenkilde MM, Voigt S. 2020. Rat cytomegalovirus-encoded γ-chemokine vXCL1 is a highly adapted, species-specific agonist for rat XCR1-positive dendritic cells. Journal of Cell Science 133.

Beck K, Meyer-König U, Weidmann M, Nern C, Hufert FT. 2003. Human cytomegalovirus impairs dendritic cell function: a novel mechanism of human cytomegalovirus immune escape. European Journal of Immunology 33:1528-1538.

Beck S, Barrell BG. 1988. Human cytomegalovirus encodes a glycoprotein homologous to MHC class-I antigens. Nature 331:269-272.

Beisser PS, Kaptein SJ, Beuken E, Bruggeman CA, Vink C. 1998a. The Maastricht strain and England strain of rat cytomegalovirus represent different betaherpesvirus species rather than strains. Virology 246:341-351.

Beisser PS, Vink C, Van Dam JG, Grauls G, Vanherle SJ, Bruggeman CA. 1998b. The R33 G protein-coupled receptor gene of rat cytomegalovirus plays an essential role in the pathogenesis of viral infection. Journal of Virology 72:2352-2363.

Bendelac A, Rivera MN, Park S-H, Roark JH. 1997. Mouse CD1-specific NK1 T cells: development, specificity, and function. Annual Review of Immunology 15:535-562.

Biron CA, Nguyen KB, Pien GC, Cousens LP, Salazar-Mather TP. 1999. Natural killer cells in antiviral defense: function and regulation by innate cytokines. Annual Review of Immunology 17:189-220.

Braun A, Worbs T, Moschovakis GL, Halle S, Hoffmann K, Bölter J, Münk A, Förster R. 2011. Afferent lymph–derived T cells and DCs use different chemokine receptor CCR7–dependent routes for entry into the lymph node and intranodal migration. Nature Immunology 12:879.

Brinkman CC, Rouhani SJ, Srinivasan N, Engelhard VH. 2013. Peripheral tissue homing receptors enable T cell entry into lymph nodes and affect the anatomical distribution of memory cells. The Journal of Immunology 191:2412-2425.

Bruggeman C, Meijer H, Bosman F, Van Boven C. 1985. Biology of rat cytomegalovirus infection. Intervirology 24:1-9.

Bruggeman C, Meijer H, Dormans P, Debie W, Grauls G, Van Boven C. 1982. Isolation of a cytomegalovirus-like agent from wild rats. Archives of Virology 73:231-241.

Busche A, et al. 2013. Priming of CD8+ T cells against cytomegalovirus-encoded antigens is dominated by cross-presentation. The Journal of Immunology 190:2767-2777.

Campbell AE, Cavanaugh VJ, Slater JS. 2008. The salivary glands as a privileged site of cytomegalovirus immune evasion and persistence. Medical Microbiology and Immunology 197:205-213.

Catusse J, Spinks J, Mattick C, Dyer A, Laing K, Fitzsimons C, Smit MJ, Gompels UA. 2008. Immunomodulation by herpesvirus U51A chemokine receptor via CCL5 and FOG-2 down-regulation plus XCR1 and CCR7 mimicry in human leukocytes. European Journal of Immunology 38:763-777.

Cavanaugh VJ, Deng Y, Birkenbach MP, Slater JS, Campbell AE. 2003. Vigorous innate and virus-specific cytotoxic T-lymphocyte responses to murine cytomegalovirus in the submaxillary salivary gland. Journal of Virology 77:1703-1717.

Cha T-a, Tom E, Kemble GW, Duke GM, Mocarski ES, Spaete RR. 1996. Human cytomegalovirus clinical isolates carry at least 19 genes not found in laboratory strains. Journal of Virology 70:78-83.

Chee M, Satchwell S, Preddie E, Weston K, Barrell B. 1990. Human cytomegalovirus encodes three G protein-coupled receptor homologues. Nature 344:774-777.

Cirone M, Conte V, Farina A, Valia S, Trivedi P, Granato M, Santarelli R, Frati L, Faggioni A. 2012. HHV-8 reduces dendritic cell migration through down-regulation of cell-surface CCR6 and CCR7 and cytoskeleton reorganization. Virology Journal 9:1-5.

Clark-Lewis I, Kim KS, Rajarathnam K, Gong JH, Dewald B, Moser B, Baggiolini M, Sykes BD. 1995. Structure-activity relationships of chemokines. Journal of Leukocyte Biology 57:703-711.

Collins TM, Quirk MR, Jordan MC. 1994. Biphasic viremia and viral gene expression in leukocytes during acute cytomegalovirus infection of mice. Journal of Virology 68:6305-6311.

Cooper MA, Fehniger TA, Caligiuri MA. 2001. The biology of human natural killer-cell subsets. Trends in Immunology 22:633-640.

Cooper MA, Fehniger TA, Fuchs A, Colonna M, Caligiuri MA. 2004. NK cell and DC interactions. Trends in Immunology 25:47-52.

Crozat K, Guiton R, Contreras V, Feuillet V, Dutertre C-A, Ventre E, Manh T-PV, Baranek T, Storset AK, Marvel J. 2010. The XC chemokine receptor 1 is a conserved selective marker of mammalian cells homologous to mouse CD8α+ dendritic cells. Journal of Experimental Medicine 207:1283-1292.

Dalod M, Hamilton T, Salomon R, Salazar-Mather TP, Henry SC, Hamilton JD, Biron CA. 2003. Dendritic cell responses to early murine cytomegalovirus infection: subset functional specialization and differential regulation by interferon α/β. Journal of Experimental Medicine 197:885-898.

Davison AJ, Dolan A, Akter P, Addison C, Dargan DJ, Alcendor DJ, McGeoch DJ, Hayward GS. 2003. The human cytomegalovirus genome revisited: comparison with the chimpanzee cytomegalovirus genomeFN1. Journal of General Virology 84:17-28.

De Smedt T, Pajak B, Muraille E, Lespagnard L, Heinen E, De Baetselier P, Urbain J, Leo O, Moser M. 1996. Regulation of dendritic cell numbers and maturation by lipopolysaccharide in vivo. Journal of Experimental Medicine 184:1413-1424.

Dorner BG, Dorner MB, Zhou X, Opitz C, Mora A, Güttler S, Hutloff A, Mages HW, Ranke K, Schaefer M. 2009. Selective expression of the chemokine receptor XCR1 on cross-presenting dendritic cells determines cooperation with CD8+ T cells. Immunity 31:823-833.

Dorner BG, Scheffold A, Rolph MS, Hüser MB, Kaufmann SH, Radbruch A, Flesch IE, Kroczek RA. 2002. MIP-1α, MIP-1β, RANTES, and ATAC/lymphotactin function together with IFN-γ as type 1 cytokines. Proceedings of the National Academy of Sciences 99:6181-6186.

Dorner BG, Smith HR, French AR, Kim S, Poursine-Laurent J, Beckman DL, Pingel JT, Kroczek RA, Yokoyama WM. 2004. Coordinate expression of cytokines and chemokines by NK cells during murine cytomegalovirus infection. The Journal of Immunology 172:3119-3131.

Dorner BG, Steinbach S, Hüser MB, Kroczek RA, Scheffold A. 2003. Single-cell analysis of the murine chemokines MIP-1α, MIP-1β, RANTES and ATAC/lymphotactin by flow cytometry. Journal of Immunological Methods 274:83-91.

Elkington R, Walker S, Crough T, Menzies M, Tellam J, Bharadwaj M, Khanna R. 2003. Ex vivo profiling of CD8+-T-cell responses to human cytomegalovirus reveals broad and multispecific reactivities in healthy virus carriers. Journal of Virology 77:5226-5240.

Ettinger J, Geyer H, Nitsche A, Zimmermann A, Brune W, Sandford GR, Hayward GS, Voigt S. 2012. Complete genome sequence of the English isolate of rat cytomegalovirus (Murid herpesvirus 8). Journal of Virology 86:13838-13838.

Farrell, Bruce K, Lawler C, Oliveira M, Cardin R, Davis-Poynter N, Stevenson PG. 2017. Murine cytomegalovirus spreads by dendritic cell recirculation. MBio 8:e01264-01217.

Farrell, Bruce K, Lawler C, Stevenson PG. 2019. Murine cytomegalovirus spread depends on the infected myeloid cell type. Journal of Virology:00540-00519.

Farrell, Vally H, Lynch D, Fleming P, Shellam G, Scalzo A, Davis-Poynter N. 1997. Inhibition of natural killer cells by a cytomegalovirus MHC class I homologue in vivo. Nature 386:510-514.

Faunce DE, Stein-Streilein J. 2002. NKT cell-derived RANTES recruits APCs and CD8+ T cells to the spleen during the generation of regulatory T cells in tolerance. The Journal of Immunology 169:31-38.

Fenner F. 1949. Mouse-pox (infectious ectromelia of mice): a review. The Journal of Immunology 63:341-373.

Fleming P, Davis-Poynter N, Degli-Esposti M, Densley E, Papadimitriou J, Shellam G, Farrell H. 1999. The murine cytomegalovirus chemokine homolog, m131/129, is a determinant of viral pathogenicity. Journal of Virology 73:6800-6809.

Förster R, Schubel A, Breitfeld D, Kremmer E, Renner-Müller I, Wolf E, Lipp M. 1999. CCR7 coordinates the primary immune response by establishing functional microenvironments in secondary lymphoid organs. Cell 99:23-33.

Foster-Cuevas M, Westerholt T, Ahmed M, Brown MH, Barclay AN, Voigt S. 2011. Cytomegalovirus e127 protein interacts with the inhibitory CD200 receptor. Journal of Virology 85:6055-6059.

Frascaroli G, Varani S, Moepps B, Sinzger C, Landini MP, Mertens T. 2006. Human cytomegalovirus subverts the functions of monocytes, impairing chemokine-mediated migration and leukocyte recruitment. Journal of Virology 80:7578-7589.

Frederico B, Chao B, May JS, Belz GT, Stevenson PG. 2014. A murid gamma-herpesviruses exploits normal splenic immune communication routes for systemic spread. Cell Host & Microbe 15:457-470.

Freigang S, Probst HC, van den Broek M. 2005. DC infection promotes antiviral CTL priming: the ‘Winkelried’strategy. Trends in Immunology 26:13-18.

Gerna G, Percivalle E, Lilleri D, Lozza L, Fornara C, Hahn G, Baldanti F, Revello MG. 2005. Dendritic-cell infection by human cytomegalovirus is restricted to strains carrying functional UL131–128 genes and mediates efficient viral antigen presentation to CD8+ T cells. Journal of General Virology 86:275-284.

Geyer H, Ettinger J, Möller L, Schmolz E, Nitsche A, Brune W, Heaggans S, Sandford GR, Hayward GS, Voigt S. 2015. Rat cytomegalovirus (RCMV) English isolate and a newly identified Berlin isolate share similarities with but are separate as an anciently diverged clade from mouse CMV and the Maastricht isolate of RCMV. Journal of General Virology 96:1873-1882.

Geyer H, Hartung E, Mages HW, Weise C, Belužić R, Vugrek O, Jonjić S, Kroczek RA, Voigt S. 2014. Cytomegalovirus expresses the chemokine homologue vXCL1 capable of attracting XCR1+ CD4− dendritic cells. Journal of Virology 88:292-302.

Grandage V, Gale R, Linch D, Khwaja A. 2005. PI3-kinase/Akt is constitutively active in primary acute myeloid leukaemia cells and regulates survival and chemoresistance via NF-kB, MAPkinase and p53 pathways. Leukemia 19:586-594.

Granelli-Piperno A, Finkel V, Delgado E, Steinman RM. 1999. Virus replication begins in dendritic cells during the transmission of HIV-1 from mature dendritic cells to T cells. Current Biology 9:21-29.

Granzow H, Weiland F, Jöns A, Klupp BG, Karger A, Mettenleiter TC. 1997. Ultrastructural analysis of the replication cycle of pseudorabies virus in cell culture: a reassessment. Journal of Virology 71:2072-2082.

Greenwald RJ, Freeman GJ, Sharpe AH. 2005. The B7 family revisited. Annual Review of Immunology 23:515-548.

Gros M, Amigorena S. 2019. Regulation of antigen export to the cytosol during cross-presentation. Frontiers in Immunology 10:41.

Grosjean I, Caux C, Bella C, Berger I, Wild F, Banchereau J, Kaiserlian D. 1997. Measles virus infects human dendritic cells and blocks their allostimulatory properties for CD4+ T cells. Journal of Experimental Medicine 186:801-812.

Grundy JE, Lawson KM, MacCormac LP, Fletcher JM, Yong KL. 1998. Cytomegalovirus-infected endothelial cells recruit neutrophils by the secretion of CXC chemokines and transmit virus by direct neutrophil-endothelial cell contact and during neutrophil transendothelial migration. Journal of Infectious Diseases 177:1465-1474.

Guermonprez P, Valladeau J, Zitvogel L, Théry C, Amigorena S. 2002. Antigen presentation and T cell stimulation by dendritic cells. Annual Review of Immunology 20:621-667.

Guilliams M, Ginhoux F, Jakubzick C, Naik SH, Onai N, Schraml BU, Segura E, Tussiwand R, Yona S. 2014. Dendritic cells, monocytes and macrophages: a unified nomenclature based on ontogeny. Nature Reviews Immunology 14:571-578.

Gurka S, Hartung E, Becker M, Kroczek RA. 2015. Mouse conventional dendritic cells can be universally classified based on the mutually exclusive expression of XCR1 and SIRPα. Frontiers in Immunology 6:35.

Hedrick JA, Saylor V, Figueroa D, Mizoue L, Xu Y, Menon S, Abrams J, Handel T, Zlotnik A. 1997. Lymphotactin is produced by NK cells and attracts both NK cells and T cells in vivo. The Journal of Immunology 158:1533-1540.

Hidi R, Riches V, Al-Ali M, Cruikshank WW, Center DM, Holgate ST, Djukanović R. 2000. Role of B7-CD28/CTLA-4 costimulation and NF-κB in allergen-induced T cell chemotaxis by IL-16 and RANTES. The Journal of Immunology 164:412-418.

Hochrein H, O'Keeffe M, Wagner H. 2002. Human and mouse plasmacytoid dendritic cells. Human Immunology 63:1103-1110.

Holtappels R, Böhm V, Podlech J, Reddehase MJ. 2008. CD8 T-cell-based immunotherapy of cytomegalovirus infection:"proof of concept" provided by the murine model. Medical Microbiology and Immunology 197:125-134.

Hou W-S, Van Parijs L. 2004. A Bcl-2-dependent molecular timer regulates the lifespan and immunogenicity of dendritic cells. Nature Immunology 5:583-589.

Hubert F-X, Voisine C, Louvet C, Heslan J-M, Ouabed A, Heslan M, Josien R. 2006. Differential pattern recognition receptor expression but stereotyped responsiveness in rat spleen dendritic cell subsets. The Journal of Immunology 177:1007-1016.

ICTV. 2019. International Committee on Taxonomy of Viruses (ICTV). (12.06.2019 https://ictv.global/taxonomy/)

Jahn G, Stenglein S, Riegler S, Einsele H, Sinzger C. 1999. Human cytomegalovirus infection of immature dendritic cells and macrophages. Intervirology 42:365-372.

Jancic C, Savina A, Wasmeier C, Tolmachova T, El-Benna J, Dang PM-C, Pascolo S, Gougerot-Pocidalo M-A, Raposo G, Seabra MC. 2007. Rab27a regulates phagosomal pH and NADPH oxidase recruitment to dendritic cell phagosomes. Nature Cell Biology 9:367-378.

Jarvis MA, Nelson JA. 2002. Mechanisms of human cytomegalovirus persistence and latency. Frontiers in Bioscience 7:d1575-d1582.

Joffre OP, Segura E, Savina A, Amigorena S. 2012. Cross-presentation by dendritic cells. Nature Reviews Immunology 12:557-569.

Jonjić S, Del Val M, Keil GM, Reddehase MJ, Koszinowski UH. 1988. A nonstructural viral protein expressed by a recombinant vaccinia virus protects against lethal cytomegalovirus infection. Journal of Virology 62:1653-1658.

Jonjić S, Pavić I, Lucin P, Rukavina D, Koszinowski UH. 1990. Efficacious control of cytomegalovirus infection after long-term depletion of CD8+ T lymphocytes. Journal of Virology 64:5457-5464.

Jordan S, Krause J, Prager A, Mitrovic M, Jonjic S, Koszinowski UH, Adler B. 2011. Virus progeny of murine cytomegalovirus bacterial artificial chromosome pSM3fr show reduced growth in salivary Glands due to a fixed mutation of MCK-2. Journal of Virology 85:10346-10353.

Kaptein SJ, van Cleef KW, Gruijthuijsen YK, Beuken EV, van Buggenhout L, Beisser PS, Stassen FR, Bruggeman CA, Vink C. 2004. The r131 gene of rat cytomegalovirus encodes a proinflammatory CC chemokine homolog which is essential for the production of infectious virus in the salivary glands. Virus Genes 29:43-61.

Karrer U, Sierro S, Wagner M, Oxenius A, Hengel H, Koszinowski UH, Phillips RE, Klenerman P. 2003. Memory inflation: continuous accumulation of antiviral CD8+ T cells over time. The Journal of Immunology 170:2022-2029.

Keen G. 1985. Human cytomegalovirus infection. South African Medical Journal= Suid-afrikaanse Tydskrif vir Geneeskunde 68:159-161.

Kelch M. 2020. Characterization of a RCMV-B gamma-chemokine knockout mutant. Master Thesis. Charite Berlin.

Kelner GS, Kennedy J, Bacon KB, Kleyensteuber S, Largaespada DA, Jenkins NA, Copeland NG, Bazan JF, Moore KW, Schall TJ. 1994. Lymphotactin: a cytokine that represents a new class of chemokine. Science 266:1395-1399.

Kennedy J, Kelner GS, Kleyensteuber S, Schall TJ, Weiss MC, Yssel H, Schneider PV, Cocks BG, Bacon KB, Zlotnik A. 1995. Molecular cloning and functional characterization of human lymphotactin. The Journal of Immunology 155:203-209.

Kopp EB, Ghosh S. 1995. NF-kB and Rel proteins in innate immunity. Advances in Immunology 58.

Kroczek RA, Henn V. 2012. The role of XCR1 and its ligand XCL1 in antigen cross-presentation by murine and human dendritic cells. Frontiers in Immunology 3:14.

La Rosa C, Diamond DJ. 2012. The immune response to human CMV. Future Virology 7:279-293.

Lande R, Giacomini E, Grassi T, Remoli ME, Iona E, Miettinen M, Julkunen I, Coccia EM. 2003. IFN-αβ released by Mycobacterium tuberculosis-infected human dendritic cells induces the expression of CXCL10: selective recruitment of NK and activated T cells. The Journal of Immunology 170:1174-1182.

Lefkowitz EJ, Dempsey DM, Hendrickson RC, Orton RJ, Siddell SG, Smith DB. 2017. Virus taxonomy: the database of the International Committee on Taxonomy of Viruses (ICTV). Nucleic Acids Research 46:D708-D717.

Lei Y, Takahama Y. 2012. XCL1 and XCR1 in the immune system. Microbes and Infection 14:262-267.

Lenschow DJ, Walunas TL, Bluestone JA. 1996. CD28/B7 system of T cell costimulation. Annual Review of Immunology 14:233-258.

Liu L, Zhang M, Jenkins C, MacPherson GG. 1998. Dendritic cell heterogeneity in vivo: two functionally different dendritic cell populations in rat intestinal lymph can be distinguished by CD4 expression. The Journal of Immunology 161:1146-1155.

Ljunggren H-G, Kärre K. 1990. In search of the ‘missing self’: MHC molecules and NK cell recognition. Immunology Today 11:237-244.

Lü F, Jacobson R. 2007. Oral mucosal immunity and HIV/SIV infection. Journal of Dental Research 86:216-226.

Luo J, Luo Z, Zhou N, Hall JW, Huang Z. 1999. Attachment of C-terminus of SDF-1 enhances the biological activity of its N-terminal peptide. Biochemical and Biophysical Research Communications 264:42-47.

Lüttichau HR. 2008. The herpesvirus 8 encoded chemokines vCCL2 (vMIP-II) and vCCL3 (vMIP-III) target the human but not the murine lymphotactin receptor. Virology Journal 5:50.

Lüttichau HR, Johnsen AH, Jurlander J, Rosenkilde MM, Schwartz TW. 2007. Kaposi sarcoma-associated herpes virus targets the lymphotactin receptor with both a broad spectrum antagonist vCCL2 and a highly selective and potent agonist vCCL3. Journal of Biological Chemistry 282:17794-17805.

Luttrell LM, Lefkowitz RJ. 2002. The role of β-arrestins in the termination and transduction of G-protein-coupled receptor signals. Journal of Cell Science 115:455-465.

MacDonald MR, Burney MW, Resnick SB, Virgin HW. 1999. Spliced mRNA encoding the murine cytomegalovirus chemokine homolog predicts a β chemokine of novel structure. Journal of Virology 73:3682-3691.

Mackay CR. 2001. Chemokines: immunology's high impact factors. Nature Immunology 2:95-101.

Malkowska M, Kokoszynska K, Dymecka M, Rychlewski L, Wyrwicz LS. 2013. Alphaherpesvirinae and Gammaherpesvirinae glycoprotein L and CMV UL130 originate from chemokines. Virology Journal 10.

Mantegazza AR, Savina A, Vermeulen M, Pérez L, Geffner J, Hermine O, Rosenzweig SD, Faure F, Amigorena S. 2008. NADPH oxidase controls phagosomal pH and antigen cross-presentation in human dendritic cells. Blood, The Journal of the American Society of Hematology 112:4712-4722.

Margulies BJ, Browne H, Gibson W. 1996. Identification of the human cytomegalovirus G protein-coupled receptor homologue encoded by UL33 in infected cells and enveloped virus particles. Virology 225:111-125.

Mathas S, Hinz M, Anagnostopoulos I, Krappmann D, Lietz A, Jundt F, Bommert K, Mechta-Grigoriou F, Stein H, Dörken B. 2002. Aberrantly expressed c-Jun and JunB are a hallmark of Hodgkin lymphoma cells, stimulate proliferation and synergize with NF-κB. The EMBO Journal 21:4104-4113.

McLellan AD, Kapp M, Eggert A, Linden C, Bommhardt U, Br cker E-B, K mmerer U, K mpgen E. 2002. Anatomic location and T-cell stimulatory functions of mouse dendritic cell subsets defined by CD4 and CD8 expression. Blood, The Journal of the American Society of Hematology 99:2084-2093.

Mettenleiter TC. 2002. Herpesvirus assembly and egress. Journal of Virology 76:1537-1547.

Michelson S, Dal Monte P, Zipeto D, Bodaghi B, Laurent L, Oberlin E, Arenzana-Seisdedos F, Virelizier J-L, Landini MP. 1997. Modulation of RANTES production by human cytomegalovirus infection of fibroblasts. Journal of Virology 71:6495-6500.

Milho R, Frederico B, Efstathiou S, Stevenson PG. 2012. A heparan-dependent herpesvirus targets the olfactory neuroepithelium for host entry. PLoS Pathogens 8:e1002986.

Miller-Kittrell M, Sparer TE. 2009. Feeling manipulated: cytomegalovirus immune manipulation. Virology Journal 6:4.

Mocarski ES, Shenk T, Paul G, F PR. 2013. Cytomegalovirus. Pages 1960-2014 in Knipe DM, Howley P, eds. Fields Virology. Philadelphia.

Moretta A. 2002. Natural killer cells and dendritic cells: rendezvous in abused tissues. Nature Reviews Immunology 2:957-965.

Mortier A, Gouwy M, Van Damme J, Proost P. 2011. Effect of posttranslational processing on the in vitro and in vivo activity of chemokines. Experimental Cell Research 317:642-654.

Moutaftsi M, Brennan P, Spector SA, Tabi Z. 2004. Impaired lymphoid chemokine-mediated migration due to a block on the chemokine receptor switch in human cytomegalovirus-infected dendritic cells. Journal of Virology 78:3046-3054.

Moutaftsi M, Mehl AM, Borysiewicz LK, Tabi Z. 2002. Human cytomegalovirus inhibits maturation and impairs function of monocyte-derived dendritic cells. Blood, The Journal of the American Society of Hematology 99:2913-2921.

Murphy. 2001. Viral exploitation and subversion of the immune system through chemokine mimicry. Nature Immunology 2:116-122.

Naik SH, Sathe P, Park H-Y, Metcalf D, Proietto AI, Dakic A, Carotta S, O'Keeffe M, Bahlo M, Papenfuss A. 2007. Development of plasmacytoid and conventional dendritic cell subtypes from single precursor cells derived in vitro and in vivo. Nature Immunology 8:1217-1226.

Nicholas J. 2007. Human herpesvirus 8-encoded proteins with potential roles in virus-associated neoplasia. Frontiers in Bioscience 12:265-281.

Noda S, Aguirre SA, Bitmansour A, Brown JM, Sparer TE, Huang J, Mocarski ES. 2006. Cytomegalovirus MCK-2 controls mobilization and recruitment of myeloid progenitor cells to facilitate dissemination. Blood 107:30-38.

Novoa RR, Calderita G, Arranz R, Fontana J, Granzow H, Risco C. 2005. Virus factories: associations of cell organelles for viral replication and morphogenesis. Biology of the Cell 97:147-172.

Owji H, Nezafat N, Negahdaripour M, Hajiebrahimi A, Ghasemi Y. 2018. A comprehensive review of signal peptides: Structure, roles, and applications. European Journal of Cell Biology 97:422-441.

Patro A. 2019. Subversion of Immune Response by Human Cytomegalovirus. Frontiers in Immunology 10:1155.

Pontejo SM, Murphy PM. 2017. Chemokines encoded by herpesviruses. Journal of Leukocyte Biology 102:1199-1217.

Priscott P, Tyrrell D. 1982. The isolation and partial characterisation of a cytomegalovirus from the brown rat, Rattus norvegicus. Archives of Virology 73:145-160.

Raftery MJ, Schwab M, Eibert SM, Samstag Y, Walczak H, Schönrich G. 2001. Targeting the function of mature dendritic cells by human cytomegalovirus: a multilayered viral defense strategy. Immunity 15:997-1009.

Rawlinson WD, Farrell HE, Barrell BG. 1996. Analysis of the complete DNA sequence of murine cytomegalovirus. Journal of Virology 70:8833-8849.

Reis e Sousa C. 2006. Dendritic cells in a mature age. Nature Reviews Immunology 6:476-483.

Revello MG, Gerna G. 2010. Human cytomegalovirus tropism for endothelial/epithelial cells: scientific background and clinical implications. Reviews in Medical Virology 20:136-155.

Ritter U, Wiede F, Mielenz D, Kiafard Z, Zwirner J, Körner H. 2004. Analysis of the CCR7 expression on murine bone marrow-derived and spleen dendritic cells. Journal of Leukocyte Biology 76:472-476.

Robertson MJ. 2002. Role of chemokines in the biology of natural killer cells. Journal of Leukocyte Biology 71:173-183.

Rölle A, Olweus J. 2009. Dendritic cells in cytomegalovirus infection: viral evasion and host countermeasures. Apmis 117:413-426.

Rollins BJ. 1997. Chemokines. Blood, The Journal of the American Society of Hematology 90:909-928.

Rossi D, Zlotnik A. 2000. The biology of chemokines and their receptors. Annual Review of Immunology 18:217-242.

Ryckman BJ, Rainish BL, Chase MC, Borton JA, Nelson JA, Jarvis MA, Johnson DC. 2008. Characterization of the human cytomegalovirus gH/gL/UL128-131 complex that mediates entry into epithelial and endothelial cells. Journal of Virology 82:60-70.

Sacher T, Andrassy J, Kalnins A, Dölken L, Jordan S, Podlech J, Ruzsics Z, Jauch K-W, Reddehase MJ, Koszinowski UH. 2011. Shedding light on the elusive role of endothelial cells in cytomegalovirus dissemination. PLoS Pathogens 7:e1002366.

Saederup N, chun Lin Y, Dairaghi DJ, Schall TJ, Mocarski ES. 1999. Cytomegalovirus-encoded β chemokine promotes monocyte-associated viremia in the host. Proceedings of the National Academy of Sciences 96:10881-10886.

Sallusto F, Palermo B, Lenig D, Miettinen M, Matikainen S, Julkunen I, Forster R, Burgstahler R, Lipp M, Lanzavecchia A. 1999. Distinct patterns and kinetics of chemokine production regulate dendritic cell function. European Journal of Immunology 29:1617-1625.

Sánchez-Sánchez N, Riol-Blanco L, Rodríguez-Fernández JL. 2006. The multiple personalities of the chemokine receptor CCR7 in dendritic cells. The Journal of Immunology 176:5153-5159.

Sandford GR, Brock LE, Voigt S, Forester CM, Burns WH. 2001. Rat cytomegalovirus major immediate-early enhancer switching results in altered growth characteristics. Journal of Virology 75:5076-5083.

Savina A, Peres A, Cebrian I, Carmo N, Moita C, Hacohen N, Moita LF, Amigorena S. 2009. The small GTPase Rac2 controls phagosomal alkalinization and antigen crosspresentation selectively in CD8+ dendritic cells. Immunity 30:544-555.

Shivkumar M, Milho R, May JS, Nicoll MP, Efstathiou S, Stevenson PG. 2013. Herpes simplex virus 1 targets the murine olfactory neuroepithelium for host entry. Journal of Virology 87:10477-10488.

Shortman K, Liu Y-J. 2002. Mouse and human dendritic cell subtypes. Nature Reviews Immunology 2:151-161.

Sigal LJ, Crotty S, Andino R, Rock KL. 1999. Cytotoxic T-cell immunity to virus-infected non-haematopoietic cells requires presentation of exogenous antigen. Nature 398:77.

Sinzger C, Digel M, Jahn G. 2008. Cytomegalovirus cell tropism. Pages 63-83. Human cytomegalovirus. Berlin, Heidelberg: Springer.

Sinzger C, Schmidt K, Knapp J, Kahl M, Beck R, Waldman J, Hebart H, Einsele H, Jahn G. 1999. Modification of human cytomegalovirus tropism through propagation in vitro is associated with changes in the viral genome. Journal of General Virology 80:2867-2877.

Sodeik B, Ebersold MW, Helenius A. 1997. Microtubule-mediated transport of incoming herpes simplex virus 1 capsids to the nucleus. The Journal of Cell Biology 136:1007-1021.

Sodhi A, Montaner S, Gutkind JS. 2004. Viral hijacking of G-protein-coupled-receptor signalling networks. Nature Reviews Molecular Cell Biology 5:998-1012.

Sozzani S, Allavena P, D'Amico G, Luini W, Bianchi G, Kataura M, Imai T, Yoshie O, Bonecchi R, Mantovani A. 1998. Cutting edge: differential regulation of chemokine receptors during dendritic cell maturation: a model for their trafficking properties. The Journal of Immunology 161:1083-1086.

Sozzani S, Allavena P, Mantovani A. 2001. Dendritic cells and chemokines. Dendritic Cells:203-211.

Straschewski S, Patrone M, Walther P, Gallina A, Mertens T, Frascaroli G. 2011. Protein pUL128 of human cytomegalovirus is necessary for monocyte infection and blocking of migration. Journal of Virology 85:5150-5158.

Suh W-K, Cohen-Doyle MF, Fruh K, Wang K, Peterson PA, Williams DB. 1994. Interaction of MHC class I molecules with the transporter associated with antigen processing. Science 264:1322-1326.

Swiecki M, Gilfillan S, Vermi W, Wang Y, Colonna M. 2010. Plasmacytoid dendritic cell ablation impacts early interferon responses and antiviral NK and CD8+ T cell accrual. Immunity 33:955-966.

Sylwester AW, Mitchell BL, Edgar JB, Taormina C, Pelte C, Ruchti F, Sleath PR, Grabstein KH, Hosken NA, Kern F. 2005. Broadly targeted human cytomegalovirus-specific CD4+ and CD8+ T cells dominate the memory compartments of exposed subjects. Journal of Experimental Medicine 202:673-685.

Tadagaki K, Tudor D, Gbahou F, Tschische P, Waldhoer M, Bomsel M, Jockers R, Kamal M. 2012. Human cytomegalovirus-encoded UL33 and UL78 heteromerize with host CCR5 and CXCR4 impairing their HIV coreceptor activity. Blood, The Journal of the American Society of Hematology 119:4908-4918.

Thiele S, Rosenkilde M. 2014. Interaction of chemokines with their receptors–from initial chemokine binding to receptor activating steps. Current Medicinal Chemistry 21:3594-3614.

Thomas R, Yang X. 2016. NK-DC crosstalk in immunity to microbial infection. Journal of Immunology Research.

Van Antwerp DJ, Martin SJ, Verma IM, Green DR. 1998. Inhibition of TNF-induced apoptosis by NF-κB. Trends in Cell Biology 8:107-111.

van der Strate B, Hillebrands J, a Nijeholt SL, Beljaars L, Bruggeman C, Van Luyn M, Rozing J, Meijer D, Molema G, Harmsen M. 2003. Dissemination of rat cytomegalovirus through infected granulocytes and monocytes in vitro and in vivo. Journal of Virology 77:11274-11278.

Van Dommelen SL, Tabarias HA, Smyth MJ, Degli-Esposti MA. 2003. Activation of natural killer (NK) T cells during murine cytomegalovirus infection enhances the antiviral response mediated by NK cells. Journal of Virology 77:1877-1884.

van Kooten C, Banchereau J. 2000. CD40-CD40 ligand. Journal of Leukocyte Biology 67:2-17.

Vanarsdall AL, Johnson DC. 2012. Human cytomegalovirus entry into cells. Current Opinion in Virology 2.

Varani S, Frascaroli G, Homman-Loudiyi M, Feld S, Landini MP, Söderberg-Nauclér C. 2005. Human cytomegalovirus inhibits the migration of immature dendritic cells by down-regulating cell-surface CCR1 and CCR5. Journal of Leukocyte Biology 77:219-228.

Varnum SM, Streblow DN, Monroe ME, Smith P, Auberry KJ, Paša-Tolić L, Wang D, Camp DG, Rodland K, Wiley S. 2004. Identification of proteins in human cytomegalovirus (HCMV) particles: the HCMV proteome. Journal of Virology 78:10960-10966.

Villadangos JA, Schnorrer P. 2007. Intrinsic and cooperative antigen-presenting functions of dendritic-cell subsets in vivo. Nature Reviews Immunology 7:543-555.

Vink C, Beuken E, Bruggeman CA. 2000. Complete DNA sequence of the rat cytomegalovirus genome. Journal of Virology 74:7656-7665.

Vischer HF, Siderius M, Leurs R, Smit MJ. 2014. Herpesvirus-encoded GPCRs: neglected players in inflammatory and proliferative diseases? Nature Reviews Drug Discovery 13:123-139.

Voigt S, Hayward GS. 2011. Create species Murid herpesvirus 8 in the genus Muromegalovirus, subfamily Betaherpesvirinae, family Herpesviridae, order Herpesvirales. (https://talk.ictvonline.org/ICTV/proposals/2011.014aV.A.v2.Muromegalovirus-Sp.pdf)

Voigt S, Mesci A, Ettinger J, Fine JH, Chen P, Chou W, Carlyle JR. 2007. Cytomegalovirus evasion of innate immunity by subversion of the NKR-P1B: Clr-b missing-self axis. Immunity 26:617-627.

Voigt S, Sandford GR, Hayward GS, Burns WH. 2005. The English strain of rat cytomegalovirus (CMV) contains a novel captured CD200 (vOX2) gene and a spliced CC chemokine upstream from the major immediate-early region: further evidence for a separate evolutionary lineage from that of rat CMV Maastricht. Journal of General Virology 86:263-274.

von Heijne G. 1990. The signal peptide. The Journal of Membrane Biology 115:195-201.

Vremec D, Pooley J, Hochrein H, Wu L, Shortman K. 2000. CD4 and CD8 expression by dendritic cell subtypes in mouse thymus and spleen. The Journal of Immunology 164:2978-2986.

Vyas JM, Van der Veen AG, Ploegh HL. 2008. The known unknowns of antigen processing and presentation. Nature Reviews Immunology 8:607.

Wagner FM, Brizic I, Prager A, Trsan T, Arapovic M, Lemmermann NA, Podlech J, Reddehase MJ, Lemnitzer F, Bosse JB. 2013. The viral chemokine MCK-2 of murine cytomegalovirus promotes infection as part of a gH/gL/MCK-2 complex. PLoS Pathogens 9.

Wang D, Bresnahan W, Shenk T. 2004. Human cytomegalovirus encodes a highly specific RANTES decoy receptor. Proceedings of the National Academy of Sciences 101:16642-16647.

Wang D, Shenk T. 2005. Human cytomegalovirus virion protein complex required for epithelial and endothelial cell tropism. Proceedings of the National Academy of Sciences 102:18153-18158.

Wathen MW, Stinski MF. 1982. Temporal patterns of human cytomegalovirus transcription: mapping the viral RNAs synthesized at immediate early, early, and late times after infection. Journal of Virology 41:462-477.

Wolf SA, Epping L, Andreotti S, Reinert K, Semmler T. 2020. SCORE: Smart Consensus Of RNA Expression-a consensus tool for detecting differentially expressed genes in bacteria. Bioinformatics.

Woo YD, Koh J, Kang H-R, Kim HY, Chung DH. 2018. The invariant natural killer T cell–mediated chemokine XC motif chemokine ligand 1–XC motif chemokine receptor 1 axis promotes allergic airway hyperresponsiveness by recruiting CD103+ dendritic cells. Journal of Allergy and Clinical Immunology 142:1781-1792. e1712.

Wu L, KewalRamani VN. 2006. Dendritic-cell interactions with HIV: infection and viral dissemination. Nature Reviews Immunology 6:859.

Wyrwicz LS, Rychlewski L. 2007. Herpes glycoprotein gL is distantly related to chemokine receptor ligands. Antiviral Research 75:83-86.

Yamin R, Lecker LS, Weisblum Y, Vitenshtein A, Le-Trilling VTK, Wolf DG, Mandelboim O. 2016. HCMV vCXCL1 binds several chemokine receptors and preferentially attracts neutrophils over NK cells by interacting with CXCR2. Cell Reports 15:1542-1553.

Yanagawa Y, Onoé K. 2002. CCL19 induces rapid dendritic extension of murine dendritic cells. Blood, The Journal of the American Society of Hematology 100:1948-1956.

Yoshida T, Imai T, Kakizaki M, Nishimura M, Takagi S, Yoshie O. 1998. Identification of single C motif-1/lymphotactin receptor XCR1. Journal of Biological Chemistry 273:16551-16554.

Yoshida T, Imai T, Kakizaki M, Nishimura M, Yoshie O. 1995. Molecular cloning of a novel C or γ type chemokine, SCM-1. FEBS Letters 360:155-159.

Yrlid U, Macpherson G. 2003. Phenotype and function of rat dendritic cell subsets. Apmis 111:756-765.

Zhu, Shen Q, Ulrich M, Zheng M. 2000. Human monocyte-derived dendritic cells expressing both chemotactic cytokines IL-8, MCP-1, RANTES and their receptors, and their selective migration to these chemokines. Chinese Medical Journal 113:1124-1128.

Zhu J, Paul WE. 2010. Heterogeneity and plasticity of T helper cells. Cell Research 20:4-12.

Danksagung

An dieser Stelle möchte ich mich bei PD Dr. Sebastian Voigt bedanken, der mir die Möglichkeit gegeben hat an diesem spannenden und anspruchsvollen Projekt zu arbeiten. Zudem gilt mein Dank Herrn Prof. Dr. Krüger, der stets ein offenes Ohr für mich hatte.

Mein ganz persönlicher Dank gilt Dr. Agnieszka Bauer für die Einarbeitung in das Projekt. Mit großer Freude habe ich Seite an Seite mit ihr bis in die Nacht gearbeitet und gelacht. Sie war meine Mentorin, die mich motiviert und angefeuert hat. Weiterhin gilt mein Dank Katharina Erbe, die mich mit großem Ehrgeiz und viel Freude bei den Tierversuchen unterstützt hat. Bei Jenny Geserick, Alexander Dorn und Annette Dietrich möchte ich mich für die ausgezeichnete Betreuung der Versuchstiere bedanken. Ein großer Dank geht an Emanuel Wyler und Silver Wolf, mit deren Hilfe ich einen tiefen Einblick in die Mechanismen der dendritischen Zellen bekommen habe. Ich bedanke mich bei all meinen Studenten/-innen, die mich gefordert und unterstützt haben. Besonderer Dank gilt hier Yue Yu, die unter meiner Anleitung die CRISPR/Cas Virusmutante hergestellt hat. Ich möchte mich hiermit bei sämtlichen Kooperationspartnern/-innen bedanken, die einen technischen oder theoretischen Beitrag in diesem Projekt geleistet haben. Dazu gehören Lars Möller, Vanda Juranic Lisnic, Robert Jan Lebbink, Sofie Piper, Monika Jaensch und Stephanie Gurka. Weiterhin bedanke ich mich bei den Doktoranden/-innen des RoKoDoKos, für eine tolle Atmosphäre am Institut und für den regen disziplinübergreifenden Ideenaustausch bei den Versammlungen. Für eine tolle Atmosphäre möchte ich mich auch bei Darius, Esther und Eva bedanken, die von Kollegen/-innen zu Freunden geworden sind. Renate und Dagmar danke ich ebenfalls für ihre Herzlichkeit und dass sie sich stets sehr gut um unser Labor gekümmert haben. Vielen Dank auch an Bernhard, der sehr akribisch meine Arbeit gelesen und sprachlich korrigiert hat. Ganz FG12 bin ich dankbar, für die angenehme Zeit am RKI.

Schließlich gilt mein Dank meinen Freunden und meiner Familie. Insbesondere meinem Vater, für sein stetes Interesse an meinen Fortschritten, und meinen Schwestern Jeanne, Marie und Ania, die mich vor Allem emotional unterstützt haben.

Und Stephan, vielen Dank für dein Engagement und deine Neugier an meiner Arbeit. Mich mit dir zu messen, über unsere beider Forschung zu diskutieren und innovative Ideen zu entwickeln, haben meine Motivation und meinen Ehrgeiz aufrecht gehalten und werden es auch in Zukunft tun.

Publications and presentations

Publications

Bauer, A.*, Madela, J.*, Berg, C., Daugvilaite, V., Gurka, S., Mages, H.W., Kroczek, R.A., Rosenkilde, M.M. and Voigt, S., 2020. Rat cytomegalovirus-encoded γ-chemokine vXCL1 is a highly adapted, species-specific agonist for rat XCR1-positive dendritic cells. Journal of Cell Science, 133(5)
*contributed equally

El-Mokhtar, M.A., Bauer, A., Madela, J. and Voigt, S., 2018. Cellular distribution of CD200 receptor in rats and its interaction with cytomegalovirus e127 protein. Medical Microbiology and Immunology, 207(5-6), pp.307-318

Poster

Madela, J., Bauer, A., Voigt, S., XCR1 is internalized after interaction with Rat Cytomegalovirus vXCL1, 29th Annual Meeting of the Society for Virology, Düsseldorf, 2019

Madela, J., Bauer, A., Voigt, S., Rat Cytomegalovirus γ-chemokine vXCL1 interacts with XCR1$^+$ dendritic cells, 15th International Symposium on DENDRITIC CELLS, Aachen, 2018

Madela, J., Bauer, A., Geyer, H., Voigt, S., Rat Cytomegalovirus γ-chemokine vXCL1 interacts with XCR1$^+$ dendritic cells, 28th Annual Meeting of the Society for Virology, Würzburg, 2018

Madela, J., Friedrich, N., Geyer, H., Rennert, P., Mankertz, A., Rubella virus infection leads to an upregulation of prostaglandin E2 synthesis in human fetal endothelial cells, 27th Annual Meeting of the Society for Virology, Marburg, 2017

Declaration

I hereby declare that this thesis comprises my own work and effort, except where otherwise stated. This thesis, neither in whole nor in part, has been previously submitted for any degree.

Berlin, 01.12.2020

Supplement

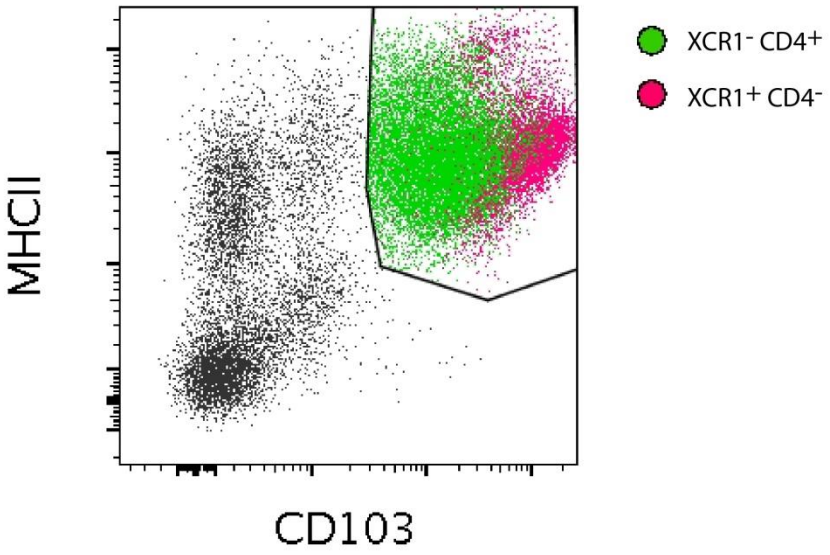

Supplement 1: CD4$^-$ DC express higher amounts of CD103. Rat spleen was digested with Collagenase D and Dnase I followed by OptiPrep density centrifugation. DC were gated by excluding dead, CD3$^+$ and CD45RA$^+$ cells. Two major DC subsets were differentiated by the expression of CD4 and XCR1. XCR1$^+$ CD4$^-$ population (pink color) and XCR1$^-$ CD4$^+$ population (green color) were then gated back into MHCII and CD103 plot to demonstrate the higher CD103 expression by CD4$^-$ DC.

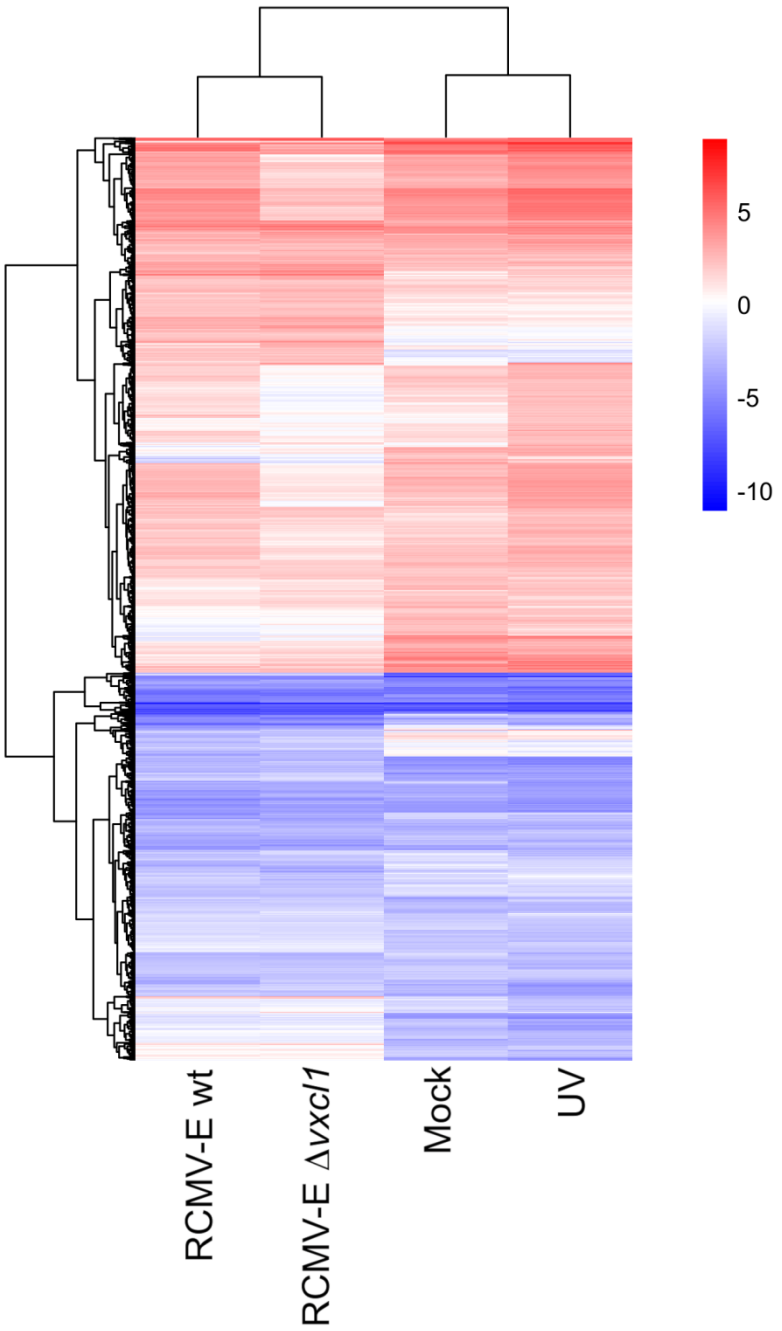

Supplement 2: Heatmap of differentially expressed genes of infected DC. Ox-62 enriched DC were infected with RCMV-E wt, UV-inactivated RCMV-E and RCMV-E Δ*vxcl1*. Mock-infected cells served as negative control. Expressed genes were normalized to freshly isolated, not cultivated DC. Designated as red are upregulated and as blue downregulated genes. Differentially expressed genes predicted by SCORE with Fold Change > 4, $p \leq 0.05$, n = 3.

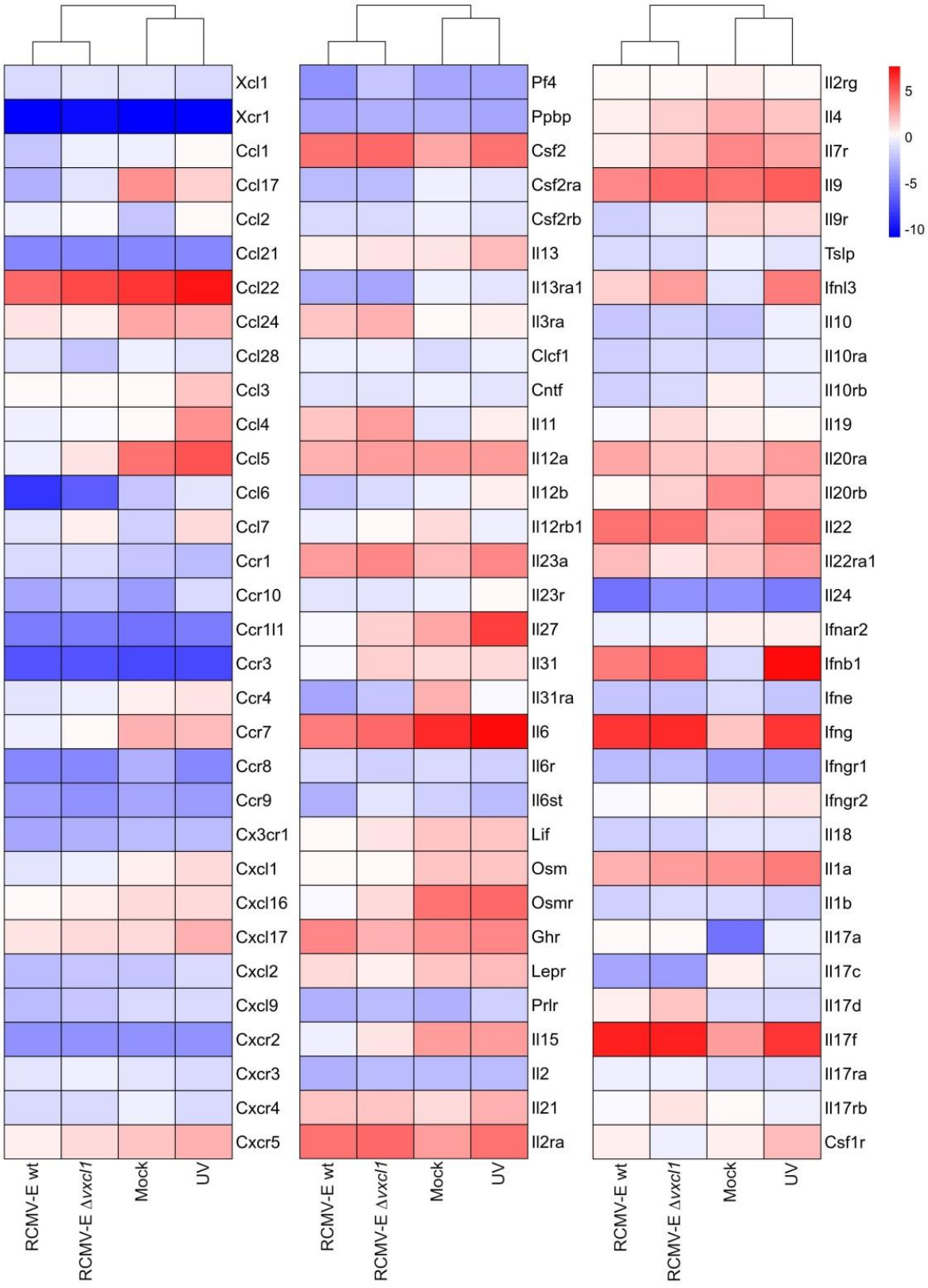

Supplement 3: Heatmap of differentially expressed cytokines of infected DC. Ox-62 enriched DC were infected with RCMV-E wt, UV-inactivated RCMV-E and RCMV-E Δ*vxcl1*. Mock-infected cells served as negative control. Expressed genes were normalized to freshly isolated, not cultivated DC. Designated as red are upregulated and as blue downregulated genes. Differentially expressed genes predicted by SCORE with Fold Change > 4, $p \leq 0.05$, n = 3.

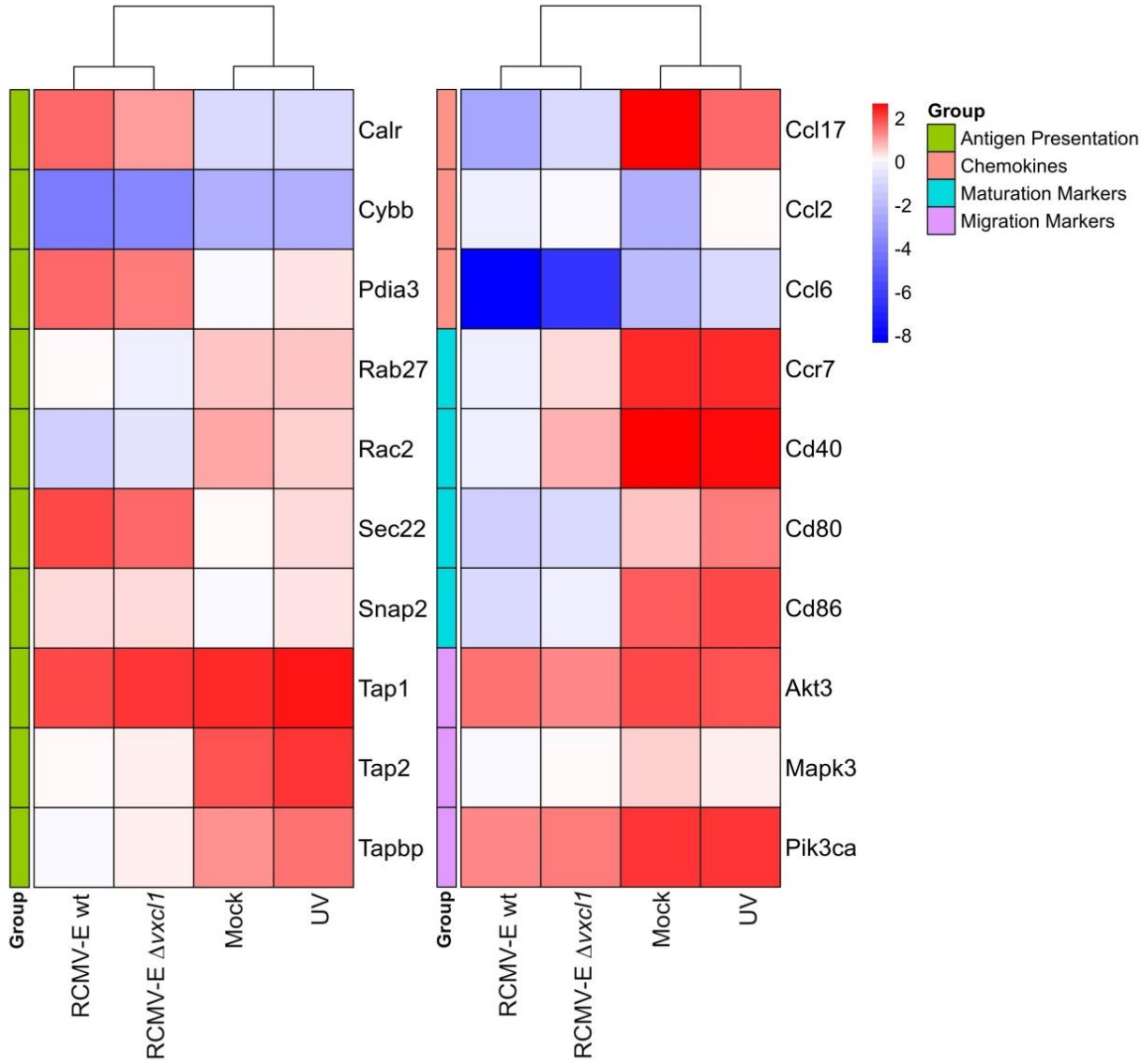

Supplement 4: Heatmap of differentially expressed genes of interest of infected DC. Ox-62 enriched DC were infected with RCMV-E wt, UV-inactivated RCMV-E and RCMV-E Δ*vxcl1*. Mock-infected cells served as negative control. Expressed genes were normalized to freshly isolated, not cultivated DC. Designated as red are upregulated and as blue downregulated genes. Differentially expressed genes predicted by SCORE with Fold Change > 4, $p \leq 0.05$, n = 3.

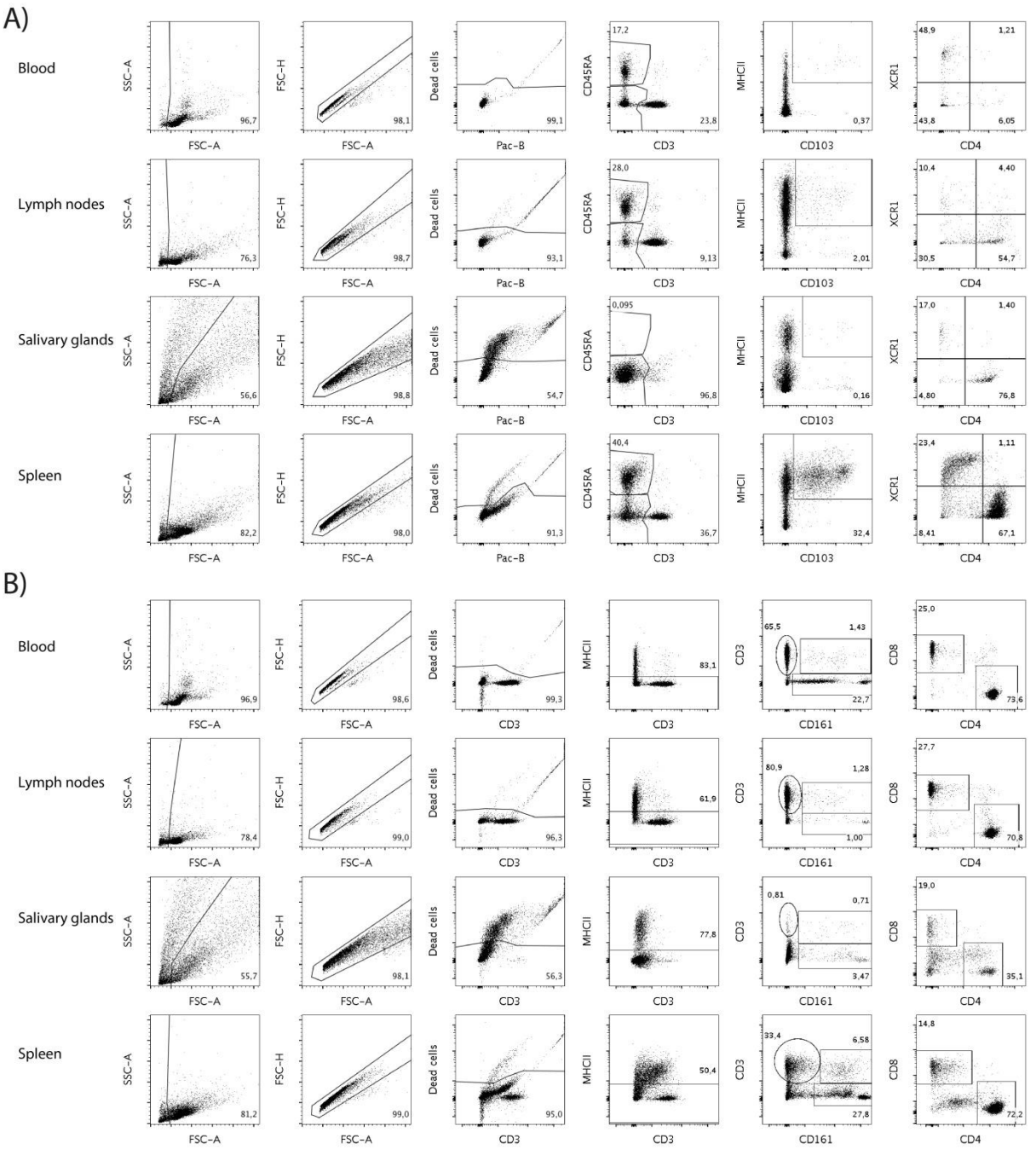

Supplement 5: Dotplots and gating of enriched leukocytes from blood, lymph nodes, salivary glands and spleen. 10-week-old male rats were infected with $1*10^6$ pfu of RCMV-B. After 3, 5, 16 and 90 days post infection, blood, lymph nodes, salivary glands and spleen were collected and processed for cell isolation. A) Cells were stained to analyze DC ($MHCII^+$ $CD103^+$) and B cells ($CD45RA^+$). B) Cells were stained to analyze T cells ($CD3^+$), NK ($CD161^+$), and NKT ($CD161^+$ $CD3^+$) cells.

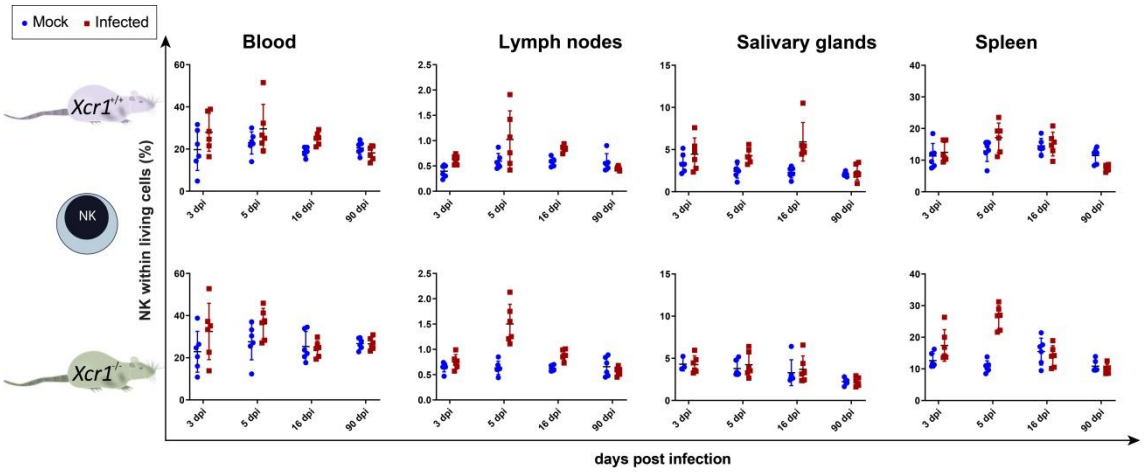

Supplement 6: NK cell population within living cells. 10-week-old male Sprague Dawley rats were infected with $1*10^6$ pfu of RCMV-B. Leukocytes were isolated from blood, lymph nodes, salivary glands and spleen. After surface staining, cells were gated on $CD161^+$ and $CD3^-$ to analyze NK cells. Frequency of $CD161^+$ $CD3^-$ cells within living cells is shown. Error bars represent mean ± SD, n = 6 rats.

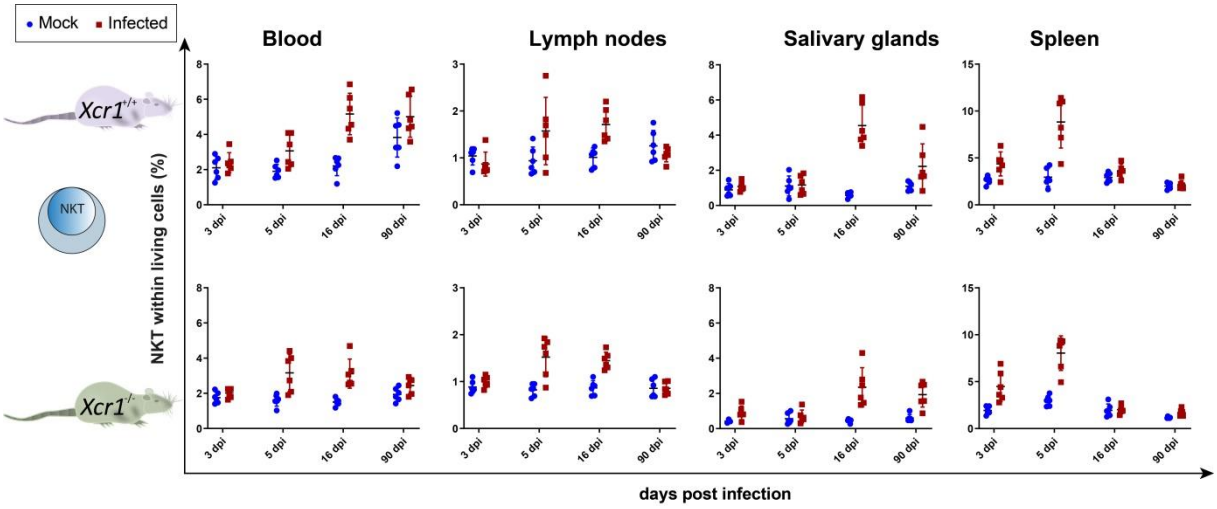

Supplement 7: NKT cell population within living cells. 10-week-old male Sprague Dawley rats were infected with $1*10^6$ pfu of RCMV-B. Leukocytes were isolated from blood, lymph nodes, salivary glands and spleen. After surface staining, cells were gated on $CD161^+$ and $CD3^+$ to analyze NKT cells. Frequency of $CD161^+$ $CD3^+$ cells within living cells is shown. Error bars represent mean ± SD, n = 6 rats.

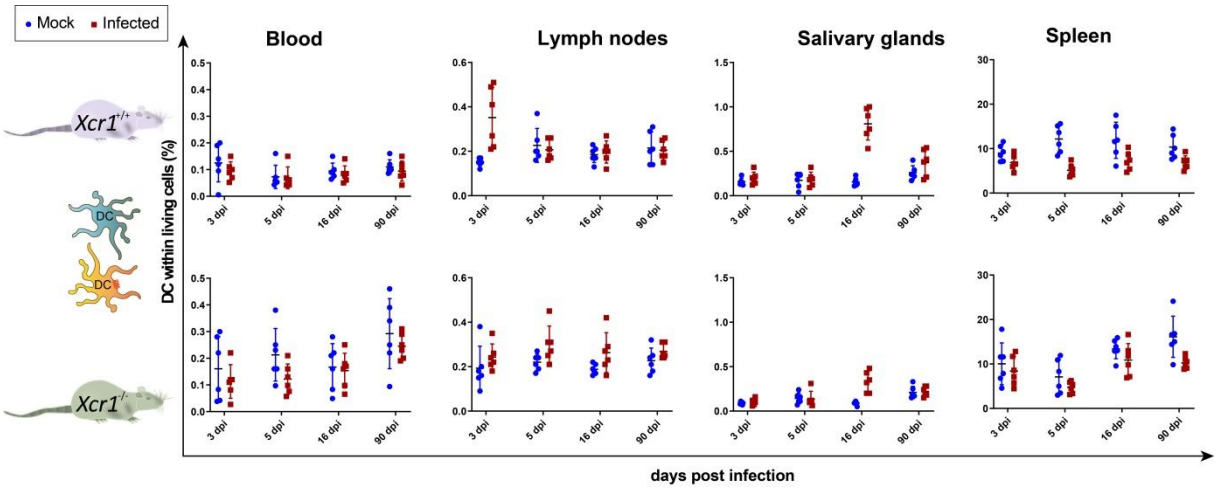

Supplement 8: Frequency of DC population within living cells. 10-week-old male Sprague Dawley rats were infected with $1*10^6$ pfu of RCMV-B. Leukocytes were isolated from blood, lymph nodes, salivary glands and spleen. After surface staining, cells were gated on MHCII$^+$ and CD103$^+$ to analyze dendritic cells. Frequency of CD103$^+$ MHCII$^+$ cells within all living cells is shown. Error bars represent mean ± SD, n = 6 rats.

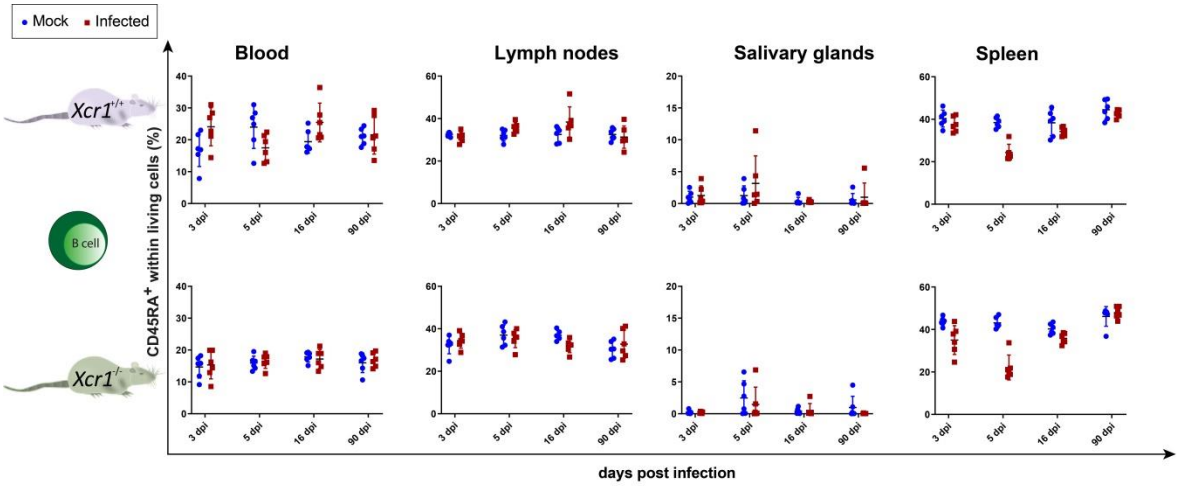

Supplement 9: Frequency of B cell population within living cells. 10-week-old male Sprague Dawley rats were infected with $1*10^6$ pfu of RCMV-B. Leukocytes were isolated from blood, lymph nodes, salivary glands and spleen. After surface staining, cells were gated on CD45RA$^+$ and MHCII$^+$ to analyze B lymphocytes. Frequency of CD45RA$^+$ MHCII$^+$ cells within living cells is shown. Error bars represent mean ± SD, n = 6 rats.

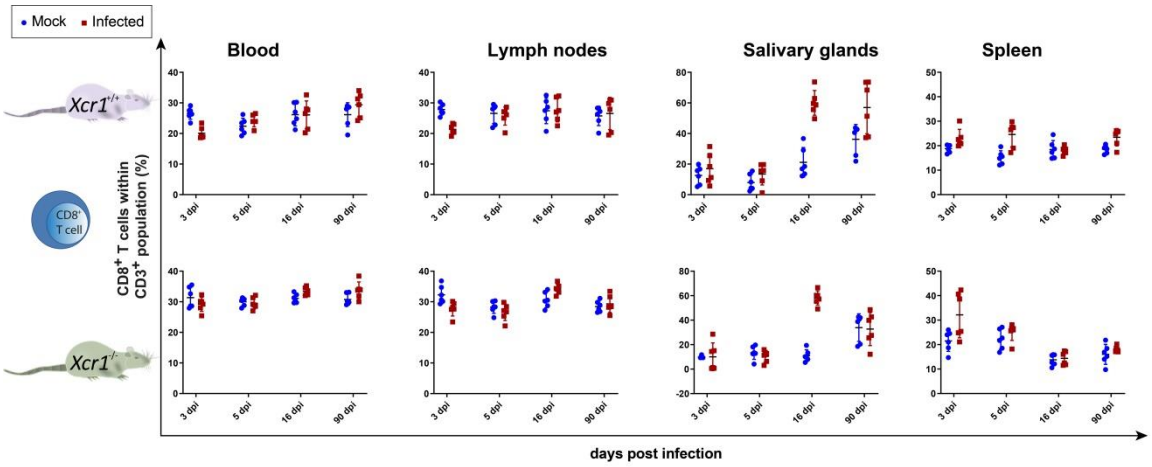

Supplement 10: Frequency of CD8⁺ T cell population within T cells. 10-week-old male Sprague Dawley rats were infected with 1*10^6 pfu of RCMV-B. Leukocytes were isolated from blood, lymph nodes, salivary glands and spleen. After surface staining, cells were gated on CD3⁺ and CD8⁺ to analyze cytotoxic T cells. Frequency of CD3⁺ CD8⁺ cells within T cell population is shown. Error bars represent mean ± SD, n = 6 rats.

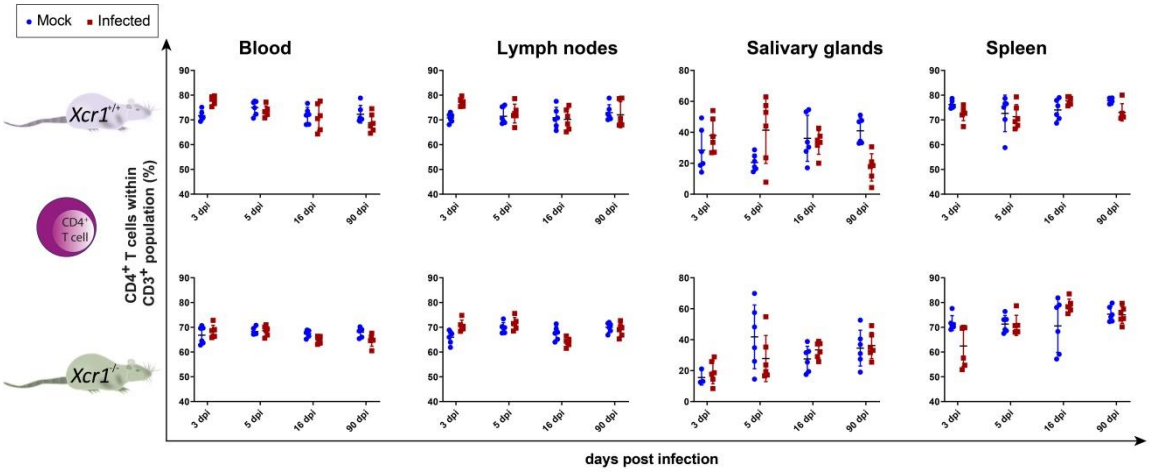

Supplement 11: Frequency of CD4⁺ T cell population within T cells. 10-week-old male Sprague Dawley rats were infected with 1*10^6 pfu of RCMV-B. Leukocytes were isolated from blood, lymph nodes, salivary glands and spleen. After surface staining, cells were gated on CD3⁺ and CD4⁺ to analyze helper T cells. Frequency of CD3⁺ CD4⁺ cells within T cell population is shown. Error bars represent mean ± SD, n = 6 rats.